7

Second- and Third-Order Nonlinear Optical Materials

Larry Dalton
Philip Sullivan
Alex K.-Y. Jen

7.1 Introduction

Second- and third-order optical nonlinearity can perhaps be best understood as the coefficients of the second and third terms in the power series expansion of molecular and macroscopic polarization in terms of applied electric fields.

$$P_i = \alpha_{ij}E_j + \beta_{ijk}E_jE_k + \gamma_{ijkl}E_jE_kE_l + \ldots \tag{7.1}$$

$$P_i = \chi^{(1)}{}_{ij}E_j + \chi^{(2)}{}_{ijk}E_jE_k + \chi^{(3)}{}_{ijkl}E_jE_kE_l + \ldots \tag{7.2a}$$

$$P_i = \chi^{(1)}{}_{ij}E_{j\omega}\cos(\omega t - kz) + (1/2)\chi^{(2)}{}_{ijj}E_{jj\omega}[1 + \cos(2\omega t - 2kz)] + \ldots \tag{7.2b}$$

The terms β and γ represent the first and second molecular hyperpolarizabilities, whereas the terms $\chi^{(2)}$ and $\chi^{(3)}$ represent the first- and second-order nonlinear material (macroscopic) susceptibilities. Each term arises from the nonlinear interaction of applied electric fields with the quasi-delocalized electron distribution of molecules and materials. Moreover, each of these terms can give rise to a variety of nonlinear responses reflecting different frequency dependences.[1–13] Second-order terms give rise to second harmonic generation (see Equation 7.2b), difference frequency (e.g., terahertz frequency) generation, optical rectification (see Equation 7.2b), and electro-optic modulation (the Pockels effect). Third-order optical nonlinearity gives rise to third harmonic generation, phase conjugation, optical

15018—Chapter7—26/8/2006—22:01—SJAPPIYAR—15018—XML MODEL CRC12a – pp. 1–126.

limiting, optical parametric effects, and all-optical modulation (the Kerr effect). As is typical for power series expansions, the second-order coefficients are larger than the third-order coefficients. Although commercial applications have been realized for both second- and third-order inorganic materials, such as lithium niobate electro-optic and titanium/sapphire optical parametric materials, organic nonlinear optical materials are still struggling to obtain a beachhead on the commercial landscape. To the present time, second-order nonlinear optical organic materials appear closer to commercial application and will thus receive greater attention in this chapter.

It is very difficult to define a universal figure-of-merit (FOM) for either second- or third-order nonlinear optical materials, as practical device performance will often depend on the details of device design as well as intrinsic material properties. However, the most simplistic and yet somewhat realistic figure-of-merit can be expressed as $\text{FOM} = \chi^{(2 \text{ or } 3)}/\tau\alpha$, where τ is the response time for the system reacting to an electric field perturbation and τ is the optical loss. For π-electron organic materials, the response time, τ is the phase relaxation time of the conjugated π-electrons, which is typically on the order of tens of femtoseconds. If device bandwidths are determined by the intrinsic material response time, bandwidths of tens of terahertz are possible. The optical loss, α, typically includes both absorption and scattering contributions. Optical loss will, thus, be influenced by material heterogeneity as well as molecular structure. Of course, practical device applications may also require many additional material properties including stability (e.g., thermal and photochemical) and processability (e.g., solubility in spin-casting solvent, appropriate sublimation temperatures for vapor deposition, appropriate glass transition temperatures for nanoimprint lithography). The FOM defined above is most commonly used in ranking third-order nonlinear optical materials. With second-order nonlinear optical materials, other factors such as the resistivity of metal electrodes used in electro-optic modulator devices can limit bandwidths, so the material FOM is commonly simplified to $\chi^{(2)}/\alpha$ or as $\chi^{(2)}/\alpha\varepsilon$, where ε is the material dielectric constant. For example, for electro-optic applications, it is important to match the velocity of propagating optical and radiofrequency waves. Velocity matching is optimized when $n^2 = \varepsilon$, where n is the material index of refraction.

Quantum mechanical calculations have proven useful in investigating the relationship of β and γ to molecular (chromophore) structure.[14–24] For simple polyenes, the variation of molecular hyperpolarizability with the length of the conjugated π-electron structure and with bond length alternation is reasonably well predicted by theoretical calculations. Third-order nonlinear optical activity can be observed for both isotropic and anisotropic materials. From the above polarization equations, it can be seen that the symmetry requirement for second-order optical nonlinearity requires chromophores to exhibit either dipolar[23,24] or octupolar[25–27] symmetry. For materials to exhibit second-order optical nonlinearity, macroscopic dipolar or octupolar symmetry must exist; such symmetry is frequently introduced by electric field poling or by sequential synthesis/self assembly from a functionalized surface. Because of the additional symmetry requirement for second-order nonlinear optical materials, statistical mechanical calculations have proven useful in guiding the optimization of desired nano- and mesoscopic order.

In the following discussion, greater attention will be paid to second-order nonlinear optical organic materials than for third-order materials. The reason for this disproportionate focus relates to the fact that more commercial attention has been focused on second-order materials, whose design issues have therefore received more intense research scrutiny. For example, very little attention has been given to the optical loss and photostability of third-order nonlinear optical materials, whereas these properties have been extensive studied for a number of second-order materials.

7.2 Second-Order Nonlinear Optical Materials

The primary applications of second-order nonlinear optical organic materials include electro-optic modulation, second harmonic generation, optical rectification, and terahertz radiation generation and detection. With recent success in the development of visible wavelength lasers and light emitting diodes,

second harmonic generation has received less attention. Also, absorption at visible wavelengths of second harmonic light by organic materials is problematic and has inhibited the practical utilization of materials for this application. An excellent review of second harmonic generation, including an extensive discussion of the concept of phase-matching, has been given by Stegeman.[28] This review remains highly relevant.

The most common application of organic second-order nonlinear optical materials is electro-optic modulation. Electro-optic modulation involves the application of a low (relative to optical frequencies) frequency electrical field to a material. This low frequency field is often referred to as a radiofrequency field, although actual frequencies can range from DC to tens of terahertz. The applied field perturbs the π-electron distribution of the material, which in turn alters the velocity of light propagating in the material. Thus, electro-optic activity can be viewed as voltage control of the refraction index of a material. The primary focus of this chapter will be a review of organic electro-optic materials and devices.

An increasingly popular application of second-order nonlinear optical materials is terahertz generation and detection. This phenomenon is relevant to a variety of sensing applications, ranging from homeland security to medical imaging. Organic materials also have potential for promoting the development and increased utilization of terahertz spectroscopy. Terahertz generation is an example of optical rectification or "difference frequency" phenomena. Like second harmonic generation, terahertz generation involves the interaction of two optical fields with the charge density of the material.

7.2.1 Electro-Optic Materials

Organic electro-optic materials include single crystal materials such as 4′-dimethylamino-*N*-methyl-4-stibazolium tosylate (DAST),[13,29] chromophore/polymer composite materials,[30–33] polymeric materials containing covalently incorporated chromophores (including heavily crosslinked materials),[30,31,34–40] single-chromophore-containing dendrimers,[24,41–44] multichromophore-containing dendrimers,[44,45] chromophore-containing dendronized polymers,[44,46–51] doped chromophore materials (including binary chromophore systems),[52] and materials prepared by sequential synthesis/self-assembly of chromophores from a functionalized surface by Langmuir–Blodgett or modified Merrifield techniques.[13,53–57] The vast majority of systems studied involve dipolar chromophores; the reader is referred elsewhere for an introduction to octupolar materials.[25–27] In like manner, most devices are currently prepared by electric field poling of polymeric or dendritic materials. For materials prepared by electric field poling or by sequential synthesis/self-assembly, only two nonzero electro-optic tensor elements (r_{33} and r_{13}) exist. These are given approximately by:

$$r_{33} = 2Nf(0)\beta_{zzz} < \cos^3\theta > /(n_{0e})^4 \tag{7.3a}$$

$$r_{13} = Nf(0)\beta_{zzz} < \sin^2\theta \cos\theta > /(n_{0o})^2(n_{0e})2, \tag{7.3b}$$

where N is the chromophore number density (molecules/cm^3), $f(\omega)$ are local field factors that account for the dielectric nature of the media surrounding chromophores, n_{0o} and n_{0e} are the ordinary and extraordinary linear refractive indices, and the order parameters, $<\cos^3\theta>$ and $<\sin^2\theta\ \cos\theta>$, define the orientational distribution of chromophores. Equation 7.3 neglects the minor elements of the molecular first hyperpolarizability tensor.

7.2.1.1 Optimizing Electro-Optic Activity

The process of optimizing electro-optic activity is typically a two-step process, in which quantum mechanical calculations are used to guide the improvement of molecular first hyperpolarizability,β_{ijk}, values[14–24] and statistical mechanical calculations are employed to optimize the product of the chromophore number density and the order parameter.[58–64] Quantum mechanical calculations have

guided the development of a number of chromophores, leading to dramatic improvements in molecular first hyperpolarizability, i.e., to β_0 values on the order of or greater than 1000×10^{-30} esu. The tricyanovinylfuran (TCF) acceptor moiety shown in Scheme 7.1 has facilitated the development of workhorse chromophores appropriate for prototype device development.[65–72] In recent years, the synthesis of chromophores has been greatly aided by the utilization of microwave-assisted synthesis techniques.[73,74] Of course, for a chromophore to be carried forward for development of device-appropriate materials, it must exhibit appropriate thermal, chemical, and photochemical stability, acceptably low levels of absorption at anticipated device operational wavelengths, and appropriate processability (e.g., solubility in spin casting solvents, etc.). These features will be addressed later in this chapter; note that the comments that apply for electro-optic materials also apply to other second-order materials and, to some extent, to third-order materials.

The theoretically-inspired development of chromophores with improved molecular first hyperpolarizability can be divided into two categories: (1) variations of the fundamental donor, bridge, and acceptor blocks of modular dipolar chromophores; and (2) investigation of novel chromophore architectures such as "X-shaped"[18,19,75,76] and "twisted"[20,21] chromophores. The former strategy has proven to be very effective in the past and significant future improvement may be possible following this strategy. The latter strategy is much newer, but may afford dramatic improvements in molecular first hyperpolarizability, while permitting desirable auxiliary properties such as high transparency at operating wavelengths.

Molecular first hyperpolarizability (β) values are commonly measured by hyper-Rayleigh scattering (HRS).[77–79] Such measurements are complicated by two-photon fluorescence and by molecular aggregation. A variety of modifications have been made to he HRS technique in efforts to circumvent these problems, including the use of femtosecond pulse techniques, measurements at a number of wavelengths (using laser wavelength agility afforded by optical parametric devices), and measurements as a function of concentration with measured β values determined exploiting extrapolations to zero concentration.[77–79] Moreover, HRS measurements are normally carried out to determine relative (to a standard solvent such as chloroform) β values. Absolute values are most frequently defined using an

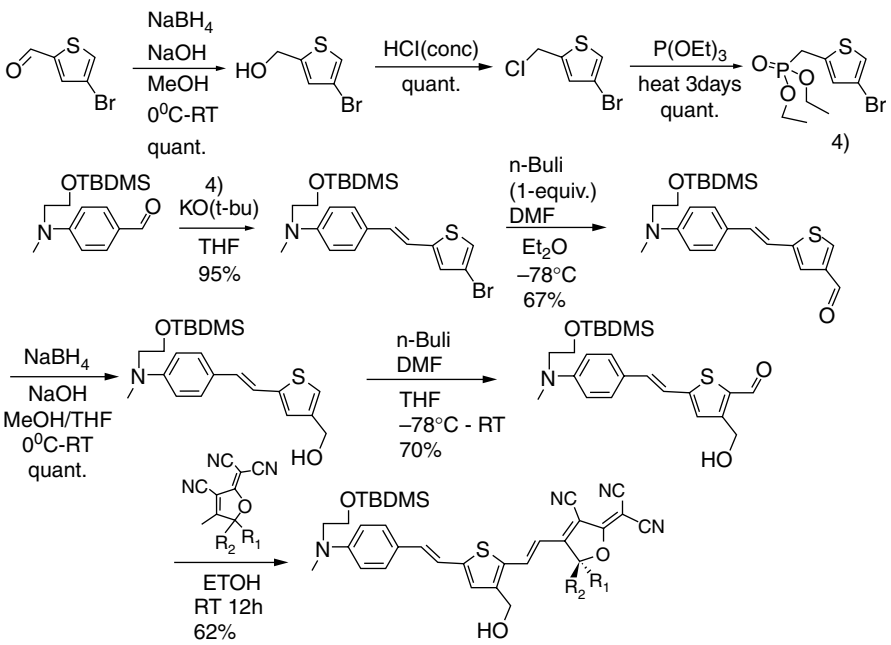

SCHEME 7.1 The synthesis of a chromophore containing the tricyanofuran (TCF) acceptor.

integrating sphere approach. A problem arises in the comparison of β values between theory and experiment. Theoretical β values are calculated for isolated particles in the long wavelength or zero frequency limit. On the other hand, experimental β values are measured in solutions of varying dielectric constants and at finite infrared wavelengths such as 1.9 μm. To avoid comparing data corresponding to different conditions, relative β values are frequently compared, e.g., both theoretical and experimental β values referenced to a standard such as paranitroaniline.[23]

The product of dipole moment, μ, and molecular first hyperpolarizability, β, is also a useful quantity, particularly as the slope of the curve of r_{33} versus N in the low concentration limit is given by $2f(0)[\mu\beta]E_p/5kTn^4$, where for the sake of simplicity the subscripts on β and n have been dropped. The product $\mu\beta$ can be measured by electric field induced second harmonic generation (EFISH) techniques. Like HRS measurements, many factors can complicate the measurements and great care must be exercised to obtain meaningful data. If molecular first hyperpolarizability values relevant to electro-optic response are to be extracted from EFISH data, then care must be exercised to avoid multiphoton resonance contributions. Again, like HRS measurements, EFISH measurements should ideally be made at a number of wavelengths.

The second aspect of optimizing electro-optic activity involves optimizing the product $N<\cos^3\theta>$. It is now well-appreciated that intermolecular electrostatic (e.g., dipole–dipole) interactions involving prolate ellipsoid-shaped π-electron chromophores can lead to serious attenuation of electro-optic activity.[58–64] The Monte Carlo calculations in Figure 7.1 illustrate this point. These calculations were carried out with the restriction that the chromophores maintain a uniform lattice distribution. Different results are obtained if a non-uniform chromophore distribution is permitted. This latter treatment

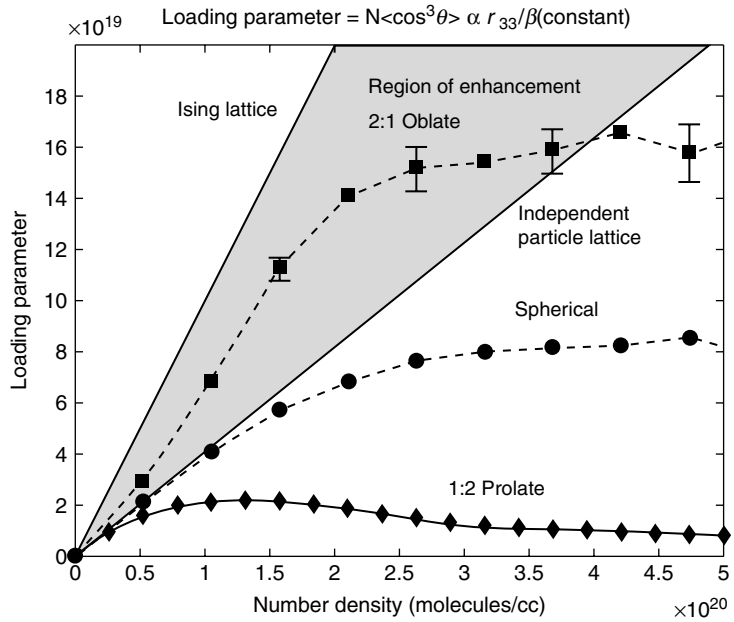

FIGURE 7.1 Calculation (employing pseudo-atomistic Monte Carlo methods) of $N<\cos^3\theta>$ vs. N for chromophore shapes ranging from prolate to oblate ellipsoidal. Calculations are based on an "on-lattice" approximation, which means that chromophores are restricted to uniform spacing among chromophores. Different results, particularly at high loading, are obtained for "off-lattice" calculations, in which chromophores are permitted to assume a non-uniform lattice distribution (e.g., to aggregate). For off-lattice calculations, results are much more sensitive to the details of chromophore structure. Pseudo-atomistic calculations mean that π-conjugated segments are treated in the united atom approximation whereas σ-bonded molecular fragments are treated fully atomistically.

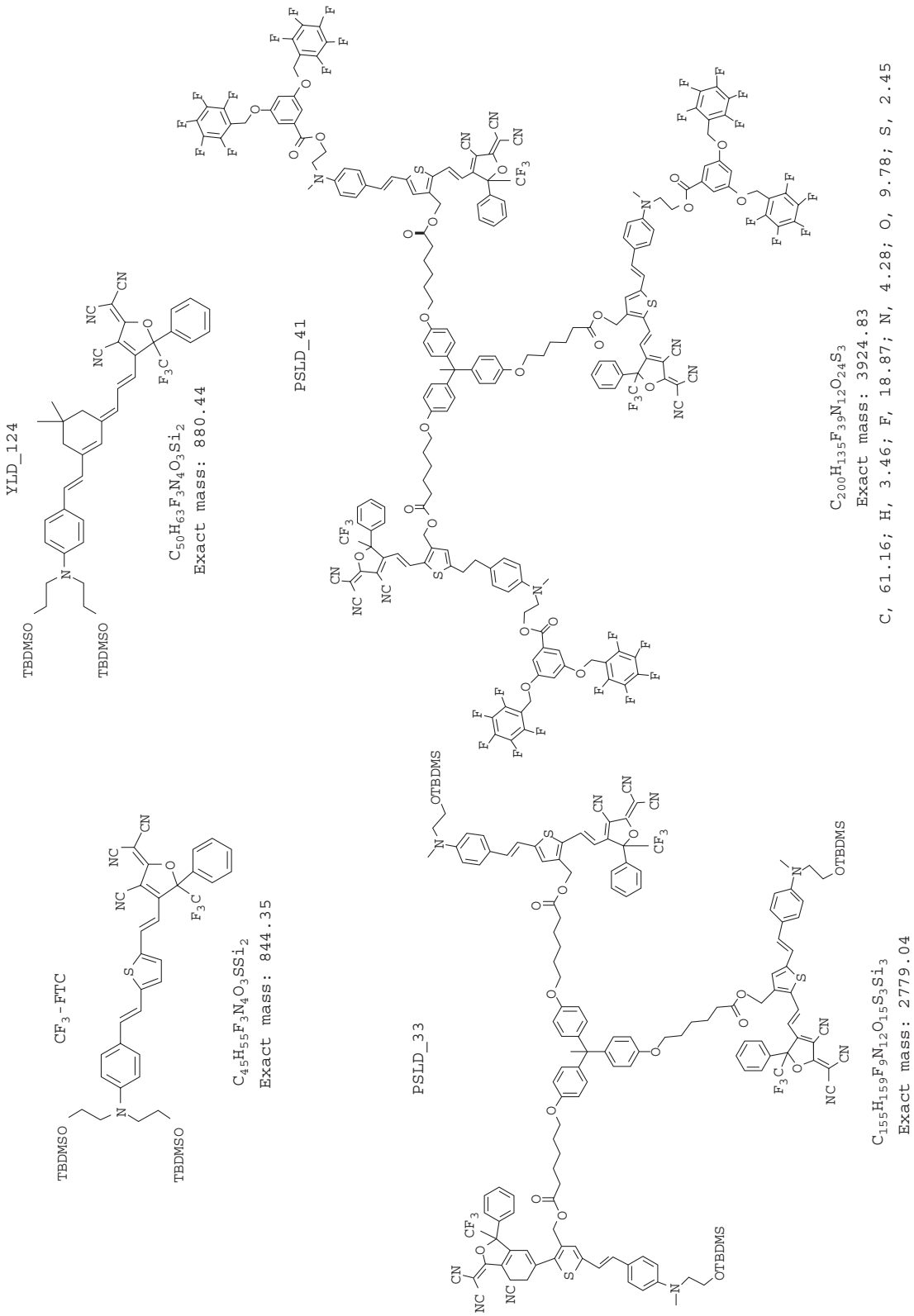

FIGURE 7.2 Four chromophore structures related to the data presented in Figure 7.3.

permits aggregation effects to be taken into account. The discussion of this latter treatment, which can be critical for considering very large number densities (high chromophore loading), is sufficiently complicated to be beyond the discussion presented here. In the present discussion, we restrict our consideration to the more simplistic case of a uniform chromophore distribution. As shown in this figure, intermolecular electrostatic interactions can also augment poling-induced noncentrosymmetric order. It has been suggested in at least two studies that chromophore-polymer interactions can also influence order.[80,81] Indeed, in addition to chromophore shape effects illustrated in Figure 7.1, the spatial and dynamical restrictions associated with covalent bonds impact poling-induced order. This is illustrated in studies of multichromophore-containing dendrimers (MCCD), as depicted in Figure 7.2 and Figure 7.3. In Figure 7.3, a significant enhancement in electro-optic activity is observed for a MCCD, relative to the behavior observed for the same chromophore in a polymer composite material. Indeed, behavior for the MCCD lies between that expected for a chromophore in a spherically-symmetric environment and the independent particle limit (see Figure 7.1). Even more intriguing behavior is observed when a second chromophore is doped into the MCCD. The electro-optic activity, as shown in Figure 7.3, increased nearly linearly with a slope more than twice the initial slope of the r_{33} versus N plot for the same chromophore in an amorphous polycarbonate (APC) polymer host.[32,33] A simplistic analysis suggests that such behavior may reflect intermolecular electrostatic interactions, acting to increase $N<\cos^3\theta>$ in a manner analogous to that seen in Figure 7.1. However, unlike the case for chromophore/polymer composite and undoped dendrimer materials, this behavior has not yet been quantitatively reproduced by theoretical calculations. Moreover, all necessary control experiments to rule out other potential contributions to the unusual behavior shown in Figure 7.3 have not yet been completed. Nevertheless, the realization of electro-optic activities greater than 300 pm/V for doped single-chromophore-containing dendrimers, MCCDs, and dendronized polymers is an important milestone and provides the potential (providing further improvement in molecular first hyperpolarizability is forthcoming) of realizing electro-optic activity on the order of 1000 pm/V. Of course, for large electro-optic activity to be meaningful, it must be accompanied by acceptable optical transparency,

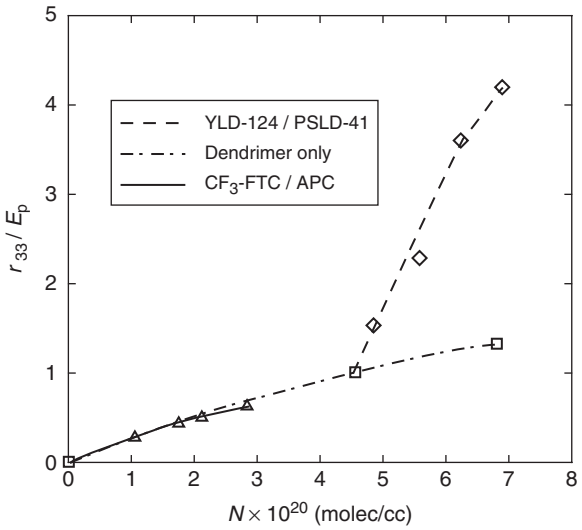

FIGURE 7.3 Data for the four chromophore structures of Figure 7.2. Since a linear dependence of electro-optic activity, r_{33}, on electric poling field strength is observed in all cases, r_{33}/E_p vs. N is plotted to facilitate comparison among data sets. Data for composite materials consisting of the chromophore CF3-FTC in amorphous polycarbonate (APC, Aldrich Chemicals) are indicated by triangles. Data for the two dendrimer materials PSLD 33 and 41 are indicated by squares. Data for samples of YLD 124 doped into PSLD 41 are indicated by diamonds.

thermal stability and photostability. We now turn attention to discussion of these issues, after a few comments about the measurement of electro-optic tensor components.

Electro-optic activity of thin film samples is most commonly measured by the following techniques: Teng-Man simple reflection[82–84] attenuated total reflection (ATR),[85–87] Fabry–Perot interferometry, FPI,[81,88,89] and two-slit interference.[90] Electro-optic activity can also be measured in a variety of waveguide (e.g., Mach Zehnder interferometry, MZI),[91–93] ring microresonator,[66,72] and etalon devices. Each technique has its particular advantages and limitations, and in general it is desirable to obtain electro-optic tensor components from multiple measurements using different techniques. It can also be important to define the dispersion of tensor components. A variety of techniques, such as ATR, FPI, and MZI devices permit both r_{33} and r_{13} to be determined. Such complete tensor determination permits a more definitive characterization of chromophore orientational order. These various characterization techniques can also be adapted by the introduction of temperature control and DC voltage application stages to provide in situ monitoring of the introduction of noncentrosymmetric order by electric field poling and the subsequent relaxation of that order.[45]

7.2.1.2 Minimizing Optical Loss

This discussion will first focus on "material" loss. Throughout the 1990s, most of the chromophores being investigated had a charge transfer absorption maxima, λ_{max}, of less than 600 nm. For such materials, optical absorption loss at 1.3 and 1.55 micron telecommunication operating wavelengths was most frequently dominated by hydrogen vibrational overtone absorptions. For dendrimer materials, optical loss values as low as 0.2 dB/cm have been observed.[94] When optical loss of greater than 2 dB/cm was observed, it was normally indicative of light scattering arising from material heterogeneity associated with various processing conditions.[35] More recently, chromophores with interband absorption maxima approaching 800 nm have come into use. For these materials, and even for some earlier materials,[32,33] absorption loss at telecommunication wavelengths is dominated by electronic charge transfer absorption. Thus, increasing $\chi^{(2)}$ may not lead to an improvement in FOM, because it is accompanied by a corresponding increase in α. The appearance of exciton bands may even lead to a decrease in FOM. In designing new chromophores for improved optical nonlinearity, it is critical to consider optical loss.

Optical loss due to electronic absorptions (both interband charge transfer and excitonic absorptions associated with aggregation) is strongly influenced by solvatochromic and line broadening effects, particularly as these effects influence the long wavelength tails of absorptions. Line broadening is frequently defined by the heterogeneity of the chromophore environment and thus can be influenced by chromophore order and by the mode of attachment of the chromophore to its surrounding matrix. The dielectric properties of the surrounding matrix will, of course, have a profound effect on solvatochromic shifts. Researchers at Lockheed Martin[32,33] appear to be the first to focus on an effort to control absorption contributions to optical loss by a systematic consideration of the roles played by the structure of the chromophore and of the surrounding matrix.

Quite different effects on absorption loss can be observed for different types of materials at telecommunication wavelengths. In this regard, dendritic materials may afford significant advantages relative to chromophore/polymer composite materials due to the fact that they permit control of the local chromophore environment and chromophore solubility in the surrounding matrix. For example, chromophores incorporated in fluorinated dendrimers typically exhibit blue (hypsochromic) shifted absorption maxima relative to the same chromophore in a polymer such as amorphous polycarbonate (APC, Aldrich Chemical). Moreover, the "solubility" of the chromophore in dendrimers is controlled by covalent bond attachment. Of course, comments made regarding dendrimers can also apply to chromophores covalently incorporated into polymers, provided that access of chromophores to each other is inhibited by the covalent incorporation. A high concentration of chromophores does not necessarily imply disastrous optical loss, as illustrated in Figure 7.4, which shows the same chromophore in a covalent-bonding-defined chromophore "bundle" and in APC.[95] The absorption maximum of the chromophore in the bundle is shifted to higher energy and no detectable line broadening is observed. The molecular hyperpolarizability of the chromophore bundle is nearly three times that of the isolated

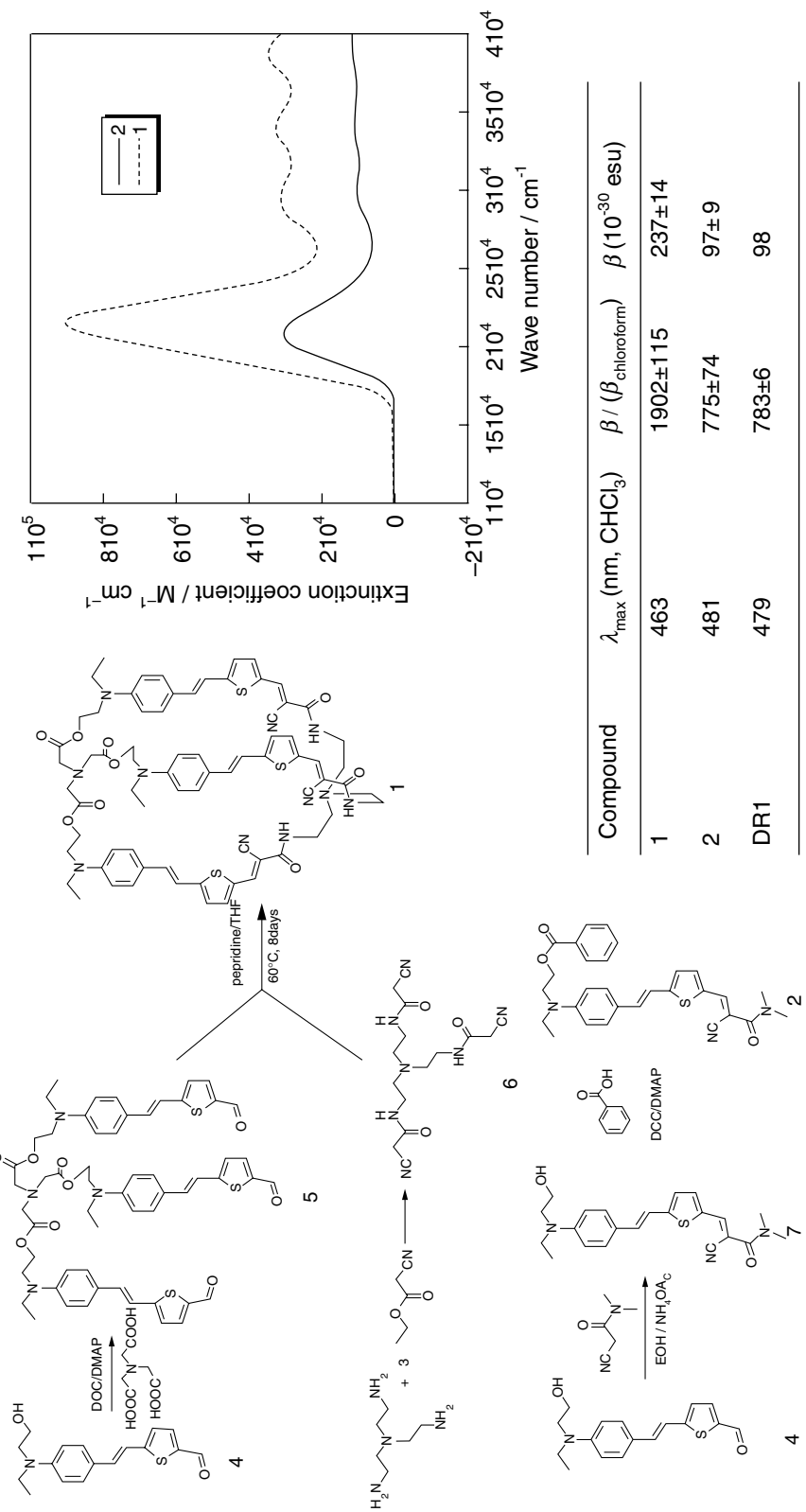

Compound	λ_{max} (nm, $CHCl_3$)	β / ($\beta_{chloroform}$)	β (10^{-30} esu)
1	463	1902±115	237±14
2	481	775±74	97± 9
DR1	479	783±6	98

FIGURE 7.4 The comparison of optical spectra and molecular hyperpolarizability for the same chromophore in APC and in a three-chromophore bundle (right hand side of figure). On the left hand side of the figure, the syntheses of the three-chromophore bundle and the analogous single chromophore are shown.

chromophore. The experimental results shown here are in good agreement with theoretical calculations carried out for the respective structures. Care should be exercised with respect to extrapolating the results of Figure 7.4 to other materials; in general, the exact optical behavior will be determined by the precise translational and orientational positioning of chromophores, which will vary from structure to structure.

Optical loss is also influenced by scattering losses. These frequently arise from material heterogeneities introduced by spin casting, electric-field poling, crosslinking (lattice hardening), and by various device processing steps (e.g., reactive ion etching of waveguides and deposition of cladding layers). The problem is typically worse (ignoring for the moment issues associated with crosslinking or lattice hardening) for chromophore/polymer composites than for chromophores covalently incorporated into dendrimers or polymers. Again, the major issue is control of chromophore "solubility." For chromophore/polymer composites, problems include: the differential solubility of the chromophore and polymer host in spin casting solvents; sublimation of chromophores during baking (to drive off residual spin casting solvents); sublimation of chromophores during electric field poling; and "electrophoretic" phase separation during poling. "Covalent-tailoring" of chromophores and their incorporation into host materials is a very attractive means of controlling chromophore solubility and packing (void volumes) in the final material. As we shall see shortly, crosslinking (or lattice hardening) is typically necessary to achieve adequate thermal stability. Some crosslinking chemistries can lead to phase separation and lattice strain and thus dramatic increases in optical loss due to light scattering. New cycloaddition crosslinking chemistries involving the "soft" free-radical chemistry of the fluorovinyl ether group or the Diels-Alder/retro-Diels-Alder reaction lead not only to lattice hardening without attenuation of poling efficiency, but also to materials with low optical loss.

Optical loss can also arise from the process of fabricating buried channel waveguides. When this is done by techniques such as reactive ion etching, care must be exercise to avoid pitting (waveguide wall roughness) due to reactive ions with excess kinetic energy (i.e., a physical rather than chemical etch). When care is employed, the excess waveguide loss can be 0.01 dB/cm or less.[96] Loss can also be introduced in deposition of cladding layers if the solvent used to deposit the cladding layer attacks the electro-optic material. For both reactive ion etching and deposition of cladding layers, the lowest loss is typically observed when very hard electro-optic materials are used. Loss can also arise from material damage (dielectric breakdown) during electric field poling.

Optical loss can be influenced by the structure of the device, e.g., bending loss for ring microresonators. Of course, one of the greatest contributions to total device insertion loss is coupling loss. With organic electro-optic materials, the dominant contribution to coupling loss arises from a mismatch in mode size and shape between light propagating in silica transmission fibers and that in the organic EO waveguides. The solution to this problem is typically to employ a "mode transformer" structure.[97–101] Mode transformers permit per facet coupling losses to be kept to a few tenths of a dB. The overall objective is typically to achieve a total insertion loss of less than 5 dB (the current standard for lithium niobate devices). Thus, if device lengths of 2 cm or less are to be used, then material loss must be kept to less than 2 dB/cm. Short device lengths, of course, have the advantage of permitting greater operational bandwidths by minimizing loss occurring in metal drive electrodes. The calculated performance of a Mach Zehnder device for typical EO, cladding, and electrode material conditions is shown in Figure 7.5.

7.2.1.3 Maximizing Thermal Stability

The stability of electro-optic activity following the cessation of electric field poling is critical for device applications. In the simplest sense, thermal stability relates to the temperature difference between the operating temperature and the material glass transition temperature, T_g. With composite materials, incorporation of chromophores results in plasticization and a corresponding reduction of glass transition temperature with increasing dopant (chromophore) concentration. Thus, to realize sufficient thermal stability to satisfy Telcordia standards, it is necessary to use a host polymer material with an initial glass transition temperature on the order of 150°C or greater. Polycarbonates, polyquinolines, and polyimides have been the most commonly employed polymers for producing composite materials appropriate for

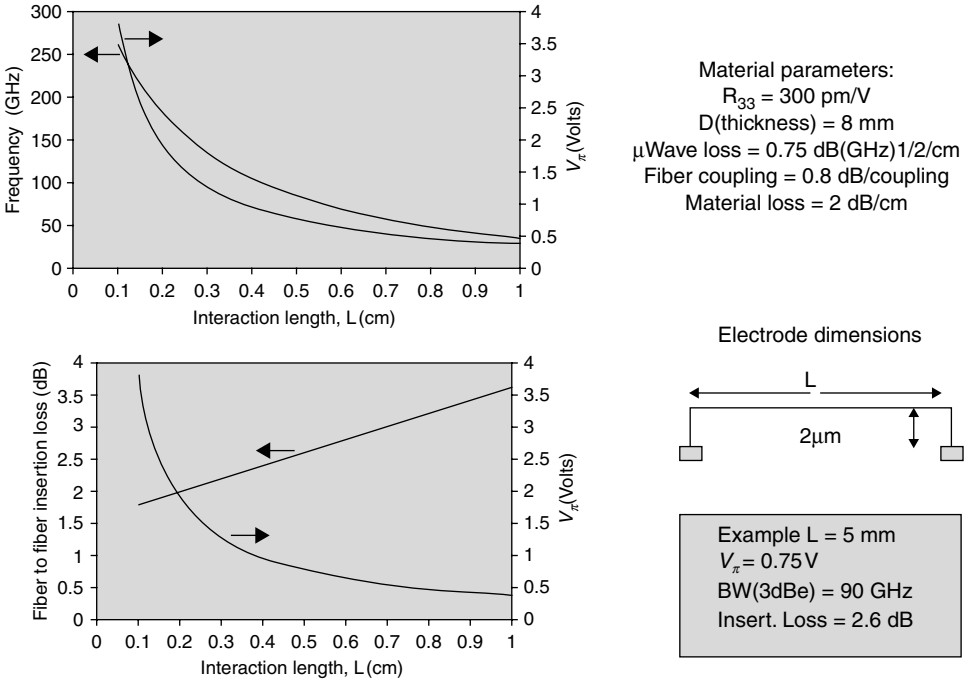

FIGURE 7.5 The variation of critical Mach Zehnder device parameters (bandwidth, drive voltage, fiber-to-fiber insertion loss) with device (electrical/optical field interaction) length. An example of performance for a 5-mm length Mach Zehnder electro-optic modulator expected with current materials is also shown.

prototype device fabrication. One of the problems with very high-glass-transition-temperature composite materials, such as polyimides, is that very high poling temperatures are required. Such temperatures promote chromophore sublimation and the decomposition of chromophores, and can also be incompatible with processing methodologies such as nanoimprint lithography. High glass transition materials also commonly exhibit poor solubility in solvents used for spin casting. A convenient means of avoiding this requirement for high temperature processing at intermediate stages of electro-optic material production is to achieve thermal stability by crosslinking (lattice hardening) in the final stages of electro-optic material production. With crosslinking, thermal stability will be defined by the density of crosslinks and the flexibility of intervening segments. Throughout the 1990s, crosslinking chemistries used to elevate final material glass transitions temperatures frequently involved condensation (e.g., urethane and sol gel) chemistry.[34,35] Such reactions give off water as an elimination product and are influenced by atmospheric moisture. Moreover, the expulsion of gaseous elimination products can result in lattice disruption and increased light scattering. As the condensation reaction proceeds, increased lattice strain (e.g., lattice contraction) can also be a problem, which can be serious with sol-gel glasses. Both thermal and photo-induced crosslinking chemistries have been explored.[30,31] The latter has been plagued by competition for light absorption involving the photo-initiator and the EO chromophore. More recently, cycloaddition chemistries[36–38,44,46–52,102] have become popular for realizing high glass transition temperature (e.g., to 200°C) materials without the attenuation of electro-optic activity or an increase in optical loss associated with earlier crosslinking reactions. These chemistries are pictorially illustrated in Figure 7.6. The fluorovinyl ether crosslinking reaction illustrated in Figure 7.6a is a soft free radical reaction that has the advantage of yielding high glass transition materials that are also characterized by very low optical loss at telecommunication wavelengths due to low hydrogen content in the final material. The Diels-Alder/retro-Diels-Alder reaction of Figure 7.6b has the added advantage

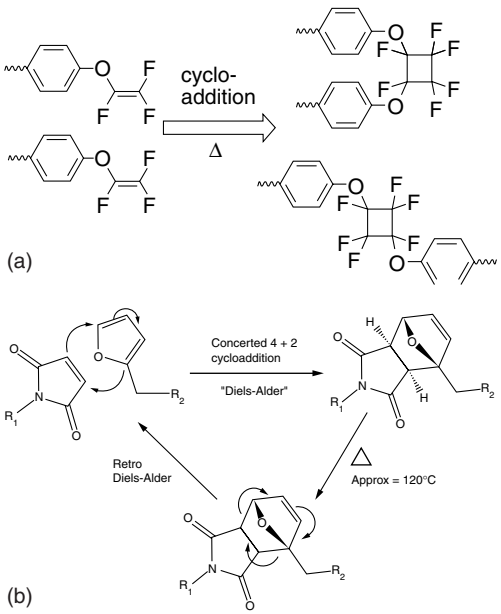

FIGURE 7.6 Fluorovinyl ether (6a) and Diels-Alder/-retro-Diels-Alder (6b) cycloaddition crosslinking reactions.

(in some cases) of reversibility. That is, the material is crosslinked below the glass transition temperature but becomes uncrosslinked at the T_g, permitting poling to be effected without being attenuated by crosslinks. Choice of diene and dienophile can permit systematic tuning of the glass transition temperature, including for the purpose of matching the poling temperature to the thermal initiation temperature of the fluorovinyl ether crosslinking reaction (when both types of cycloaddition crosslinking are used together). Obviously, for irreversible crosslinking reactions such as reaction of the fluorovinyl ether moiety, it is important to match poling temperatures to the thermal initiation temperature of the crosslinking reaction so that effective crosslinking is achieved without unwanted attenuation of poling-induced order. A final material glass transition temperature on the order of 200°C is more than adequate for satisfying Telcordia standards for thermal stability (long-term stability at an operating temperature of 85°C). Cycloaddition crosslinking has been demonstrated to be effective in providing such stability.

7.2.1.4 Maximizing Photostability

Photostability has been shown to be largely a matter of avoiding singlet oxygen chemistry.[103–108] Stegeman and coworkers[103–106] have demonstrated most of the critical features of photodecomposition of organic electro-optic materials, including the absence of contributions from multiphoton absorption. Indeed, they defined a single photostability figure-of-merit, B/σ, where B^{-1} is the probability of photodecay from the LUMO (lowest unoccupied molecular orbital) charge transfer state and σ is the interband (charge transfer) absorption coefficient. This definition has been used by subsequent researchers, although the data analysis of Stegeman and coworkers may have been somewhat overly simplistic, consequently over-estimating photo-instability. For example, more detailed analyses demonstrate that the decay data cannot be fit with a single exponential and that "observer" power in the Stegeman pump–probe experiment may lead to artificially fast decay. Moreover, Stegeman and coworkers failed to carry out measurements at telecommunication wavelengths; this was addressed in subsequent work by researchers at Corning.[107,108] The Corning group demonstrated that the photostability FOM for a given chromophore structure could vary over four orders of magnitude depending on conditions that influence singlet oxygen chemistry. Even larger variation has been observed by other groups and photostability has been shown to improve with the use of small quantities of singlet oxygen quenchers. In addition to pump-probe experiments carried out by Stegeman and coworkers, researchers at Corning, Gunter and coworkers, and Dalton and coworkers, photostability has also been investigated in operating Mach Zehnder devices by Steier and coworkers[69] and by Ashley and coworkers.[109] Again, in these studies, photo-instability could be attributed to singlet oxygen chemistry, with good photostability being observed for materials and devices where this chemistry was partially inhibited.

In summary, it appears that good photostability can be achieved with appropriate materials modification or with appropriate packaging of devices to minimize the presence of oxygen. In this latter regard, the problems faced with organic electro-optic materials are analogous (but not quite so severe) as those faced with organic light emitting device (OLED) materials. It should be noted

that dense crystals such as DAST exhibit excellent photostability, again consistent with the role played by oxygen.

7.2.1.5 Radiation Hardness

Very little work has been carried out examining the performance of organic electro-optic materials and devices in the presence of high-energy gamma rays and protons associated with space environments. Part of the problem of evaluating the impact of high-energy radiation on device performance is isolating changes attributable to organic electro-optic materials from changes of performance induced by events unrelated to the organic electro-optic materials (e.g., damage to silica input fibers). Nevertheless, the one published report[110] on this subject appears promising with respect to good stability exhibited by organic electro-optic materials.

7.2.1.6 Fabrication of Prototype Devices

The most common prototype device fabrication involves stripline Mach Zehnder modulators; however, ring microresonator, cascaded prism, and etalon structures have also been produced and evaluated. A critical issue with the fabrication of prototype devices is how to deal with the properties of cladding and electrode materials. Devices are typically multilayer structures consisting of bottom (ground) electrode/bottom cladding/electro-optic waveguide/top cladding/top (drive) electrode. If materials are poled through cladding layers, the poling field can be attenuated due to the resistivity of the cladding layers. A potential solution to this problem would be to identify cladding materials with significant conductivity. Unfortunately, cladding materials with prerequisite conductivity have also exhibited, to the present time, unacceptably high levels of optical loss. The presence of cladding layers thus makes it difficult to realize the same electro-optic activity in device structures that have been achieved in thin films. Another issue in the fabrication of prototype devices is the impact of electrode materials and device structure on performance, including operational bandwidth. For stripline devices, such as Mach Zehnder interferometers, resistive losses in metal electrodes typically define operational bandwidths. Shorter electrode structures (see Figure 7.5) lead to higher bandwidths, but at a price of increased drive voltage (V_π, the voltage required to produce a π phase shift). As already noted, shorter devices afford the advantage of reduced insertion loss and are more appropriate for high-density integration of many modulators on a single chip. For resonated devices, such as ring microresonators and etalon devices, bandwidth is limited by the optical lifetime in the resonated structure. This is defined by the quality factor, Q, of the resonant device. High quality factors have the advantage of affording reduced drive voltage operation but limit the bandwidth of the device. Very high center operational frequencies can still be obtained, but the bandwidth about the center frequency is limited by the Q. Ring microresonators have the added advantage of reduced size, which can facilitate high-density integration. In discussing bandwidth, one needs to distinguish between digital and analog signals. This point will be illustrated in the following simplified discussion of bandwidth and drive voltage requirement for resonant device structures.

For a resonator, the 3-dB electrical modulation bandwidth (the detected voltage is down by 3 dB) is given by

$$\Delta f_{3\mathrm{dBe}} = c / \lambda Q = \Delta f_{\mathrm{FWHM}}, \tag{7.4}$$

where c is the speed of light, λ is the wavelength of light, Δf_{FWHM} and is the full-width at half-maximum of the bandpass of the resonant device. The case of digital modulation is considered first.

For a 10-dB contrast in the digital pulses, the voltage induced frequency shift of the bandpass must be

$$\Delta f = 3\Delta_{\mathrm{FWHM}} / 2. \tag{7.5}$$

The frequency shift with voltage is

$$(\Delta f / V) = (n_{\text{eff}})^2 r_{33} c / (2d\lambda), \tag{7.6}$$

where d is the electrode spacing. Combining,

$$V_{10\text{dB}} = (3d\lambda\Delta f_{3\text{dBe}}) / [(n_{\text{eff}})^2 r_{33} c]. \tag{7.7}$$

In digital systems, the required bandwidth depends on the modulation format. Conservatively assuming that $\Delta f_{3\text{dBe}} = B$ (the bit rate), then

$$V_{10\text{dB}} = 3d\lambda B / [(n_{\text{eff}})^2 r_{33} c]. \tag{7.8}$$

For example, if $B = 10$ Gb/s, $n = 1.6$, $r_{33} = 300$ pm/V, $d = 6$ μm, $\lambda = 1.3$ μm, and $Q = 5 \times 10^3$, then $V_{10\text{dB}} = 1$ V (with the result obviously scaling linearly with the bit rate).

Now consider analog signal modulation. The optical wavelength is set to the point of maximum slope of the resonator transmission (bandpass) curve:

$$\Delta\lambda = \Delta\lambda_{\text{FWHM}} / (2\sqrt{3}) \tag{7.9}$$

It is helpful to define a $V\pi_{\text{equiv}}$ so that it corresponds to an equal $V\pi$ of a Mach Zehnder modulator:

$$(V_{\pi\,\text{equiv}} / \Delta f_{3\text{dBe}}) = 4\pi d\lambda / [(3\sqrt{3})(n_{\text{eff}})^2 r_{33} c]. \tag{7.10}$$

For example, if $n = 1.6$, $r_{33} = 300$ pm/V, $d = 6$ πm, and $\lambda = 1.3$ πm, then $(V\pi_{\text{equiv}}/\Delta f_{3\text{dBe}}) = 0.08$ V/GHz. It is clear from the above analyses for digital and analog signal processing that the simplest route to improving the performance of resonant devices is to increase the electro-optic coefficient, r, of the material used to fabricate the device. The current performance of organic electro-optic materials moves resonant devices close to practical application.

Device structures are most commonly fabricated using reactive ion etching, although ring microresonator and Mach Zehnder devices structures have also been made by nanoimprint lithography.[68] Nanoimprint lithography has the potential advantage of allowing complex electro-optic circuitry to be mass-produced in a cost-effective manner.

The range of application of organic electro-optic materials has been recently broadened by the incorporation of these materials into silicon photonic device structures.[66] The small dimensions of these structures and the obvious potential for convenient integration with silicon electronics is very attractive. Moreover, the small (nanoscopic) dimensions of silicon photonic circuitry result in an optical field concentration, which has recently been exploited to achieve optical rectification of light at mW optical powers.[66] Thus, the same device structure can be employed for electrical/optical and optical/electrical signal transduction.

7.2.1.7 Applications

Applications of electro-optic materials and devices include electrical-to-optical signal transduction, optical switching, optical beam steering, radiofrequency signal generation, phased array radar (radiofrequency beam steering), optical gyroscopes, analog-digital conversion, frequency conversion (time stretching), and sensing (of both physical and chemical phenomena). The term *radiofrequency* describes frequencies in the range 0–30 THz. Electro-optic technology is at the heart of "RF Photonics," or the delivery of radiofrequency signals via optical transmission. Many applications of electro-optic materials lie in the arena of defense and homeland security, but interest is growing in the areas of computer chip manufacture, transportation, telecommunications (both fiber and wireless), civil engineering, and

medicine. For example, in the development of next-generation computer chips, photonics may be used to route high frequency information among various components of the chip, avoiding the problems of signal loss and heating associated with moving electrons through metal connectors. The field of embedded network sensing combines sensors, computer processors, and communication components on a single chip. Electro-optic devices provide critical signal transduction and routing on embedded network sensing platforms. Embedded network sensing is finding increasing applications in medicine and infrastructure monitoring (civil engineering).

7.2.2 Optical Rectification Including Terahertz Radiation and Detection

Optical rectification is the difference frequency analog of second harmonic generation. Like second harmonic generation, it will occur whenever the electric field component of the optical field is large enough to produce a nonlinear perturbation of the charge distribution of the nonlinear optical material. Normally, intense laser powers are required, but the nanoscopic dimensions of silicon photonic circuitry can concentrate optical fields from milliwatt diode lasers to the point of producing optical rectification.[66] Thus, organic EO/silicon hybrid devices can act as both electrical-to-optical signal transducers and optical-to-electrical signal transducers. In other words, they have the potential to compete with photodiodes as photodetectors, providing that sufficiently large material second-order optical nonlinearity can be obtained.

Another manifestation of optical rectification/difference frequency generation is terahertz signal generation/detection. Recently, Hayden and coworkers,[111,112] Gunter and coworkers,[113] and researchers in Japan[114–116] have pioneered the use of organic electro-optic materials for terahertz applications (imaging and spectroscopy). An advantage of organic materials is that optical and terahertz waves propagate with comparable velocities in organic materials, permitting phase matching of the optical and terahertz radiation. Also, the second-order optical nonlinearity of organic materials is orders of magnitude greater than inorganic crystalline materials such as zinc telluride (ZnTe). A problem encountered with poled organic (polymer) materials is that it is difficult to effectively pole thick (millimeter) films. Such film thickness would be ideal for terahertz applications.

Among the promising sensor applications of terahertz radiation is the ability to image plastic weapons. It is an attractive alternative to magnetic (metal detector) sensing in the arena of homeland security. The possible applications in biomedical imaging are also attractive.

7.3 Third-Order Nonlinear Optical Materials

Third-order organic nonlinear optical materials have very little in common with second-order nonlinear optical materials, other than the fact that both involve significant π-conjugation. Since no symmetry requirement exists for third-order activity, a much broader range of materials can give rise to third-order optical nonlinearity, $\chi^{(3)}$. Indeed, third-order materials range from conjugated polymers such as polyacetylene, to molecules such as C_{60} and C_{70}, to metallomacrocyclic complexes. When charge transfer molecules are investigated, molecules with quadrupolar[117] symmetry (e.g., donor–acceptor–donor or acceptor–donor–acceptor) frequently exhibit larger optical nonlinearity than corresponding dipolar (donor–acceptor) molecules. Dendritic materials containing connected π-electron segments have also been observed to give rise to large third-order optical nonlinearities.

Although the third-order optical nonlinearity for organic materials has been increased over the past two decades, values are still too low for practical applications. A possible exception may be for materials incorporated into silicon photonic circuitry. Scherer and coworkers[120] have demonstrated all-optical modulation to greater than 5 THz with mW pump powers derived from a diode laser operating at telecommunication wavelengths. The concentration of optical power in waveguides of nanometer

dimensions results in an amplification of optical field intensities by orders of magnitude, permitting much smaller $\chi^{(3)}$ values to be utilized effectively.

Recently, interest in $\chi^{(3)}$ materials has increased because of potential applications of materials with large two-photon absorption coefficients. These applications range from sensor protection to biomedical imaging, photodynamic therapy, and two-photon photolithography.

Because no symmetry requirement exists for nonzero third-order optical nonlinearity, lattice hardness is a less serious problem than for second-order materials, although little research has been conducted on this feature of third-order materials. Optical loss is as important for third-order materials as it is for second-order materials, but very little research attention has been paid to this topic. Third-order materials should afford comparable advantages in processability compared to second-order organic nonlinear optical materials; however, it is unlikely that auxiliary properties will receive much attention unless significant improvement in $\chi^{(3)}$ can be achieved.

7.4 Summary

Extensive π-conjugation of organic materials leads to significant second- and third-order optical nonlinearities. However, until the present decade, values of $\chi^{(2)}$ and $\chi^{(3)}$ have been too small to promote significant commercial application. Currently, electro-optic coefficients in the range 300–400 pm/V are observed for a variety of dendrimer and dendronized polymer materials containing chromophores with large first hyperopolarizabilities. Such values are an order of magnitude greater than values for the commercial standard lithium niobate. New organic electro-optic materials afford the possibility of more compact and lightweight devices operating with bandwidths of 100 GHz or greater and with drive voltages of less than one volt. Realization of gain in RF photonics becomes a possibility for the first time. Many issues remain to be addressed before significant commercialization is likely, including the systematic control of optical loss, thermal stability, and photochemical stability. Moreover, better utilization needs to be made of the processing advantages of organic electro-optic materials, including for the production of integrated electronic/photonic circuitry exploiting a high density of organic electro-optic devices on a single chip. The integration of organic electro-optic materials with silicon photonic circuitry appears to afford some impressive new opportunities not only for high bandwidth electro-optic modulation and optical switching but also for optical rectification. One distinct advantage of organic electro-optic materials is that their processability may permit new device structures and applications to be considered. For example, new sensor technologies appear possible, e.g., by exploiting ring microresonators positioned on side-polished optical fibers.

The prognosis for third-order organic nonlinear optical materials is somewhat less optimistic, as $\chi^{(3)}$ values still need to be increased by one to two orders of magnitude for many applications. Incorporating third-order organic nonlinear optical materials into resonant structures (e.g., ring microresonators) and into silicon photonic waveguides may help reduce the performance demands on $\chi^{(3)}$ materials. At any rate, the development of third-order organic nonlinear optical materials is in a more immature stage than the development of second-order materials, as very little attention is given to auxiliary properties such as optical loss, stability, and processability. The most promising application of third-order organic materials appears to involve materials with large two-photon cross-sections for applications such as biomedical imaging, photodynamic therapy, two-photon photolithography, and ultrafast-responding sensor protection (Table 7.1 through Table 7.3).

Acknowledgments

Support from the National Science Foundation, the Air Force Office of Scientific Research, and the Defense Advanced Research Projects Agency is gratefully acknowledged. The authors thank their colleagues, particularly Professors William Steier and Bruce Robinson, for many helpful discussions.

TABLE 7.1 Experimental Results of Molecular studies. λ_{max}, Absorption Peak Wavelength of Lowest Energy Strong Trainsition; μ, Dipole Moment; β_μ (λ), EFISH Determined First Hyperpolarizability at a Fundamental Wavelength Given in Microns; β_0, as Defined in Section 6.4; S Indicates Solvatochromic Result; HR Indicates Hyper-Rayleigh Scattering Results

Structure	Solvent	λ_{max}(nm)	μ (10^{-18} esu)	$\beta_\mu(\lambda)^{ref.}$ (10^{-30} esu)
Unconjugated derivatives				
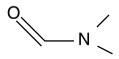	Chloroform	<240	3.5	0.5(1.9)[156]
		<200	4.6	2.3 (1.06)[37]
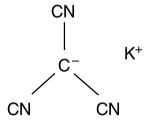	H_2O			7 (1.06HR)[265]
Benzene derivatives				
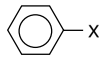				
X=CH_3	Neat		0.34	0.18 (1.06)[141]
	Neat	260	0.38	<0.2 (1.9)[46]
X=OH	Neat			0.17 (1.06)[193]
	Neat		1.5	0.17 (1.06)[191]
	p-Dioxane	270	1.5	<0.2 (1.9)[46]
X=SH	Neat		1.4	<0.2 (1.9)[46]
X=OCH_3	Neat	275	1.4	<0.2 (1.9)[46]
X=SCH_3	Neat		1.3	<0.2 (1.9)[46]
X=NH_2	Neat		1.5	0.89 (1.06)[141]
	Neat			1.2 (1.06)[193]
	Neat		1.5	1.1 (1.06)[190]
	Neat		1.5	1.2 (1.06)[191]
	Neat	284	1.5	0.55 (1.9)[46]

(continued)

15018—Chapter7—26/8/2006—22:06—SJAPPIYAR—15018—XML MODEL CRC12a – pp. 1–126.

TABLE 7.1 (Continued)

Structure	Solvent	λ_{max}(nm)	μ (10^{-18} esu)	$\beta_\mu(\lambda)^{ref.}$ (10^{-30} esu)
X=N(CH$_3$)$_2$	Neat			1.8 (1.06)[193]
	Neat		1.8	1.3 (1.06)[191]
	Neat	293	1.6	1.1 (1.9)[46]
X=F	Neat		1.5	0.44 (1.06)[141]
	Neat			0.53 (1.06)[193]
	Neat		1.6	0.70 (1.06)[191]
	Neat	266	0.63	<0.2 (1.9)[46]
X=Cl	Neat		1.5	0.28 (1.06)[141]
	Neat			0.22 (1.06)[193]
	Neat		1.7	0.33 (1.06)[191]
	Neat	272	0.44	<0.2 (1.9)[46]
X=Br	Neat		1.4	0.04 (1.06)[141]
	Neat			0.02 (1.9)[193]
	Neat		1.7	0.2 (1.06)[191]
	Neat	274	0.81	<0.2 (1.9)[46]
X=I	Neat		1.1	0.28 (1.06)[141]
	Neat			0.7 (1.06)[193]
	Neat		1.7	0.46 (1.06)[191]
	Neat	304	0.96	<0.2 (1.9)[46]
X=SO$_2$CH$_3$	*p*-Dioxane		1.1	<0.2 (1.9)[46]
X=SO$_2$F	Neat		1.7	0.3 (1.9)[46]
X=CN	Neat			0.51 (1.06)[193]
	Neat		4.1	0.48 (1.06)[191]
	Neat	230	3.9	0.36 (1.9)[46]
X=COH	Neat	320	2.8	0.8 (1.9)[46]
X=COCF$_3$	*p*-Dioxane	300	3.3	1.3 (1.9)[46]
X=NO	*p*-Dioxane	340/745	3.1	1.7 (1.9)[46]
X=NO$_2$	Neat			2.0 (1.06)[145]
	Neat			2.3 (1.06)[193]
	Neat		4.0	2.2 (1.06)[190]
	Neat		4.0	2.3 (1.06)[191]
	Hexane		4.2	1.1 (1.06)[232]
	Neat	268	4.0	1.9 (1.9)[46]
X=C$_2$H (CN)$_2$	*p*-Dioxane	303	4.8	3.1 (1.9)[46]

15018—Chapter7—26/8/2006—22:07—SJAPPIYAR—15018—XML MODEL CRC12a – pp. 1–126.

X	Y						
		p-Dioxane	310	1.6		1.3 (1.9)[46]	
$X=SO_2CH_3$	Y=OH	*p*-Dioxane	290	3.4		1.3 (1.9)[46]	
$X=SO_2CH_3$	$Y=N(CH_3)_2$	Chloroform		$\mu\beta=26\times10^{-48}$		$(1.9)^{264}$	
X=CN	$Y=CH_3$	DMSO	232	4.4		2.9 (1.9)[56]	
		Neat		4.4		0.7 (1.9) [46]	
X=CN	Y=Cl	*p*-Dioxane		2.3		0.8 (1.9)[46]	
X=CN	Y=Br	*p*-Dioxane		2.4		1.1 (1.9)[46]	
		p-Dioxane	240	2.5		2.2 (1.59)[87]	
X=CN	$Y=OC_6H_5$	*p*-Dioxane		4.1		1.2 (1.9)[46]	
X=CN	$Y=OCH_3$	DMSO	247	4.8		4.8 (1.9)[56]	
		p-Dioxane	248	4.8		1.9 (1.9)[46]	
X=CN	$Y=SCH_3$	*p*-Dioxane		4.4		2.8 (1.9)[46]	
X=CN	$Y=NH_2$	DMSO	269	5.9		13 (1.9)[56]	
		p-Dioxane	270	5.0		3.1 (1.9)[46]	
		p-Dioxane	271	6.4		2.4 (1.59)[87]	
X=CN	$Y=N(CH_3)_2$	DMSO	297	6.6		14 (1.9)[56]	
		p-Dioxane	290	5.6		5.0 (1.9)[46]	
		CCl_4	290	$\mu\beta=44\times10^{-48}$		$(1.06)^{211}$	
		Chloroform	292	$\mu\beta=50\times10^{-48}$		$(1.06)^{211}$	
		H_2CCl_2	292	$\mu\beta=53\times10^{-48}$		$(1.06)^{211}$	
		H_2CCN	291	$\mu\beta=48\times10^{-48}$		$(1.06)^{211}$	
		H_3COH	295	$\mu\beta=47\times10^{-48}$		$(1.06)^{211}$	
X=COH	$Y=CH_3$	Neat		3.0		1.7 (1.9)[46]	
X=COH	$Y=OC_6H_5$	Neat	269	2.8		1.9 (1.9)[46]	
X=COH	$Y=OCH_3$	Neat	269	3.5		2.2 (1.9)[46]	
X=COH	$Y=SCH_3$	Neat	310	3.1		2.6 (1.9)[46]	
X=COH	$Y=N(CH_3)_2$	*p*-Dioxane	326	5.1		6.3 (1.9)[46]	
$X=SO_2C_3H_7$	$Y=OCH_3$	Chloroform	290	5.4		3.3 (1.9)[46]	
$X=SC_6H_5$	$Y=NH_2$	Acetone	320	3.0		14 (1.06)[16]	
$X=COCH_3$	$Y=NH_2$	DMSO	310	4.5		2.4 (1.9)[56]	
$X=COCF_3$	$Y=OC_6H_5$	*p*-Dioxane	292	3.5		3.6 (1.9)[46]	
$X=COCF_3$	$Y=OCH_3$	*p*-Dioxane	292	4.0		3.6 (1.9)[46]	

(continued)

TABLE 7.1 (Continued)

Structure		Solvent	λ_{max}(nm)	μ (10^{-18} esu)	$\beta_\mu(\lambda)^{ref.}$ (10^{-30} esu)
X=$COCF_3$	Y=N $(CH_3)_2$	*p*-Dioxane	356	5.9	10 (1.9)[46]
X=NO	Y=N $(CH_3)_2$	*p*-dioxane	407	6.2	12 (1.9)[46]
X=NO_2	Y=CH_3	DMSO	280	4.0	8 (1.9)[56]
		p-Dioxane	272	4.2	2.1 (1.9)[46]
X=NO_2	Y=F	Neat		2.7	2.1 (1.06)[141]
X=NO_2	Y=Br	*p*-Dioxane	274	3.0	3.3 (1.9)[46]
X=NO_2	Y=OH	*p*-Dioxane	304	5.0	3.0 (1.9)[46]
X=NO_2	Y=OC_6H_5	*p*-Dioxane	294	4.2	4.0 (1.9)[46]
X=NO_2	Y=OCH_3	DMSO	314	4.5	16 (1.9)[56]
		p-Dioxane		4.9	6 (1.06)[98]
				5.3	4 (1.9S)[195]
		p-Dioxane	302	4.6	5.1 (1.9)[46]
X=NO_2	Y=SCH_3			4.6	6.7 (1.9S)[195]
		p-Dioxane	322	4.4	6.1 (1.9)[46]
		Acetone	335	4.4	20 (1.06)[16]
X=NO_2	Y=SC_6H_5	Acetone	334	4.3	19 (1.06)[16]
X=NO_2	Y=N_2H_3	*p*-Dioxane	366	6.3	7.6 (1.9)[46]
X=NO_2	Y=NH_2	Methanol			36 (1.06)[193]
		Melt		7.2	21 (1.06)[140]
		Methanol		6.2	35 (1.06)[190]
		DMSO	378	6.1	47 (1.9)[56]
		p-Dioxane			9.6 (1.91)[250]
		p-Dioxane			12 (1.37)[250]
		p-Dioxane			17 (1.06)[250]
		p-Dioxane			25 (0.91)[250]
		p-Dioxane			40 (0.83)[250]
		DMSO	384	$\mu\beta=75\times10^{-48}$	(1.58)[231]
				7.1	9.6 (1.9S)[195]
		Chloroform			23 (1.06HR)[48]
		Acetone	365	6.2	9.2 (1.9)[46]
		p-Dioxane	354	7.0	16 (1.06)[237]
		Chloroform	348	6.4	17 (1.06)[237]
		H_3CCN	366	6.2	29 (1.06)[237]
		Methanol	370	6.1	32 (1.06)[237]
		NMP	386	6.8	38 (1.06)[237]
		p-Dioxane		$\mu\beta=69\times10^{-48}$	(1.9)[107]
		Chloroform	347	6.2	20 (1.06)[117]

$X=NO_2$	$Y=NH(NH_2)$	DMSO	378	$\mu\beta=10\times10^{-47}$	$(1.36)^{231}$
$X=NO_2$	$Y=N(CH_3)_2$	DMSO	418	6.8	52 $(1.9)^{56}$
		Chloroform		$\mu\beta=14\times10^{-47}$	$(1.9)^{264}$
		Acetone	388	6.9	26 $(1.06)^{16}$
		DMSO	404	$\mu\beta=14\times10^{-47}$	$(1.36)^{231}$
		Acetone	376	6.4	12 $(1.9)^{46}$
$X=NO_2$	$Y=CN$	*p*-Dioxane		0.9	0.6 $(1.9)^{46}$
$X=NO_2$	$Y=COH$	*p*-Dioxane	376	2.5	0.2 $(1.9)^{46}$
$X=C_2H(CN)_2$	$Y=OCH_3$	*p*-Dioxane	345	5.5	9.8 $(1.9)^{46}$
$X=C_2H(CN)_2$	$Y=N(CH_3)_2$	DMSO	440	$\mu\beta=27\times10^{-47}$	$(1.36)^{231}$
		DMSO	440	$\mu\beta=62\times10^{-47}$	$(1.06)^{101}$
				7.1	12 $(1.98)^{195}$
		Chloroform	420	7.8	32 $(1.9)^{46}$
$X=C_2H(CN)_2$	$Y=N(C_2H_5)_2$	*p*-Dioxane	419	$\mu\beta=30\times10^{-47}$	$(1.9)^{106}$
$X=C_2H(CN)_2$	$Y=NC_5H_{10}$	Chloroform	440	8.5	17 $(\beta_0)^{177}$
$X=C_2H(CN)_2$	$Y=N(4\text{-}CH_3C_6H_4)_2$	Chloroform	452	7.6	25 $(\beta_0)^{177}$
$X=C_2(CN)_3$	$Y=NH_2$	CH_2Cl_2	498	7.8	39 $(1.9)^{46}$
$X=C_2(CN)_3$	$Y=N(CH_3)_2$	CH_2Cl_2	516	8.2	50 $(1.9)^{46}$
		DMSO	528	$\mu\beta=85\times10^{-47}$	$(1.36)^{231}$

$X=COH$		Chloroform		5.7	14 $(1.9)^{43}$
$X=C_2H(CN)_2$		CH_2Cl_2	458	8.0	44 $(1.9)^{46}$
		Chloroform		8.3	51 $(1.9)^{43}$
$X=C_2(CN)_3$		CH_2Cl_2	556	1.6	60 $(1.9)^{46}$
		DMSO	561	$\mu\beta=73\times10^{-47}$	$(1.36)^{231}$

		DMSO	458	$\mu\beta=36\times10^{-47}$	$(1.36)^{231}$

(continued)

TABLE 7.1 (Continued)

Structure	Solvent	λ_{max}(nm)	μ (10^{-18} esu)	$\beta_{\mu}(\lambda)^{ref.}$ (10^{-30} esu)
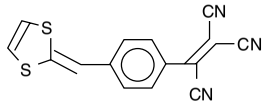	DMSO	602	$\mu\beta = 12 \times 10^{-46}$	$(1.58)^{231}$
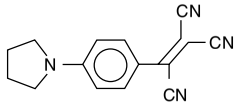	*p*-Dioxane	505	$\mu\beta = 71 \times 10^{-47}$	$(1.36)^{203}$
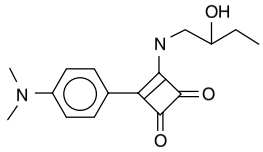		397	$\beta = 171 \times 10^{-30}$	$(1.06S)^{200}$
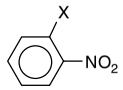				
X=CH_3	Neat		3.9	1.0 $(1.9)^{46}$
X=F	Neat		5.0	1.8 $(1.9)^{141}$
X=Br	*p*-Dioxane		4.0	0.4 $(1.9)^{46}$
X=OH	*p*-Dioxane	348	3.4	1.2 $(1.9)^{46}$
X=OCH_3	Neat	318	3.8	1.4 $(1.9)^{46}$
X=NH_2	Melt		5.0	6.4 $(1.32)^{140}$
	Acetone		4.3	10 $(1.06)^{190}$
	p-Dioxane		4.1	2.5 $(1.9)^{46}$
X=CN	*p*-Dioxane		5.5	1.2 $(1.9)^{46}$
X=COH	*p*-Dioxane		4.0	0.8 $(1.9)^{46}$

15018—Chapter7—26/8/2006—22:08—SJAPPIYAR—15018—XML MODEL CRC12a – pp. 1–126.

X = CH_3	Neat		3.9		1.5 (1.9)[46]
X = F	Neat		3.6		- 1.6 (1.06)[141]
X = Cl	Benzene		3.4		1.6 (1.06)[191]
X = Br	Benzene		3.4		1.2 (1.06)[191]
	p-Dioxane		3.4		1.0 (1.9)[46]
X = OH	*p*-Dioxane		3.6		0.8 (1.9)[46]
X = OCH_3	*p*-Dioxane	326	3.9		1.6 (1.9)[46]
X = NH_2	Melt		5.5		4.2 (1.32)[140]
	Acetone		4.9		6 (1.06)[190]
	p-Dioxane	396	4.7		1.9 (1.9)[46]
	p-Dioxane		3.7		0.8 (1.9)[46]
	p-Dioxane		2.8		1.7 (1.9)[46]
	Benzene		3.9		1.2 (1.06)[191]
	p-Dioxane				9.5 (1.91)[250]
	p-Dioxane				13 (1.37)[250]
	p-Dioxane				17 (1.06)[250]
	p-Dioxane				27 (0.91)[250]
	p-Dioxane				45 (0.83)[250]
	p-Dioxane	361	6.2		8.7 (1.9)[46]
	p-Dioxane		7.4		18 (1.06)[25]
	p-Dioxane				9.1 (1.32)[25]
	p-Dioxane				7.6 (1.91)[25]
	p-Dioxane		5.7		13 (1.06)[262]
	p-Dioxane	350	5.9		6.8 (1.9)[46]
X = CN	*p*-Dioxane		6.0		8.7 (1.9)[46]
X = COH					
X = NO_2					

(continued)

TABLE 7.1 (Continued)

Structure	Solvent	λ_{max}(nm)	μ (10^{-18} esu)	$\beta_{\mu}(\lambda)^{ref.}$ (10^{-30} esu)
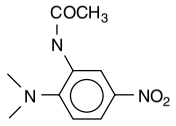	*p*-Dioxane		7.4	18 (1.06)[262]
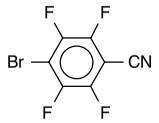			8.1	9.5 (1.06S)[195]
	p-Dioxane	240	3.5	1.4 (1.59)[87]
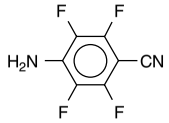	*p*-Dioxane	274	6.5	2.6 (1.59)[87]
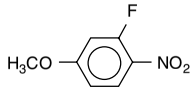	*p*-Dioxane	304	4.4	2.5 (1.9)[46]
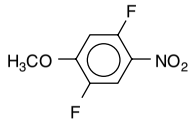	*p*-Dioxane	304	4.9	2.6 (1.9)[46]
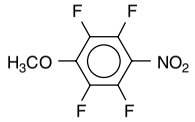	*p*-Dioxane	270	4.2	1.7 (1.9)[46]

15018—Chapter7—26/8/2006—22:08—SJAPPIYAR—15018—XML MODEL CRC12a – pp. 1–126.

		p-Dioxane	319	6.0			5.5 (1.59)[87]	
		Acetone		5.5			21 (1.06)[190]	
		p-Dioxane		$\mu\beta = 49 \times 10^{-48}$			(1.9)[107]	
		Acetone		5.6			22 (1.06)[190]	
Styrene derivatives								
X = CN	Y = OCH_3	Chloroform	304	4.2			7.0 (1.9)[45]	
X = CN	Y = $N(CH_3)_2$	Chloroform	364	6.0			23 (1.9)[45]	
X = COH	Y = Br	Chloroform	298	2.0			6.5 (1.9)[45]	
X = COH	Y = OCH_3	DMSO	320	$\mu\beta = 80 \times 10^{-48}$			(1.9)[55]	
		Chloroform	318	4.2			11 (1.9)[45]	
X = COH	Y = $N(CH_3)_2$	DMSO	387	$\mu\beta = 37 \times 10^{-47}$			(1.9)[55]	
		Chloroform	384	$\mu\beta = 32 \times 10^{-47}$			(1.34)[14]	
X = $COCH_3$	Y = OCH_3	Chloroform	384	5.6			30 (1.9)[45]	
X = $COCF_3$	Y = $N(CH_3)_2$	Chloroform	316	4.0			8.9 (1.9)[45]	
X = NO_2	Y = H	Chloroform		6.6			64 (1.9)[43]	
		Chloroform	312	3.8			8.0 (1.9)[45]	

(continued)

TABLE 7.1 (Continued)

Structure		Solvent	λ_{max}(nm)	μ (10^{-18} esu)	$\beta_{\mu}(\lambda)^{ref.}$ (10^{-30} esu)
X=NO_2	Y=OH	Chloroform	352	5.1	18 (1.9)[45]
X=NO_2	Y=OCH_3	*p*-Dioxane		5.5	12 (1.06)[98]
		Chloroform	352	4.6	17 (1.9)[45]
X=NO_2	Y=$N(CH_3)_2$	Chloroform		7.9	220 (1.06)[189]
		Chloroform	438	6.5	50 (1.9)[45]
X=$CHC(CN)_2$	Y=$N(CH_3)_2$	DMSO	500	$\mu\beta=36\times10^{-46}$	(1.06)[102]
		DMSO	500	$Re(\mu\beta)=34\times10^{-46}$	(1.06)[101]
				$Im(\mu\beta)=36\times10^{-48}$	(1.06)[101]
X=$N(CH_3)_2$	Y=NO_2	Chloroform	438	5.9	35 (1.9)[45]
	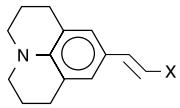				
	X=COH	Chloroform		6.3	48 (1.9)[43]
	X=NO_2	Chloroform		7.1	90 (1.9)[43]
	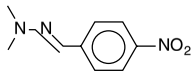	*p*-Dioxane		$\mu\beta=15\times10^{-47}$	(1.9)[107]
	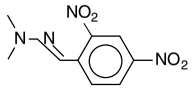	*p*-Dioxane		$\mu\beta=16\times10^{-47}$	(1.9)[107]
	Biphenyl derivatives				
	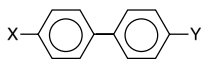				
X=CN	Y=H	*p*-Dioxane	272	4.0	1.9 (1.9)[45]

15018—Chapter7—26/8/2006—22:09—SJAPPIYAR—15018—XML MODEL CRC12a – pp. 1–126.

X = $COCH_3$	Y = H	*p*-Dioxane	280	3.1	2.0 (1.9)[45]
X = NO_2	Y = H	*p*-Dioxane	304	3.8	4.1 (1.9)[45]
X = SO_2CH_3	Y = $N(CH_3)_2$	Chloroform	340	6.0	13 (1.9)[45]
X = CN	Y = OH	*p*-Dioxane	292	4.8	6.3 (1.9)[45]
X = $COCH_3$	Y = OCH_3	*p*-Dioxane	304	3.4	4.9 (1.9)[45]
X = NO_2	Y = Br	*p*-Dioxane	306	2.7	4.4 (1.9)[45]
X = NO_2	Y = OH	*p*-Dioxane	334	4.9	7.7 (1.9)[45]
X = NO_2	Y = OCH_3	*p*-Dioxane	332	4.5	9.2 (1.9)[45]
X = NO_2	Y = NH_2	Chloroform	372	5.0	24 (1.9)[45]
X = NO_2	Y = NH_2	NMP		7.8	24 (1.9)[45]
X = NO_2	Y = $N(CH_3)_2$	Chloroform	390	5.5	50 (1.9)[45]
		Toluene	401	7.5	89 (1.06)[271]
X = NO_2	Y = N $(C_6H_{13})_2$	$C_6H_{11}CH_3$	400	7.5	73 (1.06)[271]
	Fluorene derivatives				
X = CN	Y = H	*p*-Dioxane	284	3.9	3.0 (1.9)[45]
X = NO_2	Y = H	*p*-Dioxane	328	4.1	5.1 (1.9)[45]
X = NO_2	Y = Br	*p*-Dioxane	330	2.8	6.0 (1.9)[45]
X = NO_2	Y = OCH_3	*p*-Dioxane	356	4.7	11 (1.9)[45]
X = NO_2	Y = $N(CH_3)_2$	*p*-Dioxane	410	5.6	40 (1.9)[45]
		Chloroform	417	6.0	55 (1.9)[45]
	Diphenyl ethers and derivatives				
		Chloroform	252	5.2	6.3 (1.9)[43]
		p-Dioxane		6.2	15 (1.06)[210]
		p-Dioxane	296	4.9	4.5 (1.9)[43]

(continued)

TABLE 7.1 (Continued)

Structure	Solvent	λ_{max}(nm)	μ (10^{-18} esu)	$\beta_{\mu}(\lambda)^{ref.}$ (10^{-30} esu)
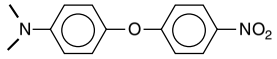	*p*-Dioxane	294	5.2	5.3 (1.9)[43]
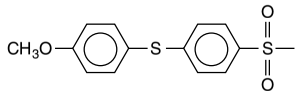	Chloroform	295	5.3	8.9 (1.9)[43]
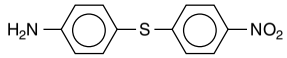	Benzene		6.0	26 (1.06)[210]
	Acetone	341	5.8	28 (1.06)[16]
	p-Dioxane	334	5	8.7 (1.9)[43]
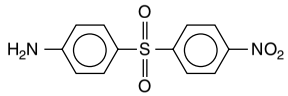	Acetone	332	8	19 (1.06)[16]
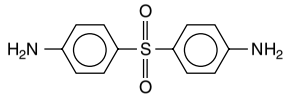	Acetone	295	7.8	8 (1.06)[16]
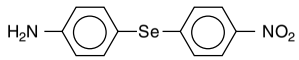	*p*-Dioxane		5.9	27 (1.06)[210]
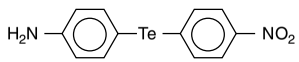	*p*-Dioxane		5.6	27 (1.06)[210]

n = 1		Chloroform	320	6		16 (1.06)[164]
n = 2		Chloroform	334	7		22 (1.06)[164]
n = 3		Chloroform	385	6.8		38 (1.06)[164]
Tolane derivatives						
X = SO_2CH_3	Y = H	*p*-Dioxane	310	5.3		3.8 (1.06)[32]
X = SO_2CH_3	Y = OCH_3	*p*-Dioxane	310	5.9		11 (1.06)[32]
X = SO_2CH_3	Y = CH_3S	*p*-Dioxane	320	5.2		16 (1.06)[32]
X = SO_2CH_3	Y = NH_2	Chloroform	338	6.5		13 (1.9)[45]
X = SO_2CH_3	Y = $N(CH_3)_2$	*p*-Dioxane	358	7.5		5.6(1.06)[32]
X = SO_2CF_3	Y = OCH_3	*p*-Dioxane	327	6.2		21 (1.06)[32]
X = SO_2CF_3	Y = $N(CH_3)_2$	*p*-Dioxane	388	8.4		40 (1.06)[32]
X = CO_2CH_3	Y = SCH_3	Chloroform	328	2.9		8 (1.9)[45]
X = CO_2CH_3	Y = NH_2	Chloroform	332	3.8		15 (1.9)[45]
X = $COCH_3$	Y = SCH_3	Chloroform	336	3.7		9.8(1.9)[45]
X = $COCH_3$	Y = NH_2	Chloroform	334	3.3		12 (1.9)[45]
X = COC_6H_5	Y = NH_2	Chloroform	352	3.7		19 (1.9)[45]
X = CN	Y = SCH_3	Chloroform	333	4.0		15 (1.9)[45]
X = CN	Y = NH_2	Chloroform	342	5.2		20 (1.9)[45]
X = CN	Y = $NHCH_3$	Chloroform	358	5.7		27 (1.9)[45]
X = CN	Y = $N(CH_3)_2$	Chloroform	372	6.1		29 (1.9)[45]
X = NO_2	Y = H	*p*-Dioxane	326	4.6		16 (1.06)[32]
X = NO_2	Y = Br	Chloroform	335	3.0		10 (1.9)[45]
X = NO_2	Y = OCH_3	*p*-Dioxane	356	4.4		14 (1.9)[45]
X = NO_2	Y = SCH_3	Chloroform	362	4.0		20 (1.9)[45]
X = NO_2	Y = NH_2	Chloroform	380	5.5		24 (1.9)[45]
		NMP	410	5.5		40 (1.9)[45]
X = NO_2	Y = $NHCH_3$	Chloroform	400	5.7		46 (1.9)[45]
X = NO_2	Y = $N(CH_3)_2$	Chloroform	415	6.1		46 (1.9)[45]
		p-Dioxane	402	7.1		102 (1.06)[32]
		Chloroform	416	6.6		33 (β_0)[177]

(continued)

TABLE 7.1 (Continued)

Structure		Solvent	λ_{max}(nm)	μ (10^{-18} esu)	$\beta_\mu(\lambda)^{ref.}$ (10^{-30} esu)
X=NO_2	Y=$N(C_6H_5)_2$	Chloroform	418	4.8	28 (β_0)[177]
	Stilbene derivatives				
	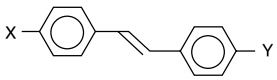				
X=H	Y=OCH_3		320	2.8	6.1 (1.06)[175]
X=H	Y=NH_2	Benzene		2.1	12 (1.06)[189]
		p-Dioxane	332	2.2	7.4 (1.9)[46]
X=H	Y=$N(CH_3)_2$	Benzene		2.4	29 (1.06)[189]
		p-Dioxane	340	2.1	10 (1.9)[46]
X=Cl	Y=H	Benzene		1.5	3.6 (1.06)[189]
X=Cl	Y=$N(CH_3)_2$	Chloroform		4.0	42 (1.06)[189]
X=CF_3	Y=OCH_3	*p*-Dioxane	323	4.3	12 (1.06)[244]
			326	4.2	16 (1.06)[175]
X=CF_3	Y=OH	*p*-Dioxane	327	4.7	12 (1.06)[244]
X=SO_2CH_3	Y=H	*p*-Dioxane	364	4.4	58 (1.06)[32]
X=SO_2CH_3	Y=OCH_3	Chloroform	336	6.5	10 (1.9)[46]
		p-Dioxane	335	6.1	9.1 (1.06)[32]
X=SO_2CH_3	Y=SC_6H_5	*p*-Dioxane	344	4.4	19 (1.06)[32]
X=SO_2CH_3	Y=$N(CH_3)_2$	*p*-Dioxane	376	6.9	66 (1.06)[32]
X=SO_2CH_3	Y=$N(CH_2C_2H_3)_2$	Chloroform	391	$\mu\beta=57\times10^{-47}$	(1.9)[264]
X=SO_2CF_3	Y=OCH_3	*p*-Dioxane	347	7.8	14 (1.9)[46]
		p-Dioxane	350	6.6	34 (1.06)[32]
X=$SO_2C_6F_{13}$	Y=$N(CH_3)_2$	Chloroform		8.0	59 (1.9)[43]
X=$COCF_3$	Y=OCH_3	*p*-Dioxane	368	4.2	16 (1.9)[46]
X=COH	Y=$N(CH_3)_2$	Chloroform	360	3.5	24 (1.9)[254]
X=CN	Y=OH	*p*-Dioxane	344	4.5	13 (1.9)[46]
X=CN	Y=OCH_3	DMSO	342	$\mu\beta=82\times10^{-47}$	(1.9)[55]
		Chloroform	340	3.8	19 (1.9)[46]
X=CN	Y=$N(CH_3)_2$	DMSO	390	$\mu\beta=98\times10^{-48}$	(1.9)[55]
		Chloroform	382	5.7	36 (1.9)[46]
X=NO_2	Y=H	Benzene		4.6	29 (1.06)[189]
		p-Dioxane	345	4.2	11 (1.9)[46]
X=NO_2	Y=CH_3	DMSO	368	$\mu\beta=20\times10^{-48}$	(1.9)[55]
		p-Dioxane	351	4.7	15 (1.9)[46]

15018—Chapter7—26/8/2006—22:10—SJAPPIYAR—15018—XML MODEL CRC12a – pp. 1–126.

$X=NO_2$	$Y=Cl$	Chloroform		3.1		39 (1.06)[189]
$X=NO_2$	$Y=Br$	*p*-Dioxane	344	3.2		14 (1.9)[46]
		Chloroform	356	3.4		18 (1.9)[46]
$X=NO_2$	$Y=OH$	Chloroform				93 (1.06HR)[48]
		p-Dioxane	370	5.5		17 (1.9)[46]
$X=NO_2$	$Y=OC_6H_5$	*p*-Dioxane	350	4.6		18 (1.9)[46]
$X=NO_2$	$Y=OCH_3$	*p*-Dioxane		5.7		81 (1.06)[98]
		Chloroform				105 (1.06HR)[48]
		p-Dioxane	364	4.5		28 (1.9)[46]
		Chloroform	370	4.5		34 (1.9)[46]
		p-Dioxane	364	4.5		60 (1.06)[32]
$X=NO_2$	$Y=SCH_3$	*p*-Dioxane	374	4.3		26 (1.9)[46]
		Chloroform	380	4.3		34 (1.9)[46]
		p-Dioxane	378	5.1		68 (1.06)[32]
$X=NO_2$	$Y=NH_2$	Acetone		7.5		260 (1.06)[189]
		Chloroform	402	5.1		40 (1.9)[46]
$X=NO_2$	$Y=N(CH_3)_2$	Acetone		7.4		450(1.06)[193]
		DMSO	447	$\mu\beta=42\times10^{-46}$		(1.9)[55]
		DMSO	453	$\mu\beta=76\times10^{-47}$		(1.36)[231]
				7.1		323 (1.06S)[195]
		Chloroform	427	6.6		73 (1.9)[46]
		NMP		7.2		70 (1.9)[46]
		p-Dioxane		$\mu\beta=58\times10^{-47}$		(1.9)[107]
		Chloroform	438	6.7		42 (β_0)[177]
$X=NO_2$	$Y=N(CH_2C_2H_3)_2$	Chloroform	452	$\mu\beta=57\times10^{-47}$		(1.9)[264]
$X=NO_2$	$Y=N(C_6H_5)_2$	Chloroform	436	4.8		37 (β_0)[177]
$X=NO_2$	$Y=COOCH_3$	CH_2Cl_2	350	4.0		4 (1.9)[46]
$X=NO_2$	$Y=COH$	*p*-Dioxane	352	4.1		6 (1.9)[46]
$X=CHC(CN)_2$	$Y=N(CH_3)_2$	Chloroform		7.8		210 (1.9)[43]
$X=CHC(CN)_2$	$Y=N(C_2H_5)_2$	CH_2Cl_2	485	8.2		180 (1.58)[54]
		p-Dioxane	468	$\mu\beta=11\times10^{-46}$		(1.9)[106]
$X=Br$	$Y=OCH_3$	*p*-Dioxane	325	4.0		25 (1.9)[46]

(continued)

TABLE 7.1 (Continued)

Structure	Solvent	λ_{max}(nm)	μ (10^{-18} esu)	$\beta_\mu(\lambda)^{ref.}$ (10^{-30} esu)
	Chloroform	438	7	96 (1.9)[46]
	Chloroform	360	3.8	4.4 (1.9)[46]
	Chloroform	370	3.7	1.6 (1.9)[46]
	Chloroform	390	3.5	3.8 (1.9)[46]
	Chloroform	320	4.4	5.5 (1.9)[46]
	Chloroform	292	3.9	4.5 (1.9)[46]

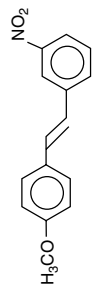	*p*-Dioxane	318	3.9	5.3 (1.9)[46]
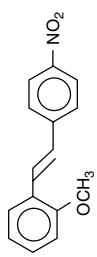	Chloroform	362	5.0	22 (1.9)[46]
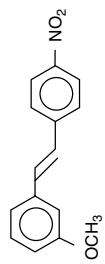	Chloroform	352	4.0	21 (1.9)[46]
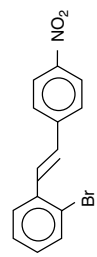	Chloroform	346	4.6	12 (1.9)[46]
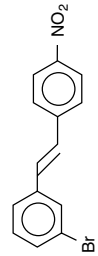	Chloroform	346	3.4	14 (1.9)[46]
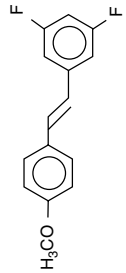		322	3.1	9.2 (1.06)[175]

(continued)

TABLE 7.1 (Continued)

Structure	Solvent	λ_{max}(nm)	μ (10^{-18} esu)	$\beta_\mu(\lambda)^{ref.}$ (10^{-30} esu)
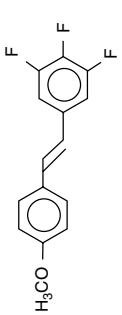		320	4.6	6.8 (1.06)[175]
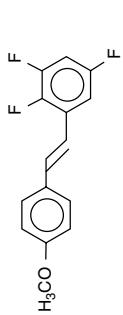		322	3.4	10 (1.06)[175]
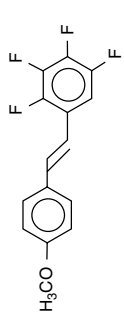		324	3.5	12 (1.06)[175]
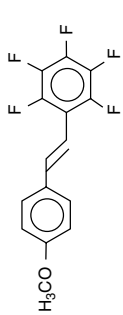		322	3.3	16 (1.06)[175]
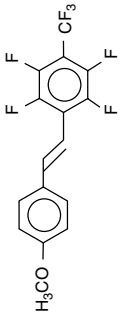		334	4.0	23 (1.06)[175]

						11 (1.06)[175]
						4.5 (1.06)[244]
X = H	4.2	4.7	326	314	*p*-Dioxane	
X = Cl		4.2		318	*p*-Dioxane	5.1 (1.06)[244]
X = Br		4.6		320	*p*-Dioxane	8.1 (1.06)[244]
X = CH_3		4.8		323	*p*-Dioxane	7.4 (1.06)[244]
X = OCH_3		5.3		340	*p*-Dioxane	15 (1.06)[244]
X = OH		5.5		348	*p*-Dioxane	16 (1.06)[244]
X = SCH_3		5.0		362	*p*-Dioxane	16 (1.06)[244]
X = $N(CH_3)_2$		6.4		410	*p*-Dioxane	29 (1.06)[244]
						26 (1.9)[46]
						23 (1.9)[46]
						18 (1.9)[46]

(continued)

TABLE 7.1 (Continued)

Structure	Solvent	λ_{max}(nm)	μ (10^{-18} esu)	$\beta_\mu(\lambda)^{ref.}$ (10^{-30} esu)
	p-Dioxane	395	4.8	32 (1.9)[46]
	p-Dioxane	361	5.3	21 (1.9)[46]
	p-Dioxane	340	4.6	8 (1.9)[46]
	p-Dioxane	382	4.1	2.1 (1.9)[46]
	p-Dioxane	355	4	10 (1.9)[46]
	p-Dioxane	354	2	5 (1.9)[46]

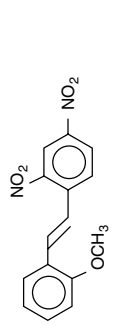	*p*-Dioxane	378	5.0	12 (1.9)[255]
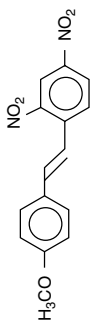	*p*-Dioxane	384	4.7	22 (1.9)[46]
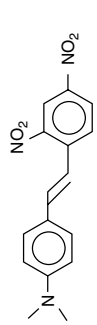	*p*-Dioxane *p*-Dioxane	466	7.0 $\mu\beta = 66 \times 10^{-47}$	57 (1.9)[255] (1.9)[107]
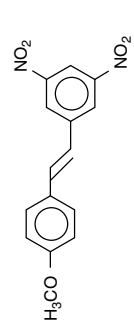	Chloroform		4.1	15 (1.9)[43]
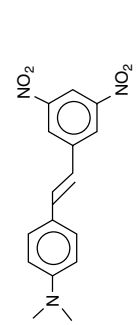	Chloroform		6.2	45 (1.9)[43]
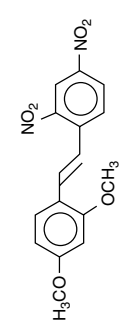	*p*-Dioxane	404	5.6	25 (1.9)[46]

(continued)

TABLE 7.1 (Continued)

Structure	Solvent	λ_{max}(nm)	μ (10^{-18} esu)	$\beta_\mu(\lambda)^{ref.}$ (10^{-30} esu)
	p-Dioxane	390	3.1	11 (1.9)[46]
	p-Dioxane	346	4.4	4.9 (1.9)[46]
	p-Dioxane	351	4.7	15 (1.9)[46]
	p-Dioxane	376	4.4	14 (1.9)[46]
	DMSO	458	$\mu\beta = 50\times10^{-47}$	(1.36)[231]
	p-Dioxane	349	5.4	6.6 (1.9)[46]

$X=SO_2CH_3$	$Y=N(C_4H_9)_2$	Chloroform	461	$\mu\beta=51\times10^{-47}$	$(1.9)^{264}$	
$X=NO_2$	$Y=NH_2$	*p*-Dioxane	420	5.8	29 $(1.9)^{46}$	
		DMSO	470	$\mu\beta=77\times10^{-47}$	$(1.36)^{231}$	
$X=NO_2$	$Y=N(CH_3)_2$	Chloroform	498	$\mu\beta=13\times10^{-46}$	$(1.9)^{264}$	
		Chloroform	480	7.7	40 $(\beta_0)^{177}$	
$X=NO_2$	$Y=N(C_2H_5)_2$	Chloroform	494	8.0	50 $(\beta_0)^{177}$	
$X=N0_2$	$Y=N(C_2H_5)(C_2H_4)OH$	CH_2Cl_2	480	8.9	90 $(1.57)^{54}$	
		p-Dioxane	455	7.0	49 $(1.9)^{46}$	
$X=NO_2$	$Y=N(C_6H_5)_2$	DMSO	508	$\mu\beta=11\times10^{-46}$	$(1.36)^{231}$	
$X=CHC(CN)_2$	$Y=N(CH_3)_2$	Chloroform	486	5.9	54 $(\beta_0)^{177}$	
$X=C_2(CN)_3$	$Y=N(C_2H_5)_2$	DMSO	492	$\mu\beta=27\times10^{-46}$	$(1.36)^{231}$	
$X=C_2(CN)_3$	$Y=N(C_2H_5)(C_2H_4)OH$	DMSO		$\mu\beta=41\times10^{-46}$	$(1.58)^{264}$	
		CH_2Cl_2	513	10	190 $(1.57)^{54}$	
	Pyridine derivatives					
		Acetone		6.5	3.7 $(1.9)^{46}$	
		p-Dioxane	376	7.2	18 $(1.06)^{25}$	
		p-Dioxane			11 $(1.32)^{25}$	
		p-Dioxane			11 $(1.91)^{25}$	
		p-Dioxane		5.5	17 $(1.06)^{262}$	
		p-Dioxane	357	6.7	13 $(1.06)^{25}$	
		p-Dioxane			9.3 $(1.32)^{25}$	
		p-Dioxane			6.0 $(1.91)^{25}$	
		p-Dioxane	361	6.8	22 $(1.06)^{25}$	
		p-Dioxane			12 $(1.32)^{25}$	
		p-Dioxane			11 $(1.91)^{25}$	

(continued)

TABLE 7.1 (Continued)

Structure	Solvent	λ_{max}(nm)	μ (10^{-18} esu)	$\beta_\mu(\lambda)^{ref.}$ (10^{-30} esu)
	p-Dioxane		6.1	15 (1.06)[262]
	p-Dioxane		3.5	2.2 (1.9)[46]
	p-Dioxane		3.5	2.2 (1.9)[46]
	Chloroform		0.9	10 (1.9)[46]
	Chloroform	335	3.8	16 (1.9)[43]
	Chloroform		1.3	8 (1.9)[46]

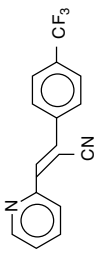	*p*-Dioxane	312	6.2	4.3 (1.06)[244]
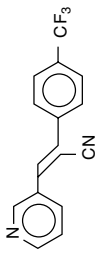	*p*-Dioxane	309	5.5	4.4 (1.06)[244]
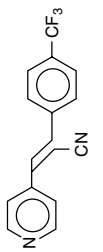	*p*-Dioxane	307	5.1	4.2 (1.06)[244]
Coumarin derivatives				
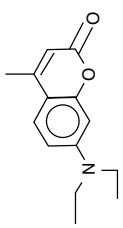	Chloroform		5	15 (1.9)[43]
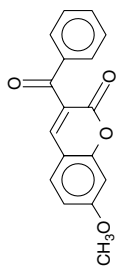	Chloroform		5	8 (1.9)[43]
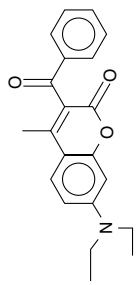	Chloroform		7.3	30 (1.9)[43]

(continued)

TABLE 7.1 (Continued)

Structure		Solvent	λ_{max}(nm)	μ (10^{-18} esu)	$\beta_{\mu}(\lambda)^{ref.}$ (10^{-30} esu)
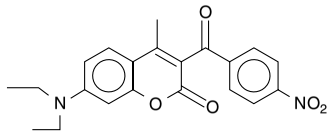		Chloroform		8.8	50 (1.9)[43]
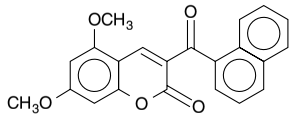		Chloroform		5.8	9.5 (1.9)[43]
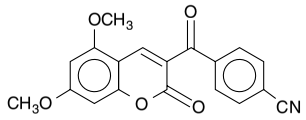		Chloroform		7.3	15 (1.9)[43]
Other polycyclic aromatic derivatives					
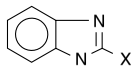					
	X=H	*p*-Dioxane		3.6	<1 (1.9)[43]
	X=SH	*p*-Dioxane		4	<1 (1.9)[43]
	X=COOH	*p*-Dioxane		2.6	<1 (1.9)[43]
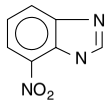		*p*-Dioxane			
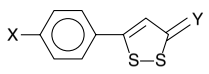					
X=H	Y=O	*p*-Dioxane	340		4.8 (1.34)[28]
X OCH_3	Y=O	*p*-Dioxane	312		13 (1.34)[28]

X = H	Y = S	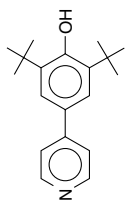	11 $(1.34)^{28}$	*p*-Dioxane	438			
X = OCH_3	Y = S		21 $(1.34)^{28}$	*p*-Dioxane	438			
		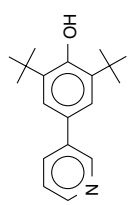	$\beta_0 = 12(S)^7$		333	4.0		
		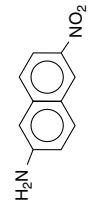	$\beta_0 = 11(S)^7$		356	6.2		
		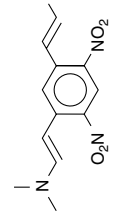	$(1.36)^{231}$	DMSO		$\mu\beta = 23 \times 10^{-47}$		
			36 $(1.9)^{43}$	Chloroform		7.6		
		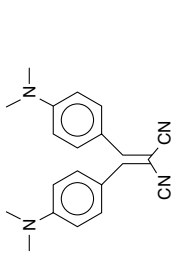	20 $(1.9)^{43}$	Chloroform		7.3.		

(continued)

TABLE 7.1 (Continued)

Structure	Solvent	λ_{max}(nm)	μ (10^{-18} esu)	$\beta_\mu(\lambda)^{ref.}$ (10^{-30} esu)
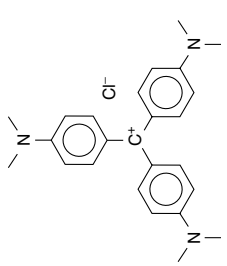	CCl_4	590		580 (1.06HR)[291]
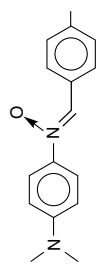	Chloroform		4	10 (1.9)[43]
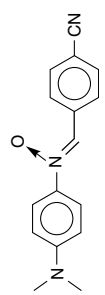	Chloroform	400	6.7	31 (1.9)[43]
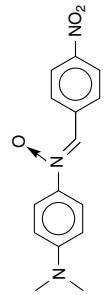	Chloroform	423	7	45 (1.9)[43]
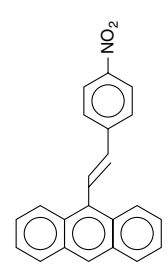	*p*-Dioxane		6	5 (1.9)[43]

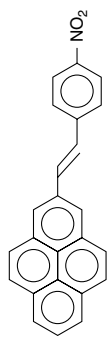	*p*-Dioxane	8		11 (1.9)[43]
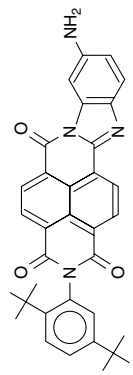	*p*-Dioxane	575	$\mu\beta = 30 \times 10^{-47}$	($\approx$2)[226]
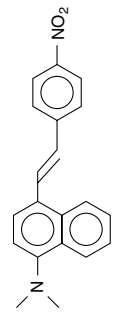	Chloroform	6.5		35 (1.9)[43]
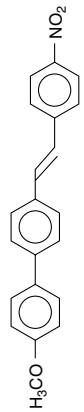	NMP	364	7	18 (1.9)[43]
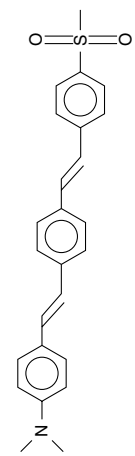	NMP	406	8	30 (1.9)[43]
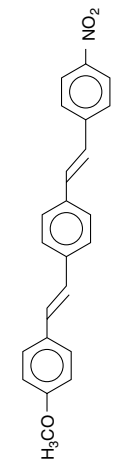	Chloroform	394	8	52 (1.9)[43]
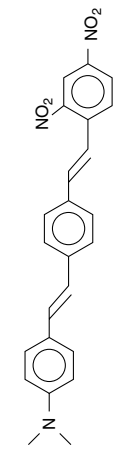	*p*-Dioxane		$\mu\beta = 13 \times 10^{-46}$	(1.9)[107]

(continued)

TABLE 7.1 (Continued)

Structure			Solvent	λ_{max}(nm)	μ (10^{-18} esu)	$\beta_{\mu}(\lambda)^{ref.}$ (10^{-30} esu)
Polyene derivatives						
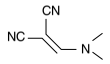			Chloroform	352	7.6	1 (1.9)[156]
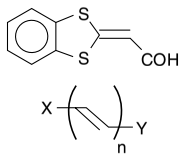			Chloroform	372	$\mu\beta = 30 \times 10^{-48}$	(1.34)[14]
$n=1$	X=COH	Y=$N(CH_3)_2$	Chloroform	284	6.3	3.3 (1.9)[156]
$n=2$	X=COH	Y=$N(C_2H_5)_2$	Chloroform	363	6.5	20 (1.9)[156]
$n=3$	X=COH	Y=$N(CH_3)_2$	Chloroform	422	6.9	53 (1.9)[156]
$n=1$	X=$CHC(CN)_2$	Y=$N(CH_3)_2$	Chloroform	374	8.9	6.1 (1.9)[156]
$n=2$	X=$CHC(CN)_2$	Y=$N(C_2H_5)_2$	Chloroform	476	10.7	45 (1.9)[156]
$n=3$	X=$CHC(CN)_2$	Y=$N(CH_3)_2$	Chloroform	550	9.9	211 (1.9)[156]
$n=1$	X=NO_2	Y=$N(CH_3)_2$	Chloroform		6.3	4.8 (1.9)[43]
$n=2$	X=NO_2	Y=$N(CH_3)_2$	Chloroform		6.7	21 (1.9)[43]
$n=3$	X=NO_2	Y=$N(CH_3)_2$	Chloroform		8.4	73 (1.9)[43]
$n=3$	X=SO_2CF_3	Y=$N(CH_3)_2$	Chloroform		9.8	40 (1.9)[43]
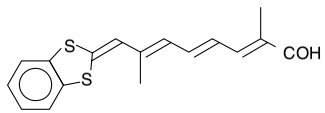			Chloroform	456	$\mu\beta = 12 \times 10^{-46}$	(1.34)[14]
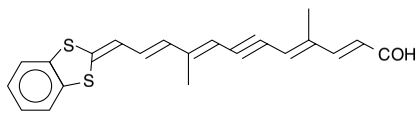			Chloroform	466	$\mu\beta = 22 \times 10^{-46}$	(1.34)[14]

15018—Chapter7—26/8/2006—22:14—SJAPPIYAR—15018—XML MODEL CRC12a – pp. 1–126.

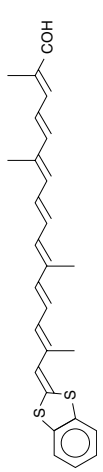	Chloroform	500	$\mu\beta = 73 \times 10^{-46}$ (1.34)[14]
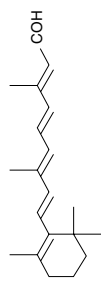	DMSO	380	$\mu\beta = 23 \times 10^{-47}$ (1.06)[101]
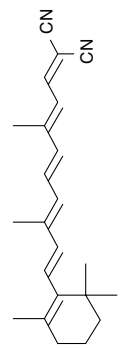	DMSO	470	$\mathrm{Re}(\mu\beta) = 13 \times 10^{-46}$ (1.06)[101] $\mathrm{Im}(\mu\beta) = 15 \times 10^{-46}$ (1.06)[101]
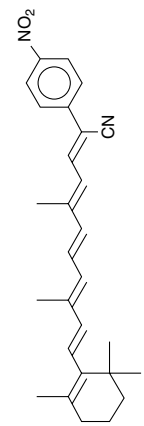	DMSO	480	$\mathrm{Re}(\mu\beta) = 14 \times 10^{-46}$ (1.06)[101] $\mathrm{Im}(\mu\beta) = 35 \times 10^{-46}$ (1.06)[101]
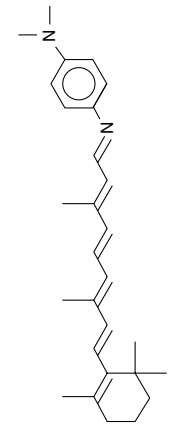	DMSO	440	$\mathrm{Re}(\mu\beta) = 15 \times 10^{-46}$ (1.06)[101] $\mathrm{Im}(\mu\beta) = 17 \times 10^{-46}$ (1.06)[101]
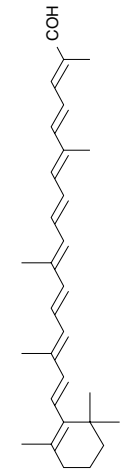	$Cl_2CHCHCl_2$	470	$\mathrm{Re}(\mu\beta) = 10 \times 10^{-47}$ (1.06)[101] $\mathrm{Im}(\mu\beta) = 44 \times 10^{-46}$ (1.06)[101]
	Chloroform	476	$\mu\beta = 96 \times 10^{-47}$ (1.9)[53]

(continued)

TABLE 7.1 (Continued)

Structure			Solvent	λ_{max}(nm)	μ (10^{-18} esu)	$\beta_\mu(\lambda)^{ref.}$ (10^{-30} esu)
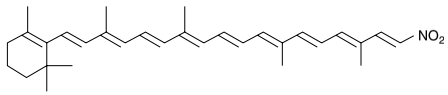			$Cl_2CHCHCl_2$	500	$Re(\mu\beta) = -20\times10^{-46}$ $Im(\mu\beta) = 25\times10^{-46}$	$(1.06)^{101}$ $(1.06)^{101}$
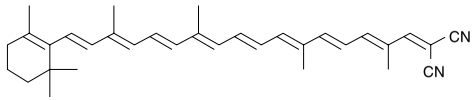			$Cl_2CHCHCl_2$	570	$Re(\mu\beta) = 35\times10^{-46}$ $Im(\mu\beta) = 47\times10^{-46}$	$(1.06)^{101}$ $(1.06)^{101}$
			Chloroform	566	$\mu\beta = 44\times10^{-46}$	$(1.9)^{53}$
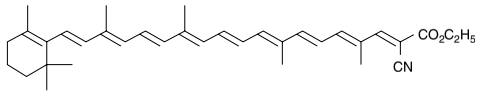			$Cl_2CHCHCl_2$	510	$Re(\mu\beta) = -12\times10^{-45}$ $Im(\mu\beta) = 73\times10^{-46}$	$(1.06)^{101}$ $(1.06)^{101}$
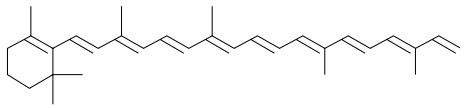			Chloroform	502	$\mu\beta = 15\times10^{-46}$	$(1.9)^{53}$
α-Phenylpolyene Derivatives						
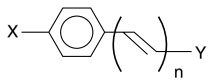						
$n=2$	X=COH	Y=OCH_3	Chloroform	350	4.3	28 $(1.9)^{45}$
$n=3$	X=COH	Y=OCH_3	Chloroform	376	4.6	42 $(1.9)^{45}$
$n=2$	X=COH	Y=$N(CH_3)_2$	Chloroform	412	6.0	52 $(1.9)^{45}$
$n=3$	X=COH	Y=$N(CH_3)_2$	Chloroform	434	6.3	88 $(1.9)^{45}$
			Chloroform		6.6	105 $(1.9)^{43}$

15018—Chapter7—26/8/2006—22:14—SJAPPIYAR—15018—XML MODEL CRC12a – pp. 1–126.

$n=4$	X=COH	Y=N(CH$_3$)$_2$	Chloroform		8.0		138 (1.9)[43]	
$n=2$	X=COCF$_3$	Y=N(CH$_3$)$_2$	Chloroform		6.6		126 (1.9)[43]	
$n=2$	X=NO$_2$	Y=OCH$_3$	DMSO	370	$\mu\beta=81\times10^{-48}$		(1.06)[102]	
			Chloroform		4.6		42 (1.9)[45]	
$n=3$	X=NO$_2$	Y=OCH$_3$	DMSO	400	$\mu\beta=30\times10^{-47}$		(1.06)[102]	
$n=2$	X=NO$_2$	Y=N(CH$_3$)$_2$	Acetone		8.8		630 (1.06)[189]	
			DMSO	460	$\mu\beta=17\times10^{-46}$		(1.06)[102]	
			Chloroform	466	6.5		140 (1.9)[254]	
$n=3$	X=NO$_2$	Y=N(CH$_3$)$_2$	DMSO	490	$\mu\beta=55\times10^{-46}$		(1.06)[102]	
			Chloroform	487	6.6		240 (1.9)[254]	
$n=4$	X=NO$_2$	Y=N(CH$_3$)$_2$	Chloroform	502	7.6		280 (1.9)[254]	
$n=2$	X=CHC(CN)$_2$	Y=N(CH$_3$)$_2$	DMSO	500	$\mu\beta=36\times10^{-46}$		(1.06)[102]	
			Chloroform	520	9.0		163 (1.9)[45]	
$n=3$	X=CHC(CN)$_2$	Y=N(CH$_3$)$_2$	Chloroform		8.8		432 (1.9)[43]	
$n=3$		X=COH	Chloroform		7.1		162 (1.9)[43]	
$n=3$		X=NO$_2$	Chloroform		7.8		287 (1.9)[43]	
$n=4$		X=NO$_2$	Chloroform		$\mu\beta=26\times10^{-46}$		(1.9)[43]	
$n=3$		X=CHC(CN)$_2$	Chloroform		8.7		485 (1.9)[43]	
			Chloroform	450	$\mu\beta=20\times10^{-46}$		(1.34)[14]	
			Chloroform	461	$\mu\beta=42\times10^{-46}$		(1.34)[14]	

(continued)

TABLE 7.1 (Continued)

Structure			Solvent	λ_{max}(nm)	μ (10^{-18} esu)	$\beta_{\mu}(\lambda)^{ref.}$ (10^{-30} esu)
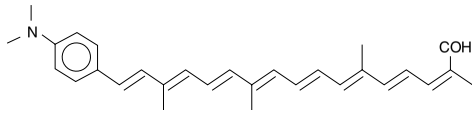			Chloroform	498	$\mu\beta = 89 \times 10^{-46}$	(1.34)[14]
Diphenylpolyene derivatives						
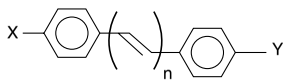						
$n=2$	X=CN	Y=OCH_3	Chloroform	360	4.3	27 (1.9)[45]
$n=3$	X=CN	Y=OCH_3	Chloroform	380	4.6	40 (1.9)[45]
$n=2$	X=NO_2	Y=Br	Chloroform	378	3.5	21 (1.9)[45]
$n=3$	X=NO_2	Y=Br	Chloroform	400	3.8	35 (1.9)[45]
$n=2$	X=NO_2	Y=OCH_3	*p*-Dioxane		6.0	135 (1.06)[98]
			Chloroform	397	4.8	47 (1.9)[45]
$n=3$	X=NO_2	Y=OCH_3	*p*-Dioxane		6.6	274 (1.06)[98]
			Chloroform	414	5.1	76 (1.9)[45]
$n=4$	X=NO_2	Y=OCH_3	*p*-Dioxane		6.7	367 (1.06)[98]
			Chloroform	430	5.8	55 (1.9)[45]
$n=5$	X=NO_2	Y=OCH_3	*p*-Dioxane		7.0	623 (1.06)[98]
$n=2$	X=NO_2	Y=SCH_3	Chloroform	398	4.5	101 (1.9)[45]
$n=2$	X=NO_2	Y=$N(CH_3)_2$	Chloroform	442	7.6	107 (1.9)[45]
			p-Dioxane		$\mu\beta = 75 \times 10^{-47}$	(1.9)[107]
$n=3$	X=NO_2	Y=$N(CH_3)_2$	Chloroform	458	8.2	131 (1.9)[45]
$N=4$	X=NO_2	Y=$N(CH_3)_2$	Chloroform	464	9	190 (1.9)[45]
$N=2$	X=C_2HCN_2	Y=$N(CH_3)_2$	DMSO	481	$\mu\beta = 13 \times 10^{-46}$	(1.36)[231]
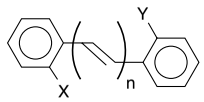						
$n=2$	X=CN	Y=OCH_3	Chloroform	354	3.8	4.5 (1.9)[45]
$n=3$	X=CN	Y=OCH_3	Chloroform	376	3.8	7.1 (1.9)[45]

$n=2$	$X=NO_2$	$Y=OCH_3$	Chloroform	376	3.7		6.4 (1.9)[45]
$n=3$	$X=NO_2$	$Y=OCH_3$	Chloroform	392	4.1		11 (1.9)[45]
$n=2$	$X=OCH_3$	$Y=CN$	Chloroform	356	3.9		2.6 (1.9)[45]
$n=3$	$X=OCH_3$	$Y=CN$	Chloroform	378	3.9		4.3 (1.9)[45]
$n=2$	$X=CN$	$Y=OCH_3$	Chloroform	358	4.9		4.3 (1.9)[45]
$n=2$	$X=OCH_3$	$Y=NO_2$	Chloroform	376	3.8		4.9 (1.9)[45]
$n=3$	$X=OCH_3$	$Y=NO_2$	Chloroform	392	3.8		11 (1.9)[45]
$n=2$	$X=NO_2$	$Y=OCH_3$	Chloroform	380	4.3		17 (1.9)[45]
$n=3$	$X=NO_2$	$Y=OCH_3$	Chloroform	412	4.8		56 (1.9)[45]
			p-Dioxane	480	7.1		98 (1.9)[255]
			p-Dioxane		$\mu\beta = 13\times10^{-46}$		(1.9)[107]
			Chloroform		6.2		71 (1.9)[255]
	α,ω-Diphenylpolyene derivatives						
$n=2$	$X=CN$	$Y=SCH_3$	Chloroform	330	3.7		17 (1.9)[45]
$n=2$	$X=CN$	$Y=NH_2$	NMP	388	$\mu\beta = 11\times10^{-47}$		(1.9)[45]

(continued)

TABLE 7.1 (Continued)

Structure			Solvent	λ_{max}(nm)	μ (10^{-18} esu)	$\beta_{\mu}(\lambda)^{ref.}$ (10^{-30} esu)
$n=2$	$X=NO_2$	$Y=SCH_3$	Chloroform	338	3.9	17 (1.9)[45]
$n=2$	$X=NO_2$	$Y=NH_2$	Chloroform	334	6.3	28 (1.9)[45]
$n=2$	$X=NO_2$	$Y=NH_2$	NMP	416	$\mu\beta=24\times10^{-47}$	(1.9)[45]
$n=3$	$X=NO_2$	$Y=NH_2$	NMP	440	$\mu\beta=41\times10^{-47}$	(1.9)[45]
	Cumulene derivatives					
	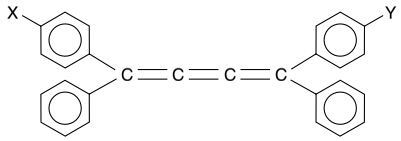					
	$X=NO_2$	$Y=H$	*p*-Dioxane	442	$\mu\beta=15\times10^{-47}$	(1.9)[61]
	$X=NO_2$	$Y=H$	*p*-Dioxane	442	$\mu\beta=66\times10^{-47}$	(1.06)[61]
	$X=NO_2$	$Y=CH_3$	*p*-Dioxane	448	$\mu\beta=60\times10^{-47}$	(1.06)[61]
	$X=NO_2$	$Y=OCH_3$	*p*-Dioxane	459	$\mu\beta=85\times10^{-47}$	(1.06)[61]
	$X=NO_2$	$Y=O(CH_2)_{11}CH_3$	*p*-Dioxane	461	$\mu\beta=28\times10^{-47}$	(1.9)[61]
	α,ω-Polyphenyl derivatives					
	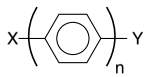					
$n=3$	$X=NO_2$	$Y=OCH_3$	*p*-Dioxane	340	5.0	11 (1.9)[45]
$n=3$	$X=NO_2$	$Y=NH_2$	NMP	360	7.8	24 (1.9)[45]
$n=4$	$X=NO_2$	$Y=NH_2$	NMP	344	7.6	16 (1.9)[45]
	Pyrrol derivatives					
	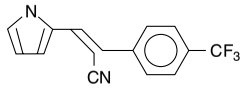		*p*-dioxane	376	5.8	11 (1.06)[244]
	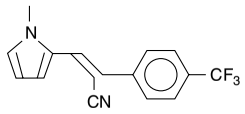		*p*-dioxane	381	7.2	12 (1.06)[244]

15018—Chapter7—26/8/2006—22:15—SJAPPIYAR—15018—XML MODEL CRC12a – pp. 1–126.

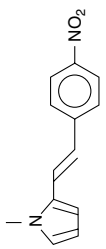	*p*-dioxane	410	5.5	26 (1.9)[43]	
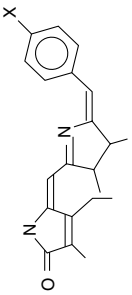					
X = OCH_3	DMSO	485	1.4	32 (1.9S)[64]	
X = $N(CH_3)_2$	DMSO	553	1.2	439 (1.9S)[64]	
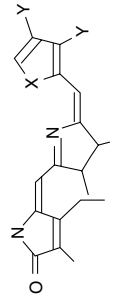					
Y = CH_3	DMSO	539	3.7	20 (1.9S)[64]	
Y = H	DMSO	493	2.5	10 (1.9S)[64]	
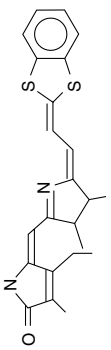					
X = NH	DMSO	553	2.5	578 (1.9S)[64]	
X = S					
Furan derivatives					
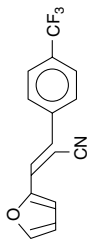	*p*-Dioxane	345	5.7	7.7 (1.06)[244]	
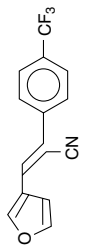	*p*-Dioxane	314	5.4	7.1 (1.06)[244]	

(*continued*)

TABLE 7.1 (Continued)

Structure	Solvent	λ_{max}(nm)	μ (10^{-18} esu)	$\beta_\mu(\lambda)^{ref.}$ (10^{-30} esu)
	Chloroform	478	6.9	83 (1.9)[45]
	Chloroform		5.9	173 (1.9)[43]
	Chloroform	488	7.2	113 (1.9)[45]
	Chloroform	400	5.2	40 (1.9)[45]
Thiophene derivatives				
	Chloroform	351	5.2	20 (1.06)[117]
	Chloroform	382	5.4	67 (1.06)[117]

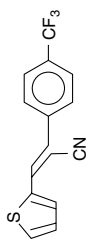	*p*-Dioxane	346	6.8	6.6 (1.06)[244]
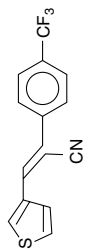	*p*-Dioxane	321	6.7	5.4 (1.06)[244]
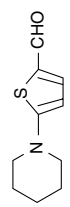	Chloroform		5.8	7.5 (1.9)[43]
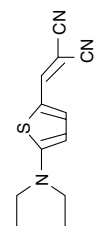	Chloroform		9.0	21 (1.9)[43]
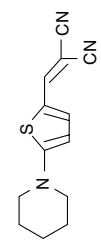	Chloroform		8.8	21 (1.9)[43]
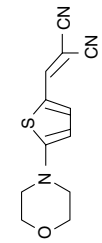	Chloroform		5.9	23 (1.9)[43]

(continued)

TABLE 7.1 (Continued)

Structure	Solvent	λ_{max}(nm)	μ (10^{-18} esu)	$\beta_\mu(\lambda)^{ref.}$ (10^{-30} esu)
	In PMMA	510	$\mu\beta_0 = 60\times10^{-47}$ (from EO at 633 nm)[165]	
	In PMMA	499	$\mu\beta_0 = 26\times10^{-47}$ (from EO at 633 nm)[165]	
	Chloroform		3.7	30 (1.9)[43]
	Chloroform	492	7.4	98 (1.9)[45]
	p-Dioxane	478	$\mu\beta = 60\times10^{-47}$	(1.9)[203]
	Chloroform		7.0	197 (1.9)[43]

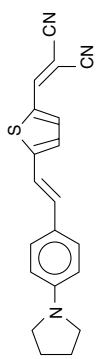	*p*-Dioxane	584	$\mu\beta = 26\times10^{-46}$	(1.9)[106]		
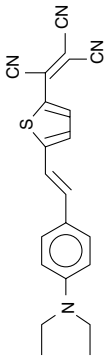	*p*-Dioxane	640	$\mu\beta = 62\times10^{-46}$	(1.9)[203]		
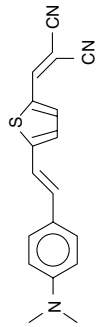	Chloroform		7.5	161 (1.9)[43]		
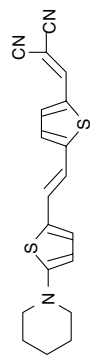	Chloroform		7.6	250 (1.9)[72]		
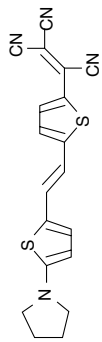	*p*-Dioxane	718	$\mu\beta = 69\times10^{-46}$	(1.9)[203]		
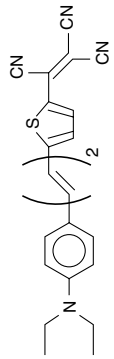	*p*-Dioxane	662	$\mu\beta = 91\times10^{-46}$	(1.9)[203]		
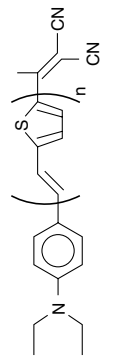	*p*-Dioxane	513	$\mu\beta = 13\times10^{-46}$	(1.9)[106]		
	p-Dioxane	547	$\mu\beta = 23\times10^{-46}$	(1.9)[106]		
	p-Dioxane	556	$\mu\beta = 38\times10^{-46}$	(1.9)[106]		

n = 1
n = 2
n = 3

(continued)

TABLE 7.1 (Continued)

Structure			Solvent	λ_{max}(nm)	μ (10^{-18} esu)	$\beta_{\mu}(\lambda)^{ref.}$ (10^{-30} esu)
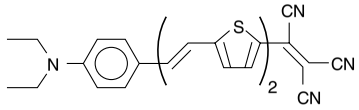			*p*-dioxane	653	$\mu\beta = 74 \times 10^{-46}$	$(1.9)^{203}$
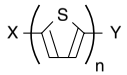						
$n=1$	$X=NO_2$	$Y=OCH_3$	CCl_4	349	5.5	7.6 $(1.06)^{271}$
$n=2$	$X=NO_2$	Y=H	$C_6H_{11}CH_3$	378	5.0	19 $(1.06)^{271}$
$n=2$	$X=NO_2$	$Y=OCH_3$	$C_6H_{11}CH_3$	411	6.0	41 $(1.06)^{271}$
$n=2$	$X=NO_2$	$Y=OCH_3$	CCl_4	418	6.0	46 $(1.06)^{271}$
$n=2$	$X=NO_2$	$Y=SCH_3$	$C_6H_{11}CH_3$	394	5.0	49 $(1.06)^{271}$
$n=2$	$X=NO_2$	$Y=N(CH_3)_2$	$C_6H_{11}CH_3$	472	8.0	319 $(1.06)^{271}$
$n=3$	$X=NO_2$	$Y=OCH_3$	CCl_4	452	6.0	162 $(1.06)^{271}$
	Azole derivatives					
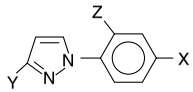						
$X=NO_2$	$Y=CH_3OC_6H_4$	Z=H	*p*-Dioxane	354	6.6	31 $(1.06)^{166}$
$X=NO_2$	$Y=C_6H_5CH–CH–$	Z=H	*p*-Dioxane	346	6.1	32 $(1.06)^{166}$
$X=NO_2$	$Y=p\text{-}CH_3OC_6H_4CH–CH–$	Z=H	*p*-Dioxane	368	5.7	40 $(1.06)^{166}$
$X=SO_2CH_3$	$Y=p\text{-}CH_3OC_6H_4CH–CH–$	Z=H	*p*-Dioxane	330	5.6	16 $(1.06)^{166}$
$X=NO_2$	$Y=p\text{-}CH_3SC_6H_4CH–CH–$	$Z=NO_2$	*p*-Dioxane	354	4.1	42 $(1.06)^{166}$
$X=CH_3O$	$Y=p\text{-}O_2NC_6H_4CH–H–$	Z=H	*p*-Dioxane	370	7.0	48 $(1.06)^{166}$

15018—Chapter7—26/8/2006—22:17—SJAPPIYAR—15018—XML MODEL CRC12a – pp. 1–126.

$X=NO_2$	$Y=p\text{-}CH_3OC_6H_4C{\equiv}C\text{–}$	$Z=H$	*p*-dioxane	340	5.6	20 (1.06)[166]	
$X=NO_2$	$Y=p\text{-}CH_3OC_6H_4CH\text{–}CH\text{–}$	$Z=H$	*p*-Dioxane	358	5.1	63 (1.06)[166]	

$X=NO_2$	$Y=CH_3OC_6H_4$	$Z=H$	*p*-Dioxane	306	6.3	13 (1.06)[166]	
$X=NO_2$	$Y=C_6H_5CH=CH\text{–}$	$Z=H$	*p*-Dioxane	298	4.6	7 (1.06)[166]	
$X=NO_2$	$Y=p\text{-}CH_3OC_6H_4CH=CH\text{–}$	$Z=H$	*p*-Dioxane	302	5.5	14 (1.06)[166]	
$X=NO_2$	$Y=p\text{-}CH_3SC_6H_4CH=CH\text{–}$	$Z=NO_2$	*p*-Dioxane	312	3.3	12 (1.06)[166]	

$X=NO_2$	$Y=p\text{-}(CH_2)_6N$	$Z=N$	Chloroform	476	8.3	79 (1.9)[176]	
$X=NO_2$	$Y=p\text{-}CH_3OC_6H_4C{\equiv}C\text{–}$	$Z=N$	*p*-Dioxane	344	8.0	53 (1.06)[176]	
$X=NO_2$	$Y=p\text{-}(CH_2)_5N$	$Z=N$	Chloroform	438	7.2	46 (1.9)[176]	
$X=O_2NC_6H_4C{\equiv}$ C-	$Y=p\text{-}CH_3OC_6H_4$	$Z=N$	*p*-Dioxane	400	8.1	69 (1.06)[176]	
$X=NO_2$	$Y=p\text{-}CH_3OC_6H_4S$	$Z=N$	*p*-Dioxane	398	6.6	56 (1.06)[176]	
$X=NO_2$	$Y=p\text{-}CH_3OC_6H_4$	$Z=N$	*p*-Dioxane	410	7.0	52 (1.06)[176]	
$X=NO_2$	$Y=p\text{-}C_4H_9CH(C_2H_5)CH_2OC_6H_4$	$Z=N$	Chloroform	416	6.3	25 (1.9)[176]	
$X=NO_2$	$Y=p\text{-}CH_3OC_6H_4$	$Z=N$	Chloroform	412	6.4	20 (1.9)[176]	
$X=SO_2C_4F_9$	$Y=p\text{-}C_4H_9CH(C_2H_5)CH_2OC_6H_4$	$Z=N$	Chloroform	384	6.5	14 (1.9)[176]	
$X=SO_2C_6H_5$	$Y=p\text{-}CH_3OC_6H_4$	$Z=N$	*p*-Dioxane	362	8.0	10 (1.06)[176]	
$X=O_2NC_6H_4C{\equiv}\text{-}$	$Y=p\text{-}CH_3OC_6H_4$	$Z=O$	*p*-Dioxane	378	7.1	64 (1.06)[176]	
$X=SO_2\text{-}C_6H_4CF_3$	$Y=p\text{-}CH_3OC_6H_4$	$Z=O$	Chloroform	370	8.0	32 (1.06)[176]	

(continued)

TABLE 7.1 (Continued)

	Structure		Solvent	λ_{max}(nm)	μ (10^{-18} esu)	$\beta_\mu(\lambda)^{ref.}$ (10^{-30} esu)
X=NO_2	Y=*p*-$CH_3OC_6H_4$	Z=O	*p*-Dioxane	390	6.3	47 (1.06)[176]
X=$SO_2C_4F_9$	Y=*p*-$CH_3OC_6H_4$	Z=O	*p*-Dioxane	378	7.9	31 (1.06)[176]
X=$SO_2C_6H_5$	Y=*p*-$CH_3OC_6H_4$	Z=O	*p*-Dioxane	358	7.0	17 (1.06)[176]
X=SO_2CH_3	Y=*p*-$CH_3OC_6H_4$	Z=O	*p*-Dioxane	352	7.0	15 (1.06)[176]
X=C_6F_{16}	Y=*p*-$CH_3OC_6H_4$	Z=O	*p*-Dioxane	344	5.7	13 (1.06)[176]
X=CF_3	Y=*p*-$CH_3OC_6H_4$	Z=O	*p*-Dioxane	338	5.3	9 (1.06)[176]
X=NO_2	Y=*p*-$CH_3OC_6H_4$	Z=S		400	8.1	21 (β_0)[176]
			Chloroform	564	6.2	71 (1.9)[43]
			Chloroform	578	6.1	83 (1.9)[43]
			Chloroform	596	6.5	75 (1.9)[43]
			CH_2Cl_2	579	8.5	260 (1.58)[54]

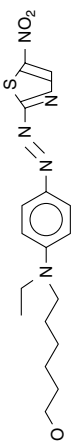	Chloroform	582	9.0	52 (β_0)[177]
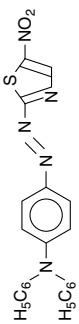	Chloroform	582	6.9	68 (β_0)[177]
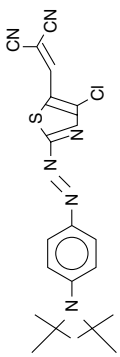	CH_2Cl_2	645	10	530 (1.58)[54]
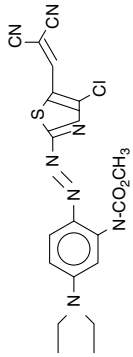	Chloroform	634	6.9	100 (1.9)[43]
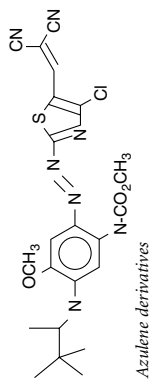	Chloroform	670	6.9	130 (1.9)[43]
Azulene derivatives				
	Chloroform		1.2	< 1 (1.9)[43]
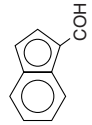	Chloroform		2.5	< 1 (1.9)[43]

(*continued*)

TABLE 7.1 (Continued)

Structure	Solvent	λ_{max}(nm)	μ (10^{-18} esu)	$\beta_\mu(\lambda)^{ref.}$ (10^{-30} esu)
Pentafulvene derivatives				
	Chloroform	4		<1 (1.9)[43]
	Chloroform	1		7 (1.9)[43]
	Chloroform	1		5 (1.9)[43]
	Chloroform	2		10 (1.9)[43]
	Chloroform		3	30 (1.9)[43]
	DMSO	420	$\mu\beta = 44\times10^{-47}$	(1.06)[102]
	DMSO	370	$\mu\beta = 70\times10^{-48}$	(1.06)[102]

Chloroform		3.6		74 (1.9)[43]	
DMSO	450	$\mu\beta = 20 \times 10^{-46}$		(1.06)[102]	
Chloroform		$\mu\beta = 73 \times 10^{-47}$		(1.9)[43]	
Chloroform		4.0		0.9 (1.9)[43]	
Chloroform		3.5		4.6 (1.9)[43]	
Methanol	444	26		−100 (1.3)[144]	
Pyridine	606	17		−210 (1.3)[144]	
DMSO	570	8		1000 (1.9)[57]	
Chloroform	590	4.0		190 (1.9)[153]	

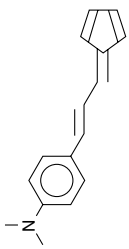

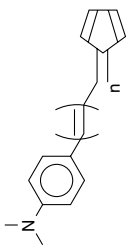

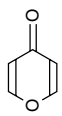

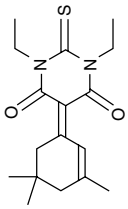

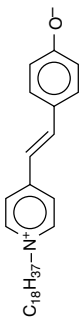

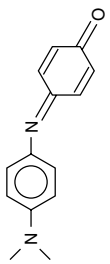

(*continued*)

TABLE 7.1 (Continued)

Structure	Solvent	λ_{max}(nm)	μ (10^{-18} esu)	$\beta_{\mu}(\lambda)^{ref.}$ (10^{-30} esu)
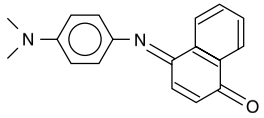	Chloroform	580	4.0	79 (1.9)[153]
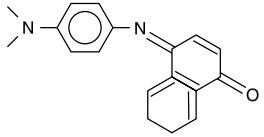	Chloroform	610	4.3	91 (1.9)[153]
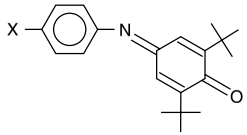				
X=H	Chloroform	428	1.5	5.9 (1.9)[154]
X=Br	Chloroform	432	1.3	13 (1.9)[154]
X=OCH_3	Chloroform	469	2.4	17 (1.9)[154]
X=OCH_3; *ortho*: OCH_3	Chloroform	498	3.4	19 (1.9)[154]
X=SCH_3	Chloroform	476	2.3	17 (1.9)[154]
X=NH_2	Chloroform	—	3.3	38 (1.9)[154]
X=$N(CH_3)_2$	Chloroform	558	3.9	78 (1.9)[154]
X=CH–CH–C_6H_4–OCH_3	Chloroform	497	2.6	48 (1.9)[154]
X=CH–CH–C_6H_4–$N(CH_3)_2$	Chloroform	512	3.7	116 (1.9)[154]
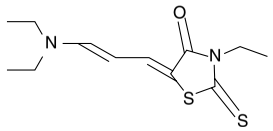	DMSO	470	$\mu\beta = 74\times10^{-47}$	(1.06)[104]
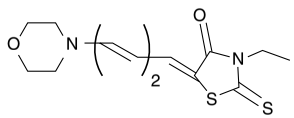	DMSO	550	$\mathrm{Re}(\mu\beta) = 48\times10^{-45}$	(1.06)[104]

					$\mathrm{Im}(\mu\beta) = 61\times10^{-45}$	$(1.06)^{104}$	
		DMSO	550		$\mathrm{Re}(\mu\beta) = 48\times10^{-45}$	$(1.06)^{104}$	
					$\mathrm{Im}(\mu\beta) = 61\times10^{-45}$	$(1.06)^{104}$	
	Y=O	DMSO	390		$\mu\beta = 12\times10^{-47}$	$(1.06)^{103}$	
	Y=S	DMSO	480		$\mathrm{Re}(\mu\beta) = 11\times10^{-46}$	$(1.06)^{103}$	
					$\mathrm{Im}(\mu\beta) = 31\times10^{-47}$	$(1.06)^{103}$	
X=N X=S							
		DMSO	530		$\mathrm{Re}(\mu\beta) = 21\times10^{-45}$	$(1.06)^{104}$	
					$\mathrm{Im}(\mu\beta) = 30\times10^{-45}$	$(1.06)^{104}$	
n=2	X=C(CH$_3$)$_2$	DMSO			$\mathrm{Re}(\mu\beta) = 17\times10^{-45}$	$(1.06)^{104}$	
					$\mathrm{Im}(\mu\beta) = 24\times10^{-45}$	$(1.06)^{104}$	
n=3	X=S	DMSO			$\mathrm{Re}(\mu\beta) = 13\times10^{-45}$	$(1.06)^{104}$	
					$\mathrm{Im}(\mu\beta) = 23\times10^{-45}$	$(1.06)^{104}$	
n=3	X=C–CH$_2$	DMSO			$\mathrm{Re}(\mu\beta) = 20\times10^{-45}$	$(1.06)^{104}$	
					$\mathrm{Im}(\mu\beta) = 27\times10^{-45}$	$(1.06)^{104}$	
n=3	X=O	Chloroform		6.9		360 $(1.9)^{43}$	
n=1	X=S	Chloroform		7.4		−46 $(1.9)^{43}$	

(continued)

TABLE 7.1 (Continued)

Structure				Solvent	λ_{max}(nm)	μ (10^{-18} esu)	$\beta_\mu(\lambda)^{ref.}$ (10^{-30} esu)
$n=2$		X=S		Chloroform		8.9	52 (1.9)[43]
$n=3$		X=S		Chloroform		9.1	300 (1.9)[43]
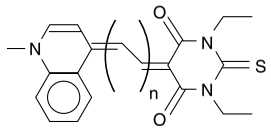				DMSO		$Re(\mu\beta)=13\times10^{-45}$	(1.06)[104]
						$Im(\mu\beta)=15\times10^{-45}$	(1.06)[104]
$n=1$				DMSO		$Re(\mu\beta)=27\times10^{-45}$	(1.06)[104]
$n=3$						$Im(\mu\beta)=49\times10^{-45}$	(1.06)[104]
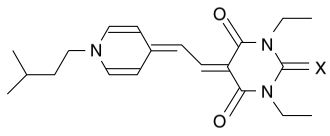							
X=O				Chloroform	510	$\mu\beta=-37\times10^{-47}$	(1.9)[60]
X=S				Chloroform	526	$\mu\beta=-60\times10^{-47}$	(1.9)[60]
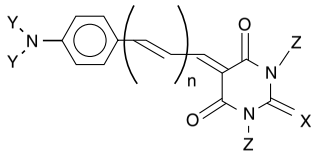							
$n=0$	X=O		Y=CH_3	Z=H	DMSO	470	$\mu\beta=63\times10^{-47}$	(1.06)[103]
$n=0$	X=O		Y=C_2H_5	Z=CH_3	Chloroform	470	6.2	20 (β_0)[177]
$n=0$	X=O		Y=4-$CH_3C_6H_4$	Z=CH_3	Chloroform	486	4.5	40 (β_0)[177]
$n=0$	X=O		Y=CH_3	Z=C_2H_5	Chloroform	464	5.1	47 (1.9)[43]
$n=1$	X=O		Y=CH_3	Z=CH_3	DMSO	540	$Re(\mu\beta)=13\times10^{-46}$	(1.06)[103]
							$Im(\mu\beta)=52\times10^{-46}$	(1.06)[103]

15018—Chapter7—26/8/2006—22:19—SJAPPIYAR—15018—XML MODEL CRC12a – pp. 1–126.

$n=1$	X=O	Y=C_2H_5	Z=C_6H_5	Chloroform	558	7.1	91 $(\beta_0)^{177}$	
$n=1$	X=O	Y=4-$CH_3C_6H_4$	Z=C_6H_5	Chloroform	560	4.0	97 $(\beta_0)^{177}$	
$n=1$	X=O	Y=CH_3	Z=C_2H_5	Chloroform	532	5.1	173 $(1.9)^{43}$	
$n=2$	X=O	Y=CH_3	Z=C_2H_5	Chloroform	554	5.8	338 $(1.9)^{43}$	
$n=3$	X=O	Y=CH_3	Z=C_2H_5	Chloroform	572	5.3	660 $(1.9)^{43}$	
$n=0$	X=S	Y=CH_3	Z=H	DMSO	500	$Re(\mu\beta)=12\times10^{-46}$ $Im(\mu\beta)=60\times10^{-47}$	$(1.06)^{103}$	
$n=0$	X=S	Y=CH_3	Z=C_2H_5	Chloroform	494	6.4	20 $(\beta_0)^{177}$	
				Chloroform	484	5.4	68 $(1.9)^{155}$	
$n=0$	X=S	Y=C_2H_5	Z=C_2H_5	Chloroform	500	7.1	20 $(\beta_0)^{177}$	
$n=0$	X=S	Y=4-$CH_3C_6H_4$	Z=C_2H_5	Chloroform	518	5.2	45 $(\beta_0)^{177}$	
$n=0$	X=S	Y=C_2H_5	Z=C_6H_5	Chloroform	502	7.6	25 $(\beta_0)^{177}$	
$n=0$	X=S	Y=4-$CH_3C_6H_4$	Z=C_6H_5	Chloroform	520	5.7	57 $(\beta_0)^{177}$	
$n=0$	X=S	Y=CH_3	Z=C_6H_5	Chloroform		5.5	58 $(1.9)^{43}$	
$n=0$	X=S	Y=CH_3	Z=4-$NO_2C_6H_4$	Chloroform		9.0	80 $(1.9)^{43}$	
$n=1$	X=S	Y=C_2H_5	Z=C_6H_5	Chloroform	588	8.3	94 $(\beta_0)^{177}$	
$n=1$	X=S	Y=4-$CH_3C_6H_4$	Z=C_6H_5	Chloroform	594	6.5	119 $(\beta_0)^{177}$	
$n=1$	X=S	Y=CH_3	Z=C_2H_5	Chloroform	572	5.7	256 $(1.9)^{155}$	
$n=2$	X=S	Y=CH_3	Z=C_2H_5	Chloroform	604	6.2	636 $(1.9)^{155}$	
$n=3$	X=S	Y=CH_3	Z=C_2H_5	Chloroform	624	6.6	1490 $(1.9)^{155}$	
				Chloroform		4.2	299 $(1.9)^{43}$	

(continued)

TABLE 7.1 (Continued)

Structure		Solvent	λ_{max}(nm)	μ (10^{-18} esu)	$\beta_{\mu}(\lambda)^{ref.}$ (10^{-30} esu)
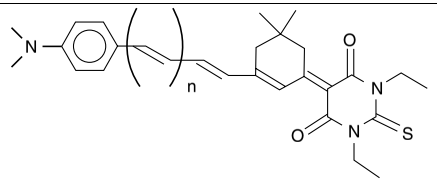					
$n=2$		Chloroform		6.8	630 (1.9)[43]
$n=3$		Chloroform		7.2	771 (1.9)[43]
$n=4$		Chloroform		7.5	893 (1.9)[43]
		Chloroform		$\mu\beta=71\times10^{-46}$	(1.9)[43]
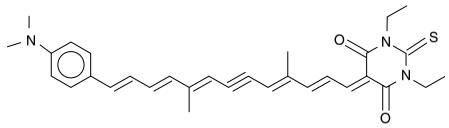					
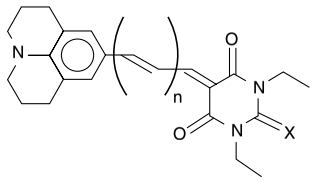					
$n=0$	X=O	Chloroform	480	5.7	64 (1.9)[43]
$n=1$	X=O	Chloroform	574	5.9	213 (1.9)[43]
$n=2$	X=O	Chloroform	616	6.5	504 (1.9)[43]
$n=3$	X=O	Chloroform		7.1	935 (1.9)[43]
$n=0$	X=S	Chloroform	522	7.0	87 (1.9)[155]
$n=1$	X=S	Chloroform	614	6.6	355 (1.9)[155]

15018—Chapter7—26/8/2006—22:20—SJAPPIYAR—15018—XML MODEL CRC12a – pp. 1–126.

X=S	Chloroform	680	6.3		1141 (1.9)[155]	
X=S	Chloroform	686	8.8		2169 (1.9)[155]	
	Chloroform			$\mu\beta = 19\times10^{-45}$	(1.9)[43]	
	Chloroform			$\mu\beta = 12\times10^{-45}$	(1.9)[43]	
	Chloroform	680		$\mu\beta = 35\times10^{-46}$	(1.9)[155]	
	Chloroform		7.9		11 (1.9)[43]	
	Chloroform		7.5		13 (1.9)[43]	
	Chloroform		5.5		14 (1.9)[43]	

(continued)

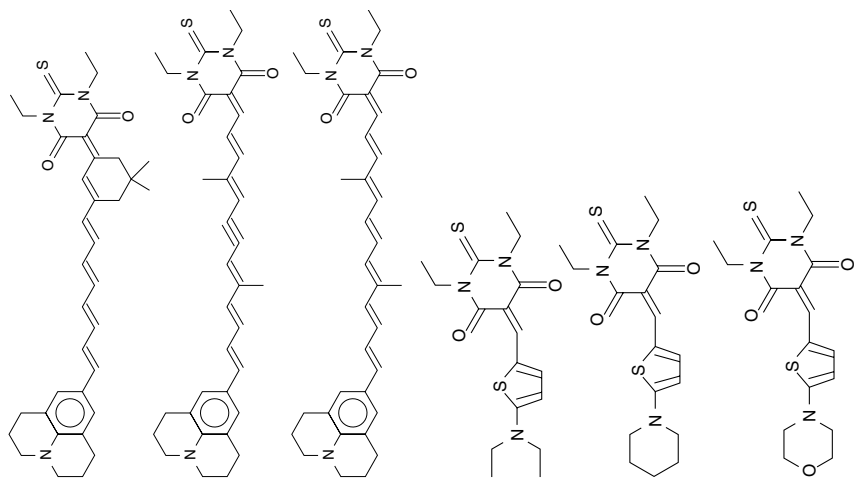

n=2
n=3

TABLE 7.1 (Continued)

Structure	Solvent	λ_{max}(nm)	μ (10^{-18} esu)	$\beta_{\mu}(\lambda)^{ref.}$ (10^{-30} esu)
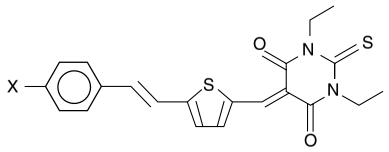				
X=OCH_3	Chloroform		2.7	171 (1.9)[43]
X=$N(CH_3)_2$	Chloroform		5.6	339 (1.9)[43]
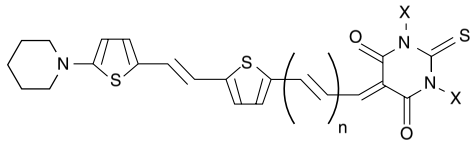				
n=0	X=C_2H_5	Chloroform	$\mu\beta=37\times10^{-46}$	(1.9)[43]
n=1	X=C_2H_5	Chloroform	$\mu\beta=71\times10^{-46}$	(1.9)[43]
n=1	X=C_6H_5	Chloroform	$\mu\beta=86\times10^{-46}$	(1.9)[74]
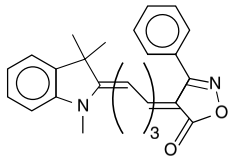		Chloroform	11	280 (1.9)[43]
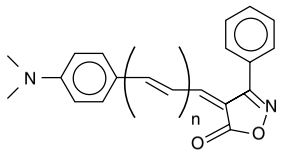				

$n=0$	Chloroform	478	8.3		37 $(1.9)^{155}$
$n=1$	Chloroform	530	8.6		140 $(1.9)^{155}$
$n=2$	Chloroform	562	8.7		362 $(1.9)^{155}$
$n=3$	Chloroform	582	8.9		918 $(1.9)^{155}$
	Chloroform			$\mu\beta=67\times10^{-45}$	$(1.9)^{43}$
$n=0$	Chloroform	504	9.5		51 $(1.9)^{155}$
$n=1$	Chloroform	586	9.1		180 $(1.9)^{155}$
$n=2$	Chloroform	620	9.0		656 $(1.9)^{155}$
$n=3$	Chloroform	640	9.8		995 $(1.9)^{155}$
	Chloroform	647		$\mu\beta=29\times10^{-45}$	$(1.9)^{155}$
	Chloroform		6.5		46 $(1.9)^{43}$

(continued)

TABLE 7.1 (Continued)

Structure		Solvent	λ_{max}(nm)	μ (10^{-18} esu)	$\beta_\mu(\lambda)^{ref.}$ (10^{-30} esu)
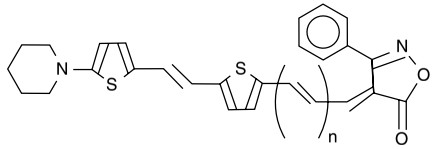					
$n=0$		Chloroform		$\mu\beta=25\times10^{-46}$	$(1.9)^{72}$
$n=1$		Chloroform		$\mu\beta=41\times10^{-46}$	$(1.9)^{72}$
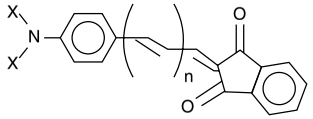		Chloroform		4.4	500 $(1.9)^{43}$
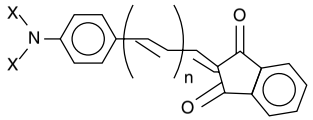					
$n=0$	$X=C_2H_5$	Chloroform	490	3.7	38 $(\beta_0)^{177}$
$n=0$	X=4-$CH_3C_5H_4$	Chloroform	498	2.0	64 $(\beta_0)^{177}$
$n=0$	$X=CH_3$	Chloroform		3.7	58 $(1.9)^{43}$
$n=1$	$X=C_2H_5$	Chloroform	552	4.4	92 $(\beta_0)^{177}$
$n=1$	X=4-$CH_3C_5H_4$	Chloroform	544	2.0	93 $(\beta_0)^{177}$
$n=1$	$X=CH_3$	Chloroform		3.6	191 $(1.9)^{43}$
$n=2$	$X=CH_3$	Chloroform		4.9	266 $(1.9)^{43}$

15018—Chapter7—26/8/2006—22:21—SJAPPIYAR—15018—XML MODEL CRC12a – pp. 1–126.

$n=3$	$X=CH_3$	Chloroform		5.3	347 (1.9)[43]
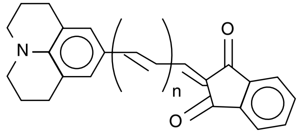					
$n=0$		Chloroform		4.0	104 (1.9)[43]
$n=1$		Chloroform		4.5	215 (1.9)[43]
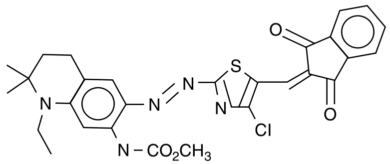		Chloroform	670	6.1	84 (1.9)[43]
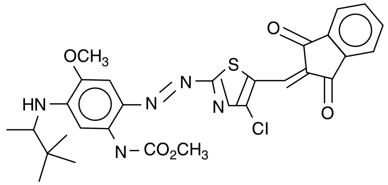		Chloroform	680	6.6	118 (1.9)[43]
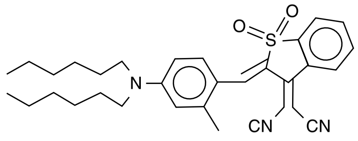		DMSO	620	6.8	163 (1.58)[34] −118 (0.95)[34]

(continued)

TABLE 7.1 (Continued)

Structure	Solvent	λ_{max}(nm)	μ (10^{-18} esu)	$\beta_\mu(\lambda)^{ref.}$ (10^{-30} esu)
$n=0$	Chloroform	5.0		98 (1.9)[43]
$n=1$	Chloroform	6.0		264 (1.9)[43]
$n=2$	Chloroform	6.9		466 (1.9)[43]
$n=3$	Chloroform	6.5		750 (1.9)[43]
$n=0$	Chloroform	6.3		124 (1.9)[43]
$n=1$	Chloroform	6.1		268 (1.9)[43]
$n=2$	Chloroform	6.8		534 (1.9)[43]
	Chloroform	5.0		98 (1.9)[43]
	Chloroform	5.6		64 (1.9)[43]

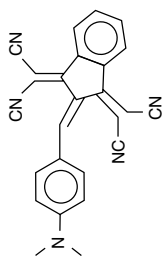	Chloroform	6.7	97 (1.9)[43]	
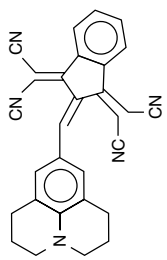	Chloroform	8.0	89 (1.9)[43]	
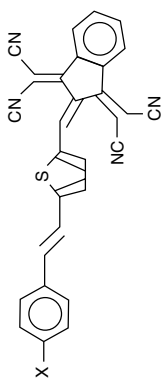	Chloroform Chloroform	6.0 6.0	165 (1.9)[43] 1024 (1.9)[43]	
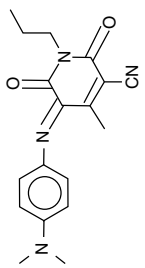	Chloroform	7.8	169 (1.9)[43]	
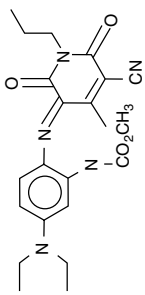	Chloroform	7.7	83 (1.9)[43]	

(continued)

TABLE 7.1 (Continued)

Structure	Solvent	λ_{max}(nm)	μ (10^{-18} esu)	$\beta_{\mu}(\lambda)^{ref.}$ (10^{-30} esu)
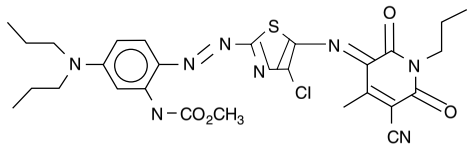	Chloroform	696	8.1	432 (1.9)[43]
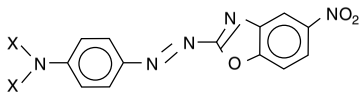				
$X=C_2H_5$; $X=HO(CH_2)_6$	Chloroform	548	9.5	60 (β_0)[177]
$X=4\text{-}CH_3C_5H_4$	Chloroform	550	7.2	72 (β_0)[177]
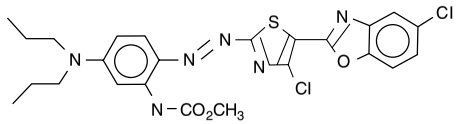	Chloroform		5.5	164 (1.9)[43]
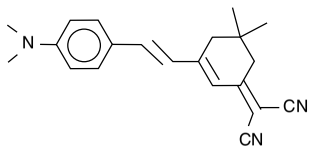	Chloroform		8.7	129 (1.9)[43]
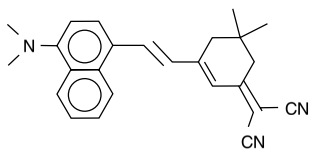	Chloroform		7.0	87 (1.9)[43]

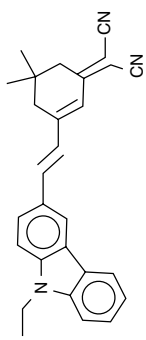	Chloroform	7.5	93 (1.9)[43]
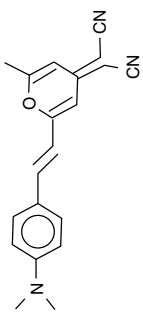	Chloroform	8.6	82 (1.9)[43]
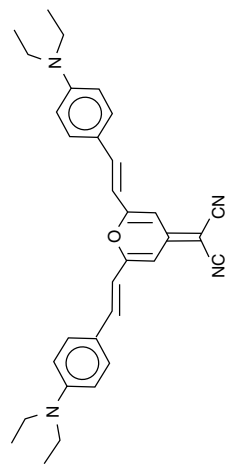	Chloroform	7.9	102 (1.9)[43]
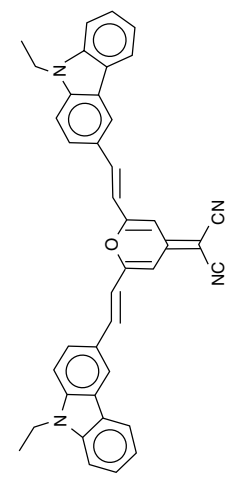	Chloroform	8.5	95 (1.9)[43]

15018—Chapter7—26/8/2006—22:22—SJAPPIYAR—15018—XML MODEL CRC12a – pp. 1–126.

TABLE 7.2 Single Crystal Results on Organic Nonlinear Materials: n_i, refractive index at 633 nm; $\lambda_{NC}(\theta)$, θ-noncritical phase-matching wavelength; $\lambda_{NC}(\lambda)$, λ-noncritical phase-matching wavelength; and at 1.064 μm: DT(τ), optical damage threshold (pulse duration); d_{eff}, effective nonlinearity (phase-matching type); $\Delta\theta l$, angular acceptance; ΔTl, temperature acceptance; $d\theta_{pm}/dT$, temperature tuning of phase-matching angle; and ρ, walk-off angle (phase-matching type)

Abstract

Structure and Nomenclature (acronym)	Point Group	SHG $d_{ij}(\lambda)$ & EO $r_{ij}(\lambda)$ (pm/v) (μm)	Cut-Off λ (nm)	Ref.	Properties
 Urea	*m*	$d_{36}(1.06) \approx 1.3$ $r_{41}(0.63) \approx 1.9$ $r_{63}(0.63) \approx 0.83$	200 & 1800	212 80 18,21, 172	DT(10 ns) = 5 GW/cm^2. $n_o = 1.485$, $n_e = 1.567$.
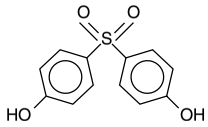 *p*,*p*′-Dihydroxydiphenyl sulfone (DHDPS)	*mm*2	$d_{33}(1.06) \approx 7$ $d_{32}(1.06) \approx 0.4$ $D_{11}(1.06) \approx 3$	300 & 1500	275	Relatively high hardness, nonhygroscopic, and photochemically stable. Crystals cleave at input power > 400 MW/cm^2, $n_x = 2.009$, $n_y = 2.000$, $n_z = 1.921$. $\lambda_{NC}(\theta) = 865$ nm.
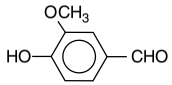 3-Methoxy-4-hydroxy-benzaldehyde (MHBA)	2	$d_{13}(1.06) \approx 13$ $d_{11}(1.06) \approx 9.8$ $d_{12}(1.06) \approx 3.9$ $d_{14}(1.06) \approx 3.2$	370	248 286	DT(10 ns) = 2 GW/cm^2. $n_x = 1.545$, $n_y = 1.685$, $n_z = 1.780$. $\Delta\theta l = 0.9$ mrad-cm. $\rho = 6°$
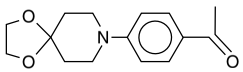 8-(4′-Acetylphenyl)-1,4-dioxa-8-azaspiro[4,5]decane(APDA)	*mm*2	$d_{33}(1.06) \approx 50$ $d_{32}(1.06) \approx 7$	384	217	$n_x = 1.56$, $n_y = 1.66$, $n_z = 1.68$. $d_{eff}(1.06) \approx 14.9$ pm/V.
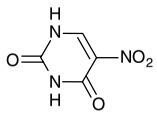 5-Nitrouracil (5NU)	222	$d_{14}(1.06) \approx 8.7$	410 & 1550	201	Relatively transparent at near IR, DT(10 ns) = 3 GW/cm^2. $n_x = 1.569$, $n_y = 1.901$, $n_z = 1.707$. $\Delta\theta l = 8$ mrad-cm, $\rho = 7°$, $\lambda_{NC}(\lambda) = 1440$ nm.

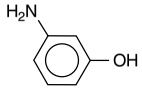 *m*-Aminophenol (*m*AP)	*mm*2	$d_{33}(1.06) \approx 3.3$ $d_{32}(1.06) \approx 2.4$ $d_{31}(1.06) \approx 0.7$	320 & 1700	36	Poor mechanical strength, $n_x = 1.659$, $n_y = 1.765$, $n_z = 1.578$.
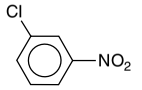 *m*-Chloronitrobenzene (*m*CNB)	*mm*2	$d_{33}(1.06) \approx 7.8$ $d_{32}(1.06) \approx 4$ $d_{31}(1.06) \approx 4.5$	400 & 2000	36	Cleaves easily, not phase-matchable for SHG at 1.064 μm, $n_x = 1.676$, $n_y = 1.684$, $n_z = 1.649$.
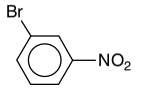 *m*-Bromonitrobenzene (*m*BNB)	*mm*2	$d_{33}(1.06) \approx 8$ $d_{32}(1.06) \approx 4.5$ $d_{31}(1.06) \approx 4$	420 & 2100	36	$\lambda_{NC}(\theta)$ at 1.064 μm for solid solution of $mC_{0.95}Br_{0.05}NB$, $n_x = 1.649$, $n_y = 1.729$, $n_z = 1.678$.
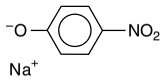 4-Nitrophenol sodium dihydrate (NPNa)	*mm*2	Type I $d_{eff}(1.06) \approx 8$	515	167	Vickers hardness: 34, good thermal conductivity.
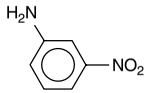 *m*-Nitroaniline (*m*NA)	*mm*2	$d_{33}(1.06) \approx 20$ $d_{32}(1.06) \approx 1.5$ $d_{31}(1.06) \approx 20$ $r_{33}(0.63) \approx 17$ $r_{23}(0.63) \approx 0.1$ $r_{13}(0.63) \approx 7.5$	500 & 1900	256 36 240	Cleaves easily, melt grown into channel waveguide (unfavourable orientation for SHG), $n_x = 1.752$, $n_y = 1.715$, $n_z = 1.665$.
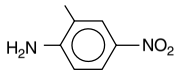 2-Methyl-4-nitroaniline (MNA)	*m*	$d_{11}(1.06) \approx 167$ $d_{12}(1.06) \approx 25$ $r_{11}(0.63) \approx 67$	500 & 1900	143 170 181 150	Melt grown into channel waveguide (orientation controlled by electric or temperature gradients). DT(20 ns) = 0.2 GW/cm^2. $n_x = 2.001$, $n_y = 1.658$, $n_z = 1.435$, near optimum molecular alignment for EO.

(continued)

15018—Chapter7—26/8/2006—22:23—SJAPPIYAR—15018—XML MODEL CRC12a – pp. 1–126.

15018—Chapter7—26/8/2006—22:23—SJAPPIYAR—15018—XML MODEL CRC12a – pp. 1–126.

TABLE 7.2 (Continued)

Structure and Nomenclature (acronym)	Point Group	SHG $d_{ij}(\lambda)$ & EO $r_{ij}(\lambda)$ (pm/v) (μm)	Cut-Off λ (nm)	Ref.	Properties
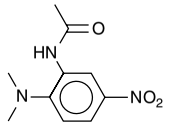 4-(*N*,*N*-dimethylamino)-3-acetamidonitrobenzene (DAN)	2	$d_{21}(1.06) \approx 1.5$ $d_{22}(1.06) \approx 5.2$ $d_{23}(1.06) \approx 50$ $d_{25}(1.06) \approx 1.5$ $r_{11}(0.63) \approx 13$	485 & 2270	121 122 123	Fiber waveguide allows full use of nonzero d_{ij}, DT(15 ns) = 80 MW/cm^2 $d_{eff} \approx 35.5$ (I) & 9 (II) pm/v. $n_x = 1.539$, $n_y = 1.682$, $n_z = 1.949$. $\Delta\theta l \approx 1.5$ mrad-cm.
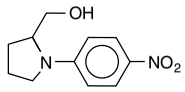 *N*-(4-nitrophenyl)-(*s*)-prolinol (NPP)	2	$d_{22}(1.06) \approx 28$ $d_{21}(1.06) \approx 85$	500 & 2000	289 138	Near optimum molecular alignment for largest d_{21}. $n_x = 2.066$, $n_y = 1.876$, $n_z = 1.478$. $\lambda_{NC}(\theta) = 1.15$ μm using d_{21} $\lambda_{NC}(\lambda) = 1.5$ μm.
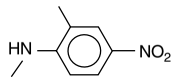 2-Methyl-4-nitro-*N*-methylaniline (MNMA)	*mm*2	$d_{33}(1.06) \approx 2.6$ $d_{31}(1.06) \approx 13$ $d_{15}(1.06) \approx 12$ $r_{13}(0.63) \approx 8$ $r_{33}(0.63) \approx 7.5$	510	245	$n_x = 2.148$, $n_x = 1.520$.
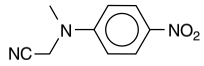 *N*-(4-nitrophenyl)-*N*-aminoacetonitrile (NPAN)	*mm*2	$d_{33}(1.06) \approx 27$ $d_{32}(1.06) \approx 57$ $d_{33}(1.34) \approx 24$ $d_{32}(1.34) \approx 48$	500	171 15	Near optimum molecular alignment for largest d_{32}. $\Delta\theta l \approx 2$ mrad-cm. $\Delta T1 \approx 5$°C-cm
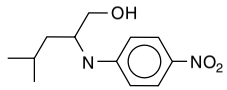 L-*N*-(5-nitro-2-pyridyl)leucinol(NPLO)	2	Type I: $d_{eff}(1.06) \approx 37$ Type II: $d_{eff}(1.06) \approx 3$	480	263	Vickers hardness: 34, nonhygroscopic, DT(8 ns) = 6 GW/cm^2. $n_x = 1.457$, $n_y = 1.631$, $n_z = 1.933$. $\rho = 0.22$ (I) & 0.24 (I) mrad.

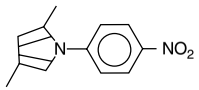 3,5-Dimethyl-1-(4-nitrophenyl) pyrazole (DMNP)	*mm*2	$d_{33}(0.84) \approx 29$ $d_{32}(0.84) \approx 90$	450	83 100	(100) oriented core fibers allow full use of d32, $\lambda_{NC}(\theta) = 944$ nm using d_{32}.
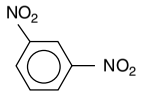 *m*-Dinitrobenzene (*m*DB)	*mm*2	$d_{33}(1.06) \approx 0.7$ $d_{32}(1.06) \approx 2.7$ $d_{31}(1.06) \approx 1.8$	400 & 2200	20	$n_x = 1.738$, $n_y = 1.680$, $n_z = 1.483$.
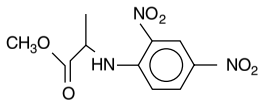 Methyl-(2,4-dinitrophenyl)-aminopropanoate (MAP)	2	$d_{22}(1.06) \approx 18$ $d_{21}(1.06) \approx 17$ $d_{23}(1.06) \approx 3.7$	500 & 2000	192	DT(10 ns) = 3 GW/cm^2. $d_{eff} \approx 3.8$ (I) & 8.8 (II) pm/v. $n_x = 1.531$, $n_y = 1.653$, $n_z = 1.935$. $\Delta\theta l \approx 1.5$ mrad-cm. $\rho = 11.5°$ (I) & 2.4°(I)
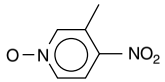 3-Methyl-4-nitropyridine-*N*-oxide (POM)	222	$d_{14}(1.06) \approx 10$ $r_{52}(0.63) \approx 5.2$	450 & 2100	288 230	DT(20 ps) = 2 GW/cm^2. $d_{eff} \approx 7.9$ (I) & 4.0 (II) pm/v. $n_x = 1.663$, $n_y = 1.829$, $n_z = 1.625$. $\rho = 6.3°$ (I) 1.4° (I).
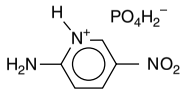 2-Amino-5-nitropyridinium-dihydrogen phosphate (2A5NPDP)	*mm*2	$d_{33}(1.06) \approx 12$ $d_{15}(1.06) \approx 7$ $d_{24}(1.06) \approx 1$	420 & 2000	135	$n_x = 1.752$, $n_y = 1.715$, $n_z = 1.665$. $\lambda_{NC}(\theta) = 1084$ & 1129 nm. $\lambda_{NC}(\lambda) = 1340$ nm. Not phase-matchable for type-II SHG at 1.064 μm. Type-I $d_{eff} \approx 2$ pm/V.. $d\theta_{pm}/dT = 2.4'/°C$ at 1.3 μm.
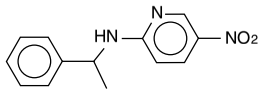 (−)2-(α-Methylbenzylamino)-5-nitropyridine (MBANP)	2	$d_{22}(1.06) \approx 60$[58] $d_{22}(1.06) \approx 35$[57]	430 & 1500	12 11 134	DT(425 ns) = 1 GW/cm^2. $n_y = 1.813$, $n_c = 1.676$. $d_{eff} \approx 1.2 \times LiIO_3 \approx 6$ pm/V.

(continued)

TABLE 7.2 (Continued)

Abstract					
Structure and Nomenclature (acronym)	Point Group	SHG $d_{ij}(\lambda)$ & EO $r_{ij}(\lambda)$ (pm/v) (μm)	Cut-Off λ (nm)	Ref.	Properties
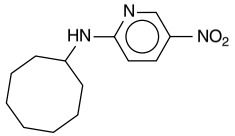 2-*N*-cyclooctylamino-5-nitropyridine (COANP)	*mm*2	$d_{33}(1.06) \approx 14$ $d_{32}(1.06) \approx 32$ $d_{31}(1.06) \approx 15$ $r_{33}(0.63) \approx 15$ $r_{13}(0.63) \approx 3.4$ $r_{23}(0.63) \approx 13$	470	77 26 27	$\lambda_{NC}(\theta) = 1023$ nm using d_{32}. $\lambda_{NC}(\theta) = 1413$ nm using d_{31}. $n_x = 1.68$, $n_y = 1.78$, $n_z = 1.64$. $d_{eff} \approx 24$ pm/V $r_{33}(0.52) \approx 28$, $r_{33}(1.06) \approx 7.7$. $r_{13}(0.52) \approx 6.8$, $r_{13}(1.06) \approx 0.9$. $r_{23}(0.52) \approx 26$, $r_{23}(1.06) \approx 6.3$.
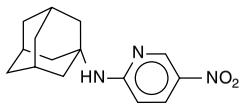 2-Adamantylamino-5-nitropyridine (AANP)	*mm*2	$d_{33}(1.06) \approx 60$ $d_{31}(1.06) \approx 80$	460	257	At 533 nm: $n_x = 1.77$, $n_y = 1.61$, $n_z = 1.86$. At 1.06 μm: $n_x = 1.67$, $n_y = 1.59$, $n_z = 1.71$.
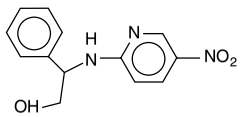 *N*-(4-nitro-2-pyridinyl)-(*s*)-phenylalaninol (NPPA)	2	$d_{22}(1.06) \approx 2.6$ $d_{21}(1.06) \approx 0.4$ $d_{23}(1.06) \approx 31$ $d_{16}(1.06) \approx 0.5$ $d_{34}(1.06) \approx 25$	480	261 247	$\lambda_{NC}(\theta)$ for SHG and SFG within absorption edge, calculated $d_{eff} \approx 31$ pm/V. $n_x = 1.524$, $n_y = 1.694$, $n_z = 1.907$.
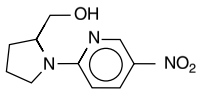 2-(*N*-prolinol)-5-nitropyridine (PNP)	2	$d_{22}(1.06) \approx 17$ $d_{21}(1.06) \approx 48$ $r_{22}(0.63) \approx 13$	490 & 2080	246 27	$\lambda_{NC}(\theta) = 1020$ nm using d_{21}. $d_{eff} \approx 47$ pm/V. $n_x = 1.990$, $n_y = 1.788$, $n_z = 1.467$. $\rho = 7°$ $r_{22}(0.52) \approx 28$, $r_{12}(0.52) \approx 20$. $r_{22}(1.06) \approx 8$, $r_{12}(1.06) \approx 9$.

15018—Chapter7—26/8/2006—22:23—SJAPPIYAR—15018—XML MODEL CRC12a – pp. 1–126.

2-Dicyanovinylanisole (DIVA)	2	$d_{22}(1.06) \approx 10$	78	$d_{eff}(1.06) \approx 20$ pm/V. $n = 1.65$.	
3-(1,1-Dicyanoethenyl)-1-phenyl-4,5-dihydro-1*H*-pyrazole (DCNP)	*m*	$r_{33}(0.63) \approx 87$	700 & 1600	3	High melting point: 190°C, near optimum molecular alignment for EO, $n_x = 1.9$, $n_z = 2.7$.
ω-(*p*-Methoxyphenyl) benzofulvene (MPBF)	*mm2*	$d_{eff}(1.06) \approx 7$	> 450	133	$d_{eff} \approx 7$ pm/V. $\Delta\theta\| = 0.32$ mrad-cm. $\Delta T1 \approx 4.6$°C-cm.
2-Cyano-3-(2-methoxyphenyl)-2-propenoic acid methyl ester (CMP-methyl)	2	$d_{22}(1.06) \approx 29$	410	183	$n_y = 1.85$
p-Methylbenzal-1,3-dimethylbarbituric acid	2	$d_{eff}(1.06) \approx 8$	460	132	Vickers hardness: 25.5.

(continued)

TABLE 7.2 (Continued)

Structure and Nomenclature (acronym)	Point Group	SHG $d_{ij}(\lambda)$ & EO $r_{ij}(\lambda)$ (pm/v) (μm)	Cut-Off λ (nm)	Ref.	Properties
			Abstract		
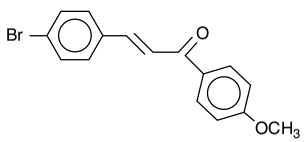 4-Br-4′-methoxychalcone	*m*	$d_{33}(1.06) \approx 6$ $d_{13}(1.06) \approx 27$	420	285	$n_x = 1.55$, $n_y = 1.47$, $n_z = 1.90$.
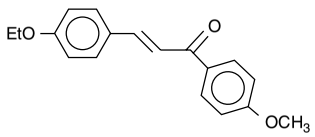 4-Ethoxy-4′-methoxychalcone	*mm*2	$d_{eff}(1.06) \approx 5.7$	430	129	Low hardness, DT(1 ns) > 30 GW/cm^2. At 532 nm: $n_x = 1.493$, $n_y = 1.710$, $n_z = 1.983$. At 1.06 μm: $n_x = 1.477$, $n_y = 1.663$, $n_z = 1.850$. $d_{eff} \approx 3.5$(I) & 5.7 (II) pm/v.
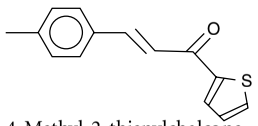 4-Methyl-2-thienylchalcone	2	$d_{eff}(1.06) \approx 7$	430	128	Low hardness, $n_x = 1.648$, $n_y = 1.696$, $n_z = 1.775$. $d_{eff} \approx 7$ pm/V. $\Delta\theta l = 0.9$ mrad-cm. $\rho = 3.6°$ $\Delta T1 = 2.2$°C-cm
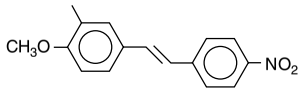 3-Methyl-4-methoxy-4′-nitrostilbene (MMONS)	*mm*2	$d_{33}(1.06) \approx 184$ $d_{32}(1.06) \approx 41$ $d_{24}(1.06) \approx 71$ $r_{33}(0.63) \approx 40$	515 & 2000	22 220	$\lambda_{NC}(\theta) = 1028$ nm using d_{24}. $d_{eff} \approx 43$ pm/V.[71] $n_x = 1.569$, $n_y = 1.693$, $n_z = 2.129$. $\rho = 9.6°$ $\Delta T1 = 0.17$°C-cm

15018—Chapter7—26/8/2006—22:24—SJAPPIYAR—15018—XML MODEL CRC12a – pp. 1–126.

	m	$d_{11}(1.06) \approx 139$ $d_{33}(1.06) \approx 0.6$ $d_{31}(1.06) \approx 41$ $r_{11}(0.63) \approx 25$	480 & 1600	8, 9	Near optimum molecular alignment for EO, $\lambda_{NC}(\theta)$ for SHG within absorption edge, $\lambda_{NC}(\lambda) =$ 1500 nm. $n_x = 1.951$, $n_y = 1.657$, $n_z = 1.510$. $d\Delta n/dT = 15.8 \times 10^{-5}\ K^{-1}$. $d_{eff} \approx 2$ pm/V.
4-Nitro-4′-methylbenzylidiene aniline (NMBA)					
	m	$d_{11}(1.06) \approx 175$ $d_{31}(1.06) \approx 2$ $d_{33}(1.06) \approx 2$ $r_{11}(0.63) \approx 29$ $r_{13}(0.63) \approx 0.5$ $r_{33}(0.63) \approx 2.4$	505	131	Near optimum molecular alignment for EO, $n_x = 2.024$, $n_y = 1.648$, $n_z = 1.583$.
4′-Nitrobenzylidene-3-acetamino-4-methoxylaniline (MNBA)					
	mm2	$d_{33}(1.06) \approx 21$	415	258	Melting point: 279°C, $n_z = 1.775$.
Cyanostilbazolium *p*-toluenesulfonate complex					
	mm2	$r_{33}(0.63) \approx 430$	600	282	Only thin-film cystal reported, $n_y = 1.31$, $n_z = 1.55$.
4′-Dimethyamino-*N*-methyl-4-stilbazolium methyl sulfate (SPCD)					
	m	$d_{11}(1.91) \approx 600$ $d_{22}(1.91) \approx 100$ $d_{12}(1.91) \approx 30$ $r_{33}(0.82) \approx 400$	700 & 2000	157 198	Near optimum molecular alignment for EO. At 820 nm: $n_x = 2.216$, $n_y = 1.66$, $n_z = 1.65$. Dielectric constant: $\varepsilon_{ab} = 5.1$, $\varepsilon_c = 3.1$.
4′-Dimethyamino-*N*-methyl-4-stilbazolium tosulate (DAST)					

TABLE 6.3 Experimental Results of Poled Polymer Studies: M_w, molecular weight; ρ#, chromophore number density; α(wavelength), optical propagation loss; τ_1 and τ_2, relaxation time in $d_{eff}(t)/d_{eff}(0) = Ae^{-t/\tau 1} + Be^{-t/\tau 2}$

Structure and Nomenclature (Ref)	Properties
Guest-host polymer composites 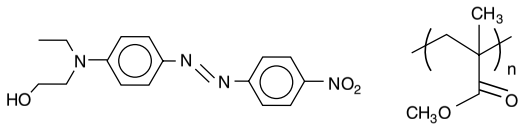 (4[*N*-ehtyl-*N*-(2-hydroxyethyl)]amino-4′-nitroazobenzene) (DR1) doped in poly-(methylmethacrylate) (PMMA) (Singer et al. 1986)	$T_g \approx 100$°C. $\lambda_{max} \approx 470$ nm. $\rho^{\#} = 2.4 \times 10^{20}$ cm^{-3} low dielectric constant: $\varepsilon = 3.6$. contact poled with 62 V/μm at 100°C. d_{33}(1.58 μm) = 2.5 pm/V. Novelty: first study of amorphous guest–host system.
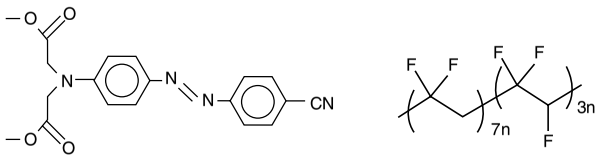 4-(4′-Cyanophenylazo)-*N*,*N*-bis-(methoxycarbonylmethyl)-aniline doped in copolymer of vinylidene fluoride and trifluoroethylene (Foraflon®, 70:30 mol%) (Pantelis et al. 1988; Hill et al. 1987)	$T_g \approx 100$°C. $\lambda_{max} = 400$ nm. UP to 10 wt% doping. α(1 μm) ≈ −1.5 dB/cm. Corona poled at 25°C. d_{33} (1.06 μm) up to 2.6 pm/V. Stable nonlinearity after 300 days at ambient condition. Novelty: ferroelectric host polymer provides a stable internal field of 150 V/μm.
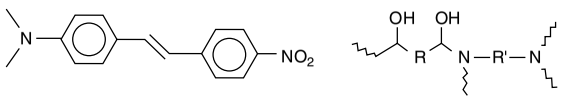 4-*N*,*N*-dimethylamino-4′-nitrostilbene doped in thermosetting epoxy (EPO-TEK® 301-2) (Hubbard et al. 1989)	Precure at 80°C prior to poling. $\lambda_{max} \approx 430$ nm. $\rho^{\#} = 0.2 \times 10^{20}$ cm^{-3} Contact poled at 60 V/μm. Temporal stability: τ_1 (25°C) = 7 days and τ_2 (25°C) = 72 days. Novelty: use of crosslinked polymer as host.
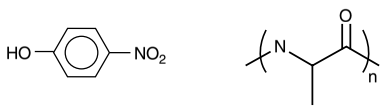 *p*-Nitrophenol doped in type A gelatin (Ho et al. 1992)	$T_g \approx 60$–70°C. $\lambda_{max} < 350$ nm. UP to 35 wt% doping. Spin coating from aqueous solution. Contact poled at 40 V/μm. r_{33} (633 nm) = 10–40 pm/V. 40% activity remains after 5 days. Novelty: use of cross-linked biopolymer as host.

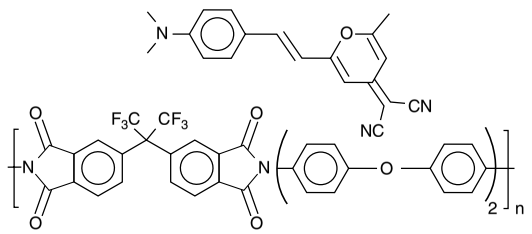

(Dicyanomethylene)-2-methyl-6-(*p*-dimethylaminostyryl-4*H*-pyran (DCM) doped in polymide (Amoco Ultradel®) (Ermer et al. 1992)

T_g = 220°C.
λ_{max} = 474 nm.
Doping level: 20 wt%
n (830 nm) = 1.651
α (830 nm) ≈ −1.5 dB/cm.
Multilayers contact poled with 312 $V/\tilde{\mu}$ 190°C.
r_{33} (830 nm) = 3.4 pm/V.
Low poling field at NLO layer due to high conductivity.
Novelty: use of high T_g host polymer.

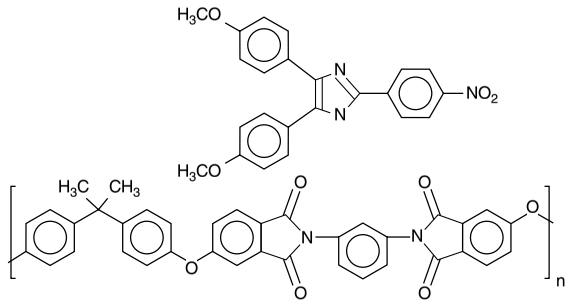

2,4,5-Triarylimidazole derivative (lophine) doped in polyimide (Ultem®) (Stahelin et al. 1992a)

T_g = 210–150°C for 0–35 wt%.
λ_{max} = 410 nm.
Chromophore: μg = 7×10^{-18}, $\beta_0 = 18\times10^{-30}$ (esu).
High loading, up to 35 wt%.
For 0–35 wt% doping, corona poling gives d_{33} (1.047 μm) = 6–17 pm/V.
For 20 wt% doping, corona poling gives T_g = 180°C, d_{33} = 10.5 pm/V., τ (80°C) = 1.5 year.
Novelty: use of thermally stable chromophore.

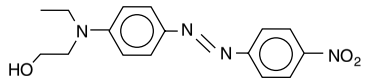

DR1 doped in phenylsiloxane polymer (Allied Signal Accuglass 204®) (Jeng et al. 1992a)

λ_{max} = 493 nm.
n (533 nm) = 1.628.
Doping level: 35 mg dye in 2 g of A204.
Corona poled at 200°C for 10 min.
d_{33} (1.06 μm) = 11.43 pm/V.
d_{33} (40 h, 100°C) = 3.8 pm/V.
Novelty: Use of sol-gel as host polymer.

(continued)

15018—Chapter7—26/8/2006—22:25—SJAPPIYAR—15018—XML MODEL CRC12a – pp. 1–126.

TABLE 6.3 (Continued)

Structure and Nomenclature (Ref)	Properties
Side-Chain acrylate polymers	$T_g = 128–134°C$ for 1–19 mol%. $\lambda_{max} = 470$ nm. $\rho^{\#}$: upto 7.5×10^{20} cm^{-3}. Contact poled with 90 V/μm at 130°C. d_{33} (1.064 μm) = 3–58 pm/V. for 1–19 mol% Novelty: high $\rho^{\#}$.
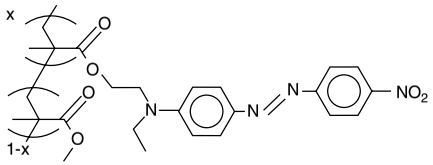 Methylmethacrylate (MMA)/DR1 functionalized methacrylate copolymer (Esselin et al. 1988)	$T_g = 127°C$. $\rho^{\#} = 8 \times 10^{20}$ cm^{-3} n (800 nm) = 1.58. Corona poled above T_g. d_{33} (1.58 μm) = 21 pm/V. r_{33} (799 nm) = 15 pm/V. 90% of activity remains stable after 35 days at ambient conditions.
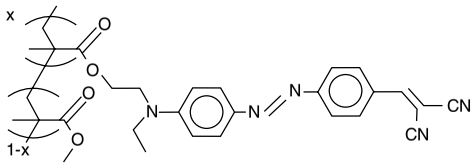 MMA/4-dicyanovinyl-4′-(*N*,*N*-dialkylamino)azobenzene functionalized methacrylate copolymer (Singer et al. 1988)	$T_g = 105°C$. $\lambda_{max} \approx 470$ nm. $M_w = 4.9 \times 10^3$. Contact poling at 190 V/μm gives d_{33} (1.06 μm) = 55 pm/V. Contact poling at 20 V/μm gives r_{33} (633 nm) = 30 pm/V. Activity remains stable for over 2 years at ambient conditions.
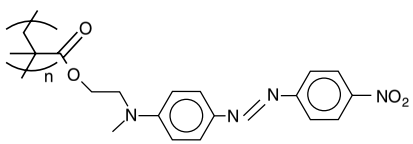 Poly-4-(4′-nitrophenylazo)-*N*-methyl-*N*-(2-acroyloxyethyl)aniline (Hill et al. 1989, 1988)	

15018—Chapter7—26/8/2006—22:25—SJAPPIYAR—15018—XML MODEL CRC12a – pp. 1–126.

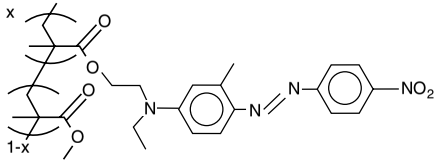

MMA/4-(*N*-ethyl-*N*-2-methacroyloxyethoxy)-2-methyl-4′-nitroazobenzene copolymer (Ore et al. 1989)

λ_{max} = 486 nm.
$M_w = 10 \times 10^3$.
$\rho^{\#} = 9.2 \times 10^{20}$ cm^{-3}
Corona poled d_{33} (1.06 μm) = 41 pm/V.
Stable nonlinearity after 75 days at ambient conditions.

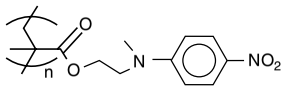

Poly-*N*-(2-methacroyloxyethyl)-*N*-methyl-4′-nitroaniline (Hayashi et al. 1992)

T_g = 100°C.
λ_{max} = 390 nm.
$M_w = 11\text{–}17 \times 10^3$.
n (633 nm) = 1.66.
Corona poled d_{33} (1.58 μm) = 30 pm/V.
Activity decays to 65% in 40 days at ambient conditions.

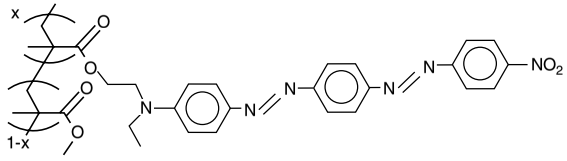

MMA/4-*N*-(2-methacroyloxyethyl)-*N*-ethyl-4′-aminophenylazo-4″-nitroazobenzene copolymer (Amano et al. 1990)

$T_g \approx 100$°C.
λ_{max} = 500 nm.
$\rho^{\#} = 4.3 \times 10^{20}$ cm^{-3}
Corona poled at 100°C.
d_{33} (1.06 μm) = 142 pm/V.
d_{33} (1.7 μm) = 70 pm/V.

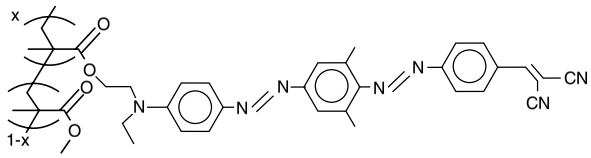

MMA/2,5-dimethyl-4-*N*-(2-methacroyloxyethyl)-*N*-ethyl-4′-aminophenylazo-4″-dicyanoazobenzene copolymer (Shuto et al. 1991)

$T_g \approx 140$°C.
λ_{max} = 510 nm.
$\rho^{\#} = 4 \times 10^{20}$ cm^{-3}
α (633 nm) = −50 dB/cm due to absorption.
Corona poling with 200 V/μm at 140°C gives d_{33} (1.06 μm) = 417 pm/V.
Contact poling at 150 V/μm at 140°C gives r_{33} (633 nm) = 40 pm/V.
Excellent temporal stability at 80°C.

(continued)

15018—Chapter7—26/8/2006—22:26—SJAPPIYAR—15018—XML MODEL CRC12a – pp. 1–126.

15018—Chapter7—26/8/2006—22:26—SJAPPIYAR—15018—XML MODEL CRC12a – pp. 1–126.

TABLE 6.3 (Continued)

Structure and Nomenclature (Ref)	Properties
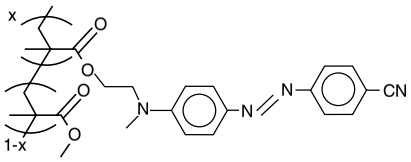 MMA/4-(*N*-methyl-*N*-2-methacroyloxyethoxy)-4′-cyanoabenzene homo-and copolymers (S'heeren et al. 1993a)	Corona poled near T_g. d_{33} values are measured 10 days after poling at 1.064 μm. dye (mol%) / T_g (°C) / Mw ($\times 10^3$) / d_{33} (pm/V) 12 / 129 / 59 / 5.2 16 / 128 / 44 / 21 32 / 134 / 59 / 68 44 / 128 / 39 / 45 49 / 125 / 98 / 32 72 / 124 / 36 / 31 100 / 181 / 15 / 26
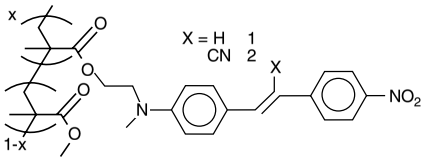 MMA/4-(*N*-methyl-*N*-2-methacroyloxyethoxy)-4′-nitrostilbene co-polymers (S'heeren et al. 1993c)	Corona poled near T_g. d_{33} values are measured several days after poling at 1.064 μm. dye (mol%) / T_g (°C) / Mw ($\times 10^3$) / d_{33} (pm/V) 1 / 11 / 122 / 69 / 18 19 / 120 / 70 / 31 31 / 124 / 69 / 44 39 / 126 / 66 / 15 52 / 120 / 48 / 66 2 / 9 / 124 / 56 / 22 18 / 131 / 62 / 41 33 / 126 / 60 / 20
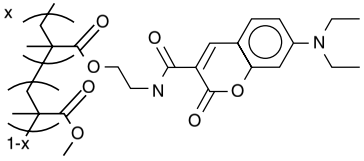 MMA/*N*-(3-methacryloxyalky)-7-diethylaminocoumarin-3-carboxamide (76:23 mol%) copolymer (Mortazavi et al. 1991)	$T_g = 135$°C. $\lambda_{max} = 410$ nm. $\rho^{\#} = 9.8 \times 10^{20}$ cm^{-3} $M_w = 89 \times 10^3$. Corona poled for SHG and contact poled with 100 V/μm for EO at 60°C. d_{33} (1.06 μm) = 13 pm/V. r_{33} (477–1100 nm) = 2–12 pm/V. d_{33} decays by 25% at 100°C in 50 h.

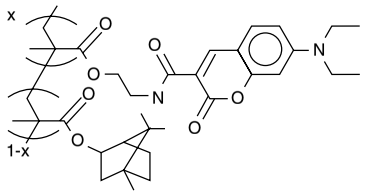

Isobornyl methacrylate/*N*-(3-methacryloxyalkyl)-7-diethlaminocoumarin-3-carboxamide (76:23 mol%) copolymer (Mortazavi et al. 1991)

$T_g = 170°C$.
$\lambda_{max} = 410$ nm.
$M_w = 50 \times 10^3$.
Corona poled at 200°C.
d_{33} (1.06 μm) = 11 pm/V.
d_{33} decays by 10% at 100°C and by 40% at 140°C in 50 h.

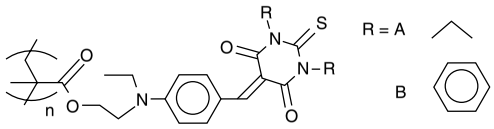

Poly(*p*-*N*-(2-methacroyloxethyl)-*N*-ethylaminobenzall-1-3-diethyl (or diphenyl thiobarbituric acid) (Cheng and Tan 1993)

Corona poled near T_g.
d_{33} and r_{33} values are measured at 1.064 μm.
At 100°C d_{33} of A(B) decays by 80% (10%) in 150 min (15 days)

	T_g(°C)	Mw ($\times 10^3$)	d_{33} (pm/V)	r_{33} (pm/V)
A	125	74	33	14
B	194	60	40	18

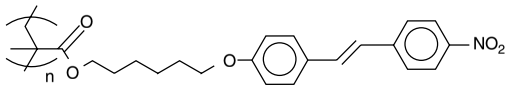

Poly-4-(6-acroyloxyhexyloxy)-4′-nitrostilbene (Huijts et al. 1989b)

$T_g = 65°C$.
$\lambda_{max} = 380$ nm.
$\rho^{\#}$:18×10^{20} cm^{-3}
n (633 nm) = 1.62.
α (1.3 μm) ≈ −1.5 dB/cm.
Contact poled with 23 V/μm at 65°C.
r_{33} (633 nm) = 0.9 pm/V.

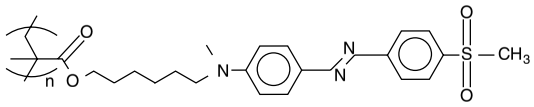

Poly-4′-*N*-(6-methacroyloxyhexyl)-*N*-methyl-amino-4-methylsulfonylazobenzene (Robello et al. 1991a, 1992)

$T_g = 99°C$.
$\lambda_{max} = 446$ nm.
$\rho^{\#} = 17 \times 10^{20}$ cm^{-3}
$M_w = 89 \times 10^3$.
n (633 nm) = 1.76.
α (830 nm) = −1 dB/cm.
Contact poled with 90 V/μm at 100°C.
r_{33} (633 nm) = 39 pm/V.; r_{33} (860 nm) = 13 pm/V.

(continued)

15018—Chapter7—26/8/2006—22:26—SJAPPIYAR—15018—XML MODEL CRC12a – pp. 1–126.

TABLE 6.3 (Continued)

Structure and Nomenclature (Ref)	Properties
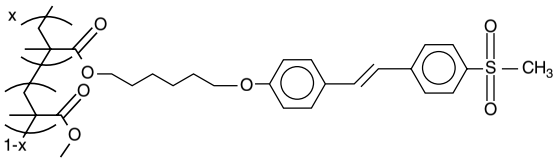 MMA/4′-(6-methacroyloxyhexloxy)-4-methylsulfonylstilbene (55:45 wt%) copolymer (Rikken et al. 1991; Seppen et al. 1991)	$T_g = 117°C$. $\lambda_{max} = 355$ nm. Low absorption at 420 nm. Corona poled with 120 V/μm at 100°C. d_{33} (820 nm) = 9 pm/V. Activity decreases to a quasi-stable 70% value after 120 days at ambient. Waveguide formation by UV photobleaching.
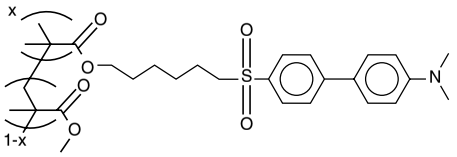 MMA/4′-(6-methacroyloxyhexylsulfony)-4-*N*,*N* dimethylamino-biphenyl (50:50 wt%) copolymer (Rikken et al. 1992)	$T_g \approx 100°C$. $\lambda_{max} = 340$ nm. Corona poled with 120 V/m at 100°C. d_{33} (820 nm) = 45 pm/V. poor temporal stability at 60°C.
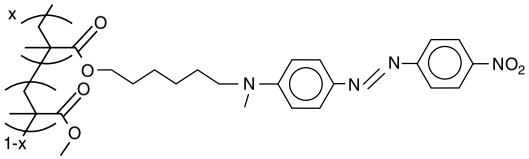 MMA/4-(4′-nitrophenylazo)-*N*-methyl-*N*-(6-methacroyloxyhexyl) aniline (81:19 mol%) copolymer (Muller et al. 1992a)	$T_g = 104°C$. $\lambda_{max} \approx 470$ nm. $M_w = 100 \times 10^3$. Thermally decomposes at 267°C. Poled with 110 V/μm. r_{33}–r_{13} (1.3 μm) = 9 pm/V.

15018—Chapter7—26/8/2006—22:26—SJAPPIYAR—15018—XML MODEL CRC12a – pp. 1–126.

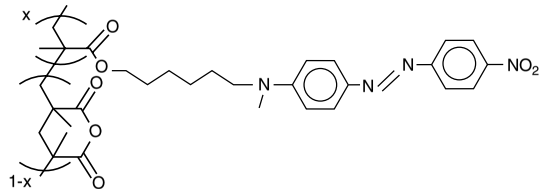

$T_g = 90°C$.
$\lambda_{max} \approx 470$ nm.
Thermally decomposes at 227°C.
Poled with 110 V/μm.
r_{33}–r_{13} (1.5 μm) = 19 pm/V.

Methacrylic anhydride/4-(4′-nitrophenylazo)-*N*-methyl-*N*-(6-methacroyloxyl)aniline (33:67 mol%) copolymer (Strohriegl 1993; Muller et al. 1992a)

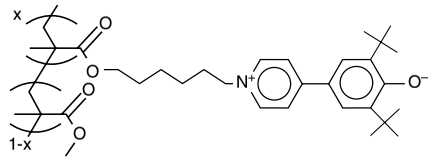

$T_g = 130°C$.
$\lambda_{max} \approx 525$ nm.
Contains zwitterionic chromophore with $\beta_0 = -30 \times 10^{-30}$ esu.
Soluble in THF.

MMA/[2,6-di-*tert*-butyl-4-(1-ω-methacroyloxyalyl)-4-pyridino]phenolates (85:15 mol%) copolymer (Combellas et al. 1992)

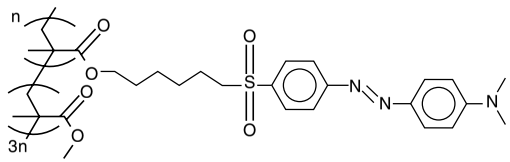

$T_g = 124°C$.
$\lambda_{max} = 437$ nm.
$M_w = 17 \times 10^3$.
Corona poled at 125°C for 45 min.
d_{33} (1.06 μm) = 100 pm/V.
Activity stabilizes at 95% value after 10 days at ambient conditions.

MMA/4′-(6-methacroyloxyhexlsulfonyl)-4-*N*,*N*-dimethylamino-azobenzene (25 mol%) copolymer (Xu et al. 1993)

(continued)

15018—Chapter7—26/8/2006—22:27—SJAPPIYAR—15018—XML MODEL CRC12a – pp. 1–126.

15018—Chapter7—26/8/2006—22:27—SJAPPIYAR—15018—XML MODEL CRC12a – pp. 1–126.

TABLE 6.3 (Continued)

Structure and Nomenclature (Ref)	Properties
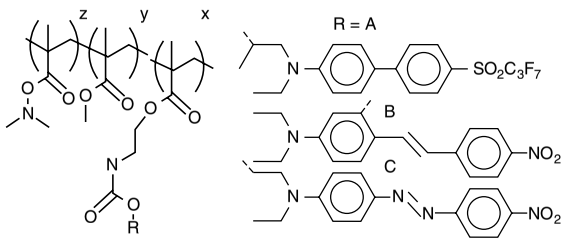 Functionalized homo-and copolymers of isocyanatoethyl methacrylate, MMA, and dimethylaminoethyl methacrylate. (Cheng et al. 1992)	Corona poled near T_g. d_{33} values are measured at 1.064 μm. d_{33} of A & C are stable at room temperature. Polymer B is stable at 80°C. $\alpha(1.06\ \mu m) \approx -(1.5–3)$ dB/cm.
Side-chain Non-acrylate polymers 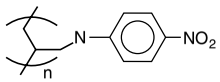 Poly-4-[*N*-(4′-nitrophenyl)amino-methyl]ethylene (Eich et al. 1989b)	(x, y, z) | T_g(°C) | ρ^a (10^{20}/cm^3) | d_{33} (pm/V) A(l, 1, 0) | 120 | 6.8 | 19 B(l, 0, 0) | 130 | 13 | 44 C(l, 0, 0) | 140 | 13 | 88 C(l, 0, 1) | 130 | 9.6 | 121 C(l, 0, 2) | 135 | 12 | 90
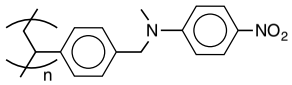 Poly-4-[*N*-methyl-*N*-(4′-nitrophenyl)amino-methyl]styrene (Hayashi 1991)	$T_g = 125$°C. $\lambda_{max} \approx 390$ nm. Thermally decomposes at 260°C. Corona poled at 140°C. d_{33} (1.06 μm) = 31 pm/V. d_{33} relaxes to 19 pm/V in 5 days.
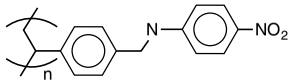 Poly-4-[*N*-(4′-nitrophenyl)amino-methyl]styrene (Hayashi et al. 1992)	$T_g = 103$°C. $\lambda_{max} = 393$ nm. $M_w = 12 \times 10^3$. $n(633\ nm) = 1.73$. α (633 nm) = −10 dB/cm. Corona poled at 110°C. d_{33} (1.06 μm) = 28 pm/V which stabilizes to 18 pm/V in 5 months at ambient conditions. $T_g = 123$°C. $\lambda_{max} = 383$ nm. $M_w = 15 \times 10^3$. $n(633\ nm) = 1.70$. Corona poled at T_g. $d_{33}(1.06\ \mu m) = 10$ pm/V. Low d_{33} due to poling-induced decomposition.

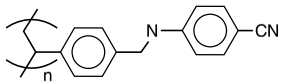

Poly-4-[*N*-(4′-cyanophenyl)amino-methyl]styrene (Hayashi, et al. 1992)

$T_g = 132°C$.
$\lambda_{max} = 288$ nm.
$M_w = 15 \times 10^3$.
$n(633\text{ nm}) = 1.65$.
Corona poled at T_g.
$d_{33}(1.06\ \mu m) = 1$ pm/V.

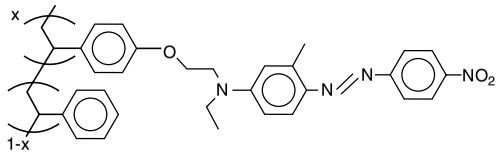

Styrene/*p*-[4-nitro-4′-(*N*-ethyl-*N*-2-oxyethyl)azobenzene] methylstyrene copolymer (88:12 mol%) (Ye et al. 1987)

$T_g = 110°C$.
$\lambda_{max} \approx 470$ nm.
Contact poled with 30 V/μm at ≈ 110°C.
d_{33} (1.06 μm) = 1.1 pm/V.
Stable activity at room temperature.

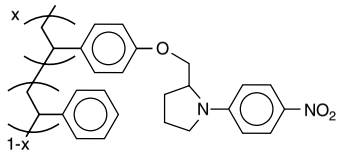

Styrene/*N*-(4-nitrophenyl)-*S*-prolinoxy methylstyrene copolymer (64:36 mol%) (Ye et al. 1989)

$T_g = 110°C$.
$\lambda_{max} \approx 380$ nm.
Contact poled with 70 V/μm at ≈ 110°C.
d_{33} (1.06 μm) = 1.6 pm/V.
Low d_{33} due to material impurity.

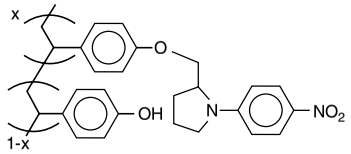

p-hydroxystyrene/*N*-(4-nitrophenyl)-*S*-prolinoxy styrene copolymer (10:90 mol%) (Ye et al. 1989)

$T_g = 96°C$.
$\lambda_{max} \approx 380$ nm.
$\rho^{\#} = 2.3 \times 10^{21}$ cm^{-3}
Corona poled at T_g.
d_{33} (1.06 μm) = 33 pm/V.
T_g increase to 146°C at 16 mol% functionalization.

(continued)

15018—Chapter7—26/8/2006—22:27—SJAPPIYAR—15018—XML MODEL CRC12a – pp. 1–126.

TABLE 6.3 (Continued)

Structure and Nomenclature (Ref)	Properties
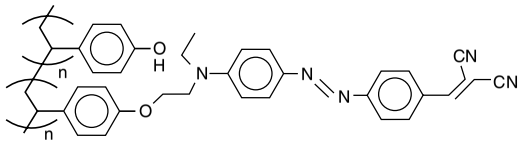	Corona poled at 117°C for 15 h. Thermal and electrochemical decomposition observed at 147°C.
p-hydroxystyrene/*p*-[4-(2,2-dicryanovinyl)-4′-(*N*-ethyl-*N*-2-oxyethyl)azobenzene] styrene copolymer (Ye et al. 1992)	
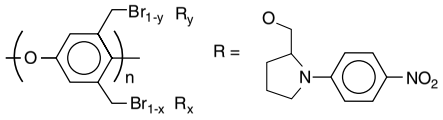	$T_g = 170$°C. $\rho^{\#} = 2.6 \times 10^{21}$ cm^{-3} n (633 nm) = 1.584. Corona poled at 190°C for 30 min. $\alpha = -1$ dB/cm. Temporal stability: τ_1(25°C) = 0.3 days and τ_2(25°C) = 39 days.
Poly-(2,6-dimethylbromo-1,4-phenylene oxide) partially functionalized with *N*-(4-nitrophenyl)-*S*-prolinol (Dai et al. 1990)	
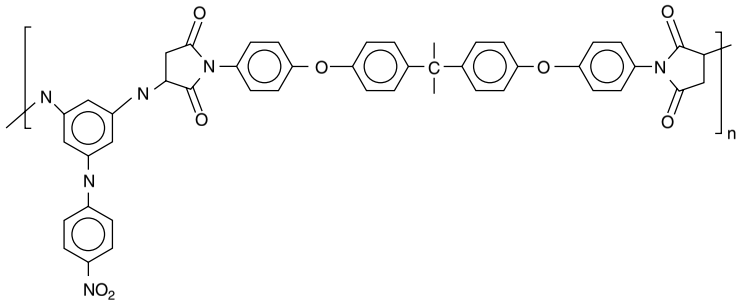	$T_g = 236$°C. $\lambda_{max} = 390$ nm. $\rho^{\#} = 7 \times 10^{20}$ cm^{-3} Films are cured and corona poled at 240°C. d_{33} (1.06 μm) = 5.4 pm/V. d_{33} (24 h, 85°C) ≈ 5 pm/V and stable.
p-nitroaniline functionalized polyimide (Lin et al. 1992)	

15018—Chapter7—26/8/2006—22:27—SJAPPIYAR—15018—XML MODEL CRC12a – pp. 1–126.

	Poly-(4-nitro-4′-(vinylooxyethyloxy)azobenzene, 1, and other poly-(vinyl ethers) (S′heeren et al. 1992)
	Poly-(4-cyano-4′-(vinylooxyethyloxy) azobenzene 2
	Poly-(4-dicyanovinyl-4′-(vinylooxyethyloxy) benzene 3
	Poly-(4-cyano-4-carbomethoxyvinyl-4′-(vinylooxyethyloxy) benzene 4
	Polyvinylalcohol/*N*-ethyl-*N*-methylamino nitroaniline copolymer(Sasaki 1993)

$T_g = 120°C$.
$\lambda_{max} \approx 380$ nm.
Corona poled at T_g.
d_{33} (1.06 μm) = 10 pm/V.
d_{33} relaxes to 7 pm/V in 40 days.

(continued)

TABLE 6.3 (Continued)

Structure and Nomenclature (Ref)	Properties
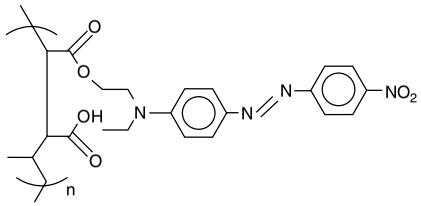 DR1/Poly(maleic anhydride-co-propylene copolymer (16:84 mol%) (Bauer et al. 1993)	$T_g = 180°C$. $\lambda_{max} \approx 470$ nm. Corona poled at 185°C. r_{33} (780 nm) = 6 pm/V. with 3°C/min heating rate, r_{33} is stable up to 100°C.
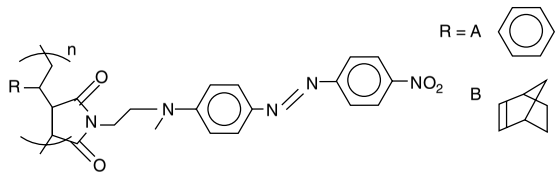 Azo dye/Poly (maleic anhydride-*co*-styrene or co-norbornadiene copolymer (Ahlheim and Lehr 1994)	T_g (°C): A 170, B 180 Mw (×10)^3: A 54 λ_{max} (nm): A 468 dye (mol%): A 92, B 96
Main-Chain Polymers 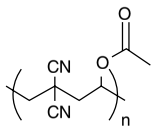 Vinylidene cyanide/vinyl acetate copolymer (50:50 mol%) (Azumai et al. 1990; Eich et al. 1988; Sato et al. 1987)	$T_g = 180°C$. $M_w = 470 \times 10^3$. n(2.94 μm) = 1.434. α(2.94 μm) = 1.4 mm^{-1}. Corona poled at 180°C for 2 h. d_{33}(1.064 μm) = 0.3 pm/V.[Eich]. Note: large discrepancy in SHG *d* coefficients.

15018—Chapter7—26/8/2006—22:28—SJAPPIYAR—15018—XML MODEL CRC12a – pp. 1–126.

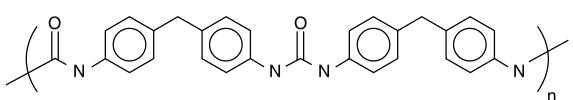

Aromatic polyurea (Nagamori et al. 1992; kajikawa et al. 1991)

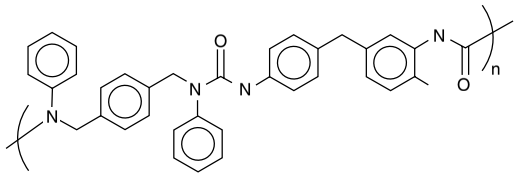

N-phenylated polyurea (Nalwa et al. 1993a; Nalwa et al. 1993b; Azumai et al. 1990; Stato et al. 1987)

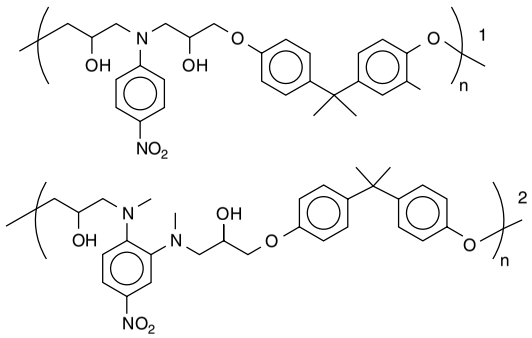

Epoxy polymers containing 4-amino-4′-nitroazobenzene (Teraoka et al. 1991)

Thin film prepared by vapor deposition polymerization.
$T_g = > 150°C$.
$\lambda_{cut\text{-}off} = 400$ nm.
Corona poled at 180°C for 3 min.
$d_{33}(1.06\ \mu m) = 1.7$ pm/V.
Negligible relaxation of activity over 2 months at ambient conditions.
Activity remains stable after short-term heating to 200°C.
$T_g = 123°C$.
$\lambda_{max} = 253$ nm.
$n(633\text{ nm}) = 1.577$.
$\alpha(633\text{ nm}) = -1.2$ dB/cm.
Corona poled at 130°C for 1 h.
$d_{33}(1.064\ \mu m) = 5.5$ pm/V.
90% of activity remains stable after 40 days at ambient.
Polymers prepared by melt condensation at 150°C under N_2.
d_{33} values are measured at 1.064 μm during corona poling.

	1	2
T_g(°C)	86	77
λ_{max} (nm)	392	412
Mw($\times 10^3$)	7	5
Poling temp. (°C)	100	85
d_{33}(pm/V)	31	12
τ(hour)	24000	770
β	0.32	0.34

(continued)

15018—Chapter7—26/8/2006—22:28—SJAPPIYAR—15018—XML MODEL CRC12a – pp. 1–126.

TABLE 6.3 (Continued)

Structure and Nomenclature (Ref)	Properties
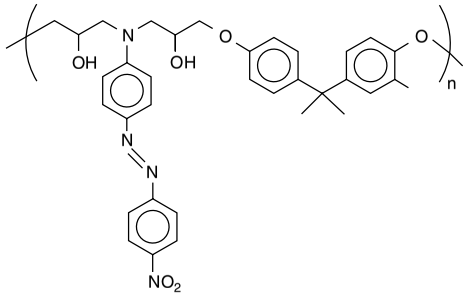	$T_g = 77°C$. $\lambda_{max} = 480$ nm. Corona poled after procuring. $d_{33}(1.06\ \mu m) = 25$ pm/V. Stable activity at ambient conditions for >20 days. Activity decreases rapidly to zero when heated above 80°C.
Epoxy polymers containing *p*-aminonitrobenzene (Gadret et al. 1991)	
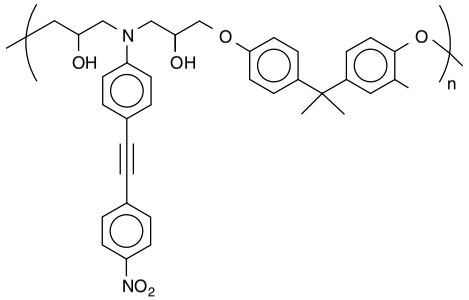	$T_g = 125°C$. $\lambda_{max} = 418$ nm. n (633 nm) = 1.71. Corona poled at 135°C for 1 h. d_{33} (1.064 μm) = 89 pm/V. r_{13} (633 nm) = 8 pm/V. Stable birefringence at ambient conditions. Birfringence decays with $\tau = 448$ h and $\beta = 0.45$ at 100°C.
Epoxy polymer containing 4-amino-4′nitrotolane (Jungbauer et al. 1991)	

15018—Chapter7—26/8/2006—22:28—SJAPPIYAR—15018—XML MODEL CRC12a – pp. 1–126.

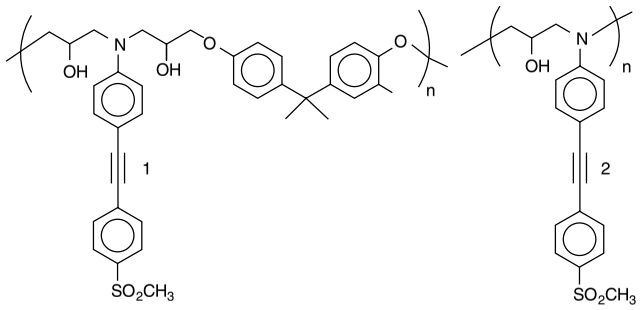

Epoxy polymers containing 4-amino-4′methylsulfonyltolane (Twieg et al. 1992)

Polymers prepared by melt condensation at 150°C.
d_{33} values are measured at 1.064 μm during corona poling.

	1	2	3
T_g (°C)	74	94	116
λ_{max} (nm)	471	476	
Mw ($\times 10^3$)	11	15	31
n (830 nm)	1.69	1.69	1.70
χ_{333} (pm/V)	14.8	10.3	

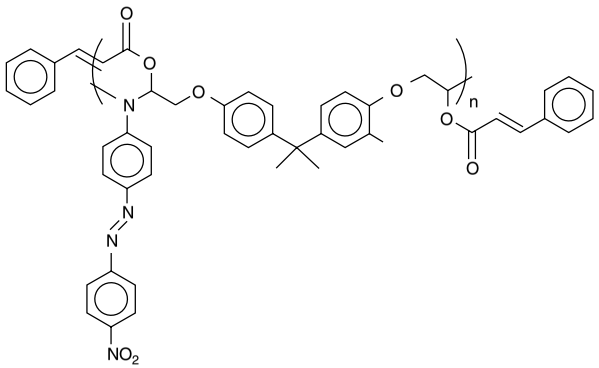

Epoxy polymers containing 4-amino-4′nitroazobenzene (Jeng et al. 1992c)

$T_g = 115$°C.
$\lambda_{max} = 461$ nm.
n (533 nm) = 1.718.
Corona poled at 115°C for 1 h.
d_{33} (1.06 μm) = 34 pm/V.
70% of SHG activity remains stable after 20 days at ambient conditions.

(continued)

15018—Chapter7—26/8/2006—22:28—SJAPPIYAR—15018—XML MODEL CRC12a – pp. 1–126.

TABLE 6.3 (Continued)

Structure and Nomenclature (Ref)	Properties
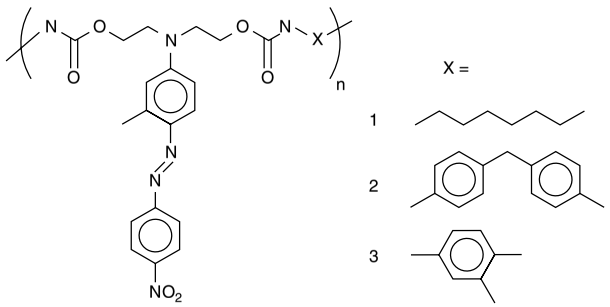 Polyurethanes containing 4-amino-4′nitroazobenzene [Meyrueix et al. 1991a, 1991b]	Polymers prepared by melt condensation at 150°C. χ_{333} ($-\omega$, ω, 0) values are measured at 830 nm after contact poling with 25 V/μm at 100°C.
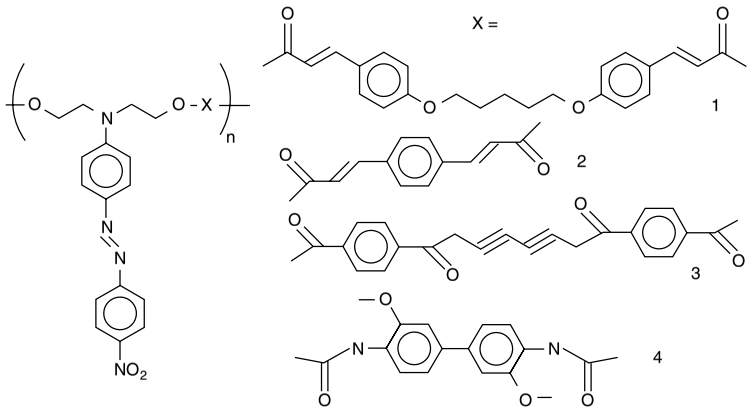 Polyurethanes containing 4-amino-4′nitroazobenzene [Chen et al. 1991]	Polymers prepared by condensation in dioxane solution. d_{33} is stabilized value measured at 1.064 μm after corona poling at about 130°C. Activity is stable at ambient conditions.

	1	2	3
T_g (°C)	74	94	116
λ_{max} (nm)	471	476	
Mw ($\times 10^3$)	11	15	31
n (830 nm)	1.69	1.69	1.70
χ_{333} (pm/V)	14.8	10.3	

	1	2	3	4
T_g (°C)	92	120	122	140
λ_{max} (nm)	460	470	455	463
Dye (wt%)	48	68	47	52
Thickness (μm)	0.04	0.05	0.22	0.28
d_{33} (pm/V)	108	250	119	223

15018—Chapter7—26/8/2006—22:29—SJAPPIYAR—15018—XML MODEL CRC12a – pp. 1–126.

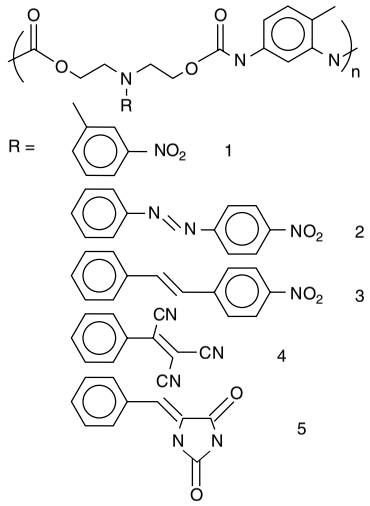

In situ corona poling during melt polymerization at 120°C.
d_{33} values are measured at 1.064 μm; stabilized values after 180 days at 25°C are given in *italics*.

	1	2	3	4	5
T_g (°C)	98	131	121	125	178
λ_{max} (nm)	373	472	431	518	388
Mw ($\times 10^3$)	2.3	2.5	2.0	1.7	2.1
d_{33} (pm/V)	9	10	2.6	3.6	2
	0.5	5.5	6	0.9	2.5

Polyurethanes derived from 2,4-toluenediisocyanate/2-methyl-4-nitro-[*N*,*N*-bis(2-hydroxyethyl)]-aniline and other diols [Kitipichai et al.1993]

(continued)

TABLE 6.3 (Continued)

Structure and Nomenclature (Ref)	Properties
1 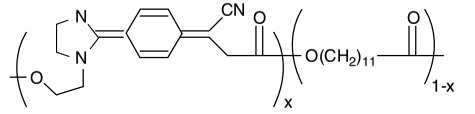 2 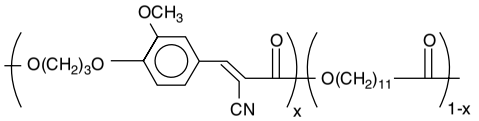 3 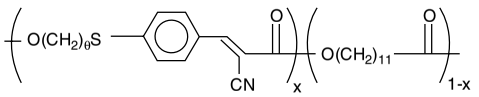 Main-chain polymers derived from (1) α-cyano-ester quinodimethanes, (2) *p*-oxy-α-cyanocinnamates, (3) *p*-thio-α-cyanocinnamates [Fuso 1991;Hall et al. 1988; Green 1987a, 1987b]	Polymers prepared by high temperature transesterification. Homopolymers are typically insoluble and high melting. Unit molecular nonlinearity $\mu\beta/n$ values are measured at 1.064 μm. **1** **2** **3** T_g (°C) None <25 45 Dye (mol%) 50 67 100 Mw ($\times 10^3$) 70 $\mu\beta/n$ ($\times 10^{-48}$ esu) 140
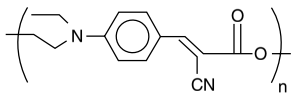 Main-chain homopolymers derived from (4-*N*-ethyl-*N*-(2-hydroxyethyl)amino-α-cyanocinnamates (1) and the corresponding acid (2) [Stenger-Smith et al. 1991, 1990]	Polymerization: (1) melt transesterification at 160°C; (2) solution polycondensation at 25°C. **1** **2** T_g (°C) 100–110 60–90 λ_{max} (nm) 442 442 Mw ($\times 10^3$) 27 5 Poling temp. (°C) 120 85–100 d_{33} (pm/V) at 1.064 μm **7** 7

15018—Chapter7—26/8/2006—22:29—SJAPPIYAR—15018—XML MODEL CRC12a – pp. 1–126.

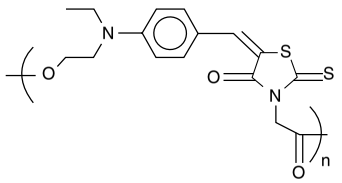

Main-chain polymer derived from 3-[(methyoxycarbonyl)methyl]-5-[4′-[*N*-ethyl-*N*-(2″-hydroxyethyl)amino] benzylidene] rhodanine [Francis et al. 1993b]

Polymers are prepared by transesterication in melt at 140°C for 8 h.
$T_g = 63$°C.
$M_w = 13 \times 10^3$.
$\lambda_{max} = 473$ nm.
n (790 nm) = 1.760.
Contact poled with 43 V/μm at 65°C.
d_{33} (1.58 μm) = 7.3 pm/V.

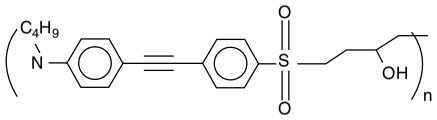

4-amino-4′-alkylsulfonyltolane main-chain polymer [Zentel et al. 1993]

Polymers are corona poled during melt polymerization at 150°C for a few hours.
$T_g = 60$°C.
$\lambda_{max} = 366$ nm.
d_{33}(1.064 μm) = 12.5 pm/V.
Activity decays by 40% in 25 days at ambient conditions.

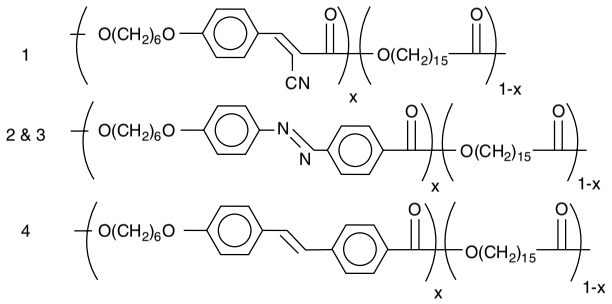

Main-chain polyesters derived from 6-hydroxyhexyloxyphenyl propenoic, azobenzoic, or ethenylbenzoic acids [S'heeren et al. 1993b]

Polymers are prepared by melt polycondensation at 220°C, 1.3 mbar for 4 h.
Films are of pale yellow in color.
d_{33} values are measured at 1.064 μm after corona poling at 10°C above T_g.

	1	2	3	4
T_g (°C)	48	41	51	53
Dye (mol%)	30	43	63	34
Mw ($\times 10^3$)		35	115	99
d_{33} (pm/V)		0.04	0.5	0.3

(continued)

15018—Chapter7—26/8/2006—22:29—SJAPPIYAR—15018—XML MODEL CRC12a – pp. 1–126.

TABLE 6.3 (Continued)

Structure and Nomenclature (Ref)	Properties
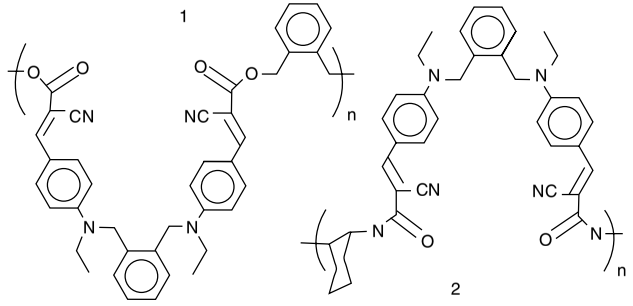 Main-chain accordionpolymers of α-cyano cinnamamides [Lindsay et al. 1992; Wang and Guan 1992]	Polymer 2 was corona poled. Activity is found to be stable at room temperature. **1** / **2** T_g (°C): 143 / 193 λ_{max} (nm): ≈425 Mw ($\times 10^3$): 55 Poling temp. (°C): 215 d_{33} (pm/V) at 1.064 μm: 3.5
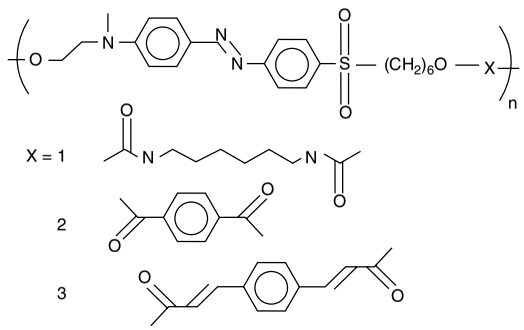 Random main-chain polymers containing 4-*N,N*-dialkylamino-4′-hexylsulfonylazobenzene [Xu et al. 1993, 1992a]	Polymers are prepared by Condensation in dioxane solution. d_{33} values are measured at 1.064 μm after corona poling at about 120°C. **1** / **2** / **3** T_g (°C): 62 / 114 / 108 λ_{max} (nm): 440 / 436 / 443 Mw ($\times 10^3$): 8 / 7 / 9 d_{33} (pm/V): 60 / 125 / 150 d_{33} (10 days) at ambient: 12 / / 140

15018—Chapter7—26/8/2006—22:30—SJAPPIYAR—15018—XML MODEL CRC12a – pp. 1–126.

Cross-linked polymers

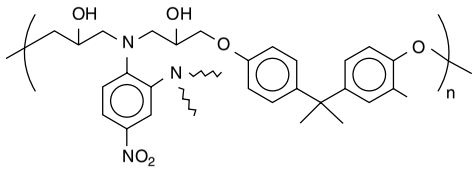

Cross-Linked epoxy polymer from 4-nitro-1, 2-phenylenediamine and bisphenol-A diglycidylether [Eich et al. 1989a]

Thermal cross-linking is achieved by procuring at 100°C for 3 h at 140°C for 16 h under a corona poling field.
λ_{max} = 410 nm.
n(633 nm) = 1.629.
d_{33} (1.06 μm) = 13.5 pm/V.
No decay of SHG activity is observed for 36 mins at 80°C.

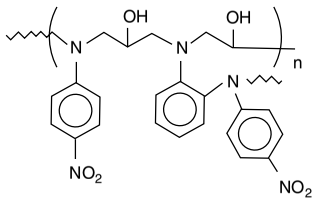

Cross-linked epoxy polymer from *N,N*-(diglycidyl)-4-nitroaniline and *N*-(2-aminophenyl)-4-nitroaniline [Jungbauer et al. 1990]

Thermal cross-linking is achieved by procuring at 130°C for 4 min and at 120°C for 24 h under a corona poling field.
λ_{max} = 397 nm.
High dye content: 63 wt%.
n (633 nm) = 1.74.
d_{33} (1.064 μm) = 50 pm/V.
Stable activity is observed at 80% of initial value at 80°C.

(continued)

TABLE 6.3 (Continued)

Structure and Nomenclature (Ref)	Properties
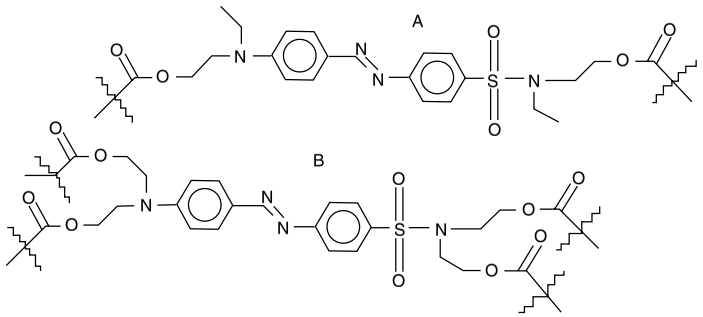 Cross-linked methacrylate polymer containing 4-*N*,*N*-dialkylamino-4′-*N*,*N*-dialkylaminosulfonylazobenzene [Wang et al. 1993; Allen et al. 1991]	Cross-linking is initiated with free radicals under a corona poling field. $\lambda_{max}=480$ nm. r_{33} (633 μm) = 36 pm/V; r_{33} (1.3 μm) = 6.6 pm/V. No decay of activity is observed over 8 months at ambient conditions for A. Higher temporal stability found for B.
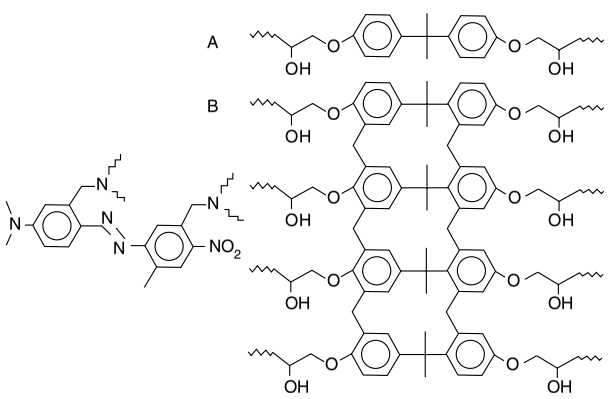 Cross-linked polymer from a reactive diamine derivative of 4-*N*, *N*-dimethylamino-4′-nitroazobenzene and oligomeric derivative of diglycidyl ether of bisphenol A [Hubbard 1992]	Thermal cross-linking is achieved procuring at 100°C for 3 h and at 130°C for 2 hour a corona poling field. $\rho^{\#}=6\times10^{20}$ cm^{-3} for B. d_{33} (1.064 μm) = 3(A)-6(B) pm/V. Temporal stability: $\tau_1(25°C)=6$(A)–4.1(B) days and $\tau_2(25°C)=$ 120(A) − 300(B) daya; $\tau_1(85°C)=1.6$(B) days and $\tau_2(85°C)=120$(B) days.

Polymers are prepared by poly-acyclotrimerization at 150°C under a poling field for several hours.
r_{33}(830 nm) = 11 pm/*V*.
High stability is observed at 85°C.

Triazine cross-linked polymer obtained from *p*(*N*,*N*-bis(4′-cyanatobenzyl)amino-p′-(2,2dicyanovinyl)azobenzene (Holland and Fang 1992; Singer et al. 1991)

(continued)

TABLE 6.3 (Continued)

Structure and Nomenclature (Ref)	Properties
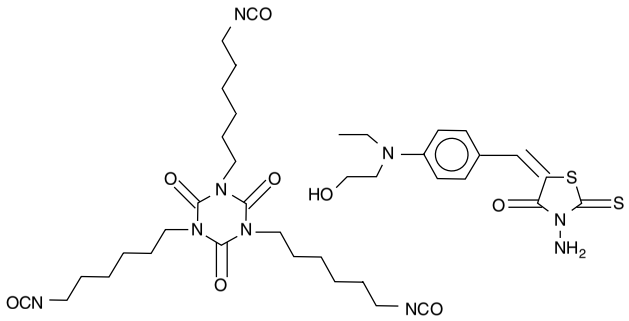 Isocyanate cross-linked polymer derived from tris-1-hexamethyleneisocyanate isocyanurate and 3-amino-5-[4′(*N*-ethyl-*N*-(2″-hydroxyethyl)amino)benzylidene]-rhodanine (Francis et al. 1993a)	Thermally cross-linked at 135°C for 16 h. λ_{max} = 470 nm. n(1.3 μm) = 1.611. Doping level: 60 mol%. Contact poled with 100 V/μm at 135°C. d_{33}(1.58 μm) = 6.9 pm/V. r_{33}(1.3 μm) = 3.6 pm/V. Activity decays by 30% in 150 days at 100°C due to thermal decomposition.
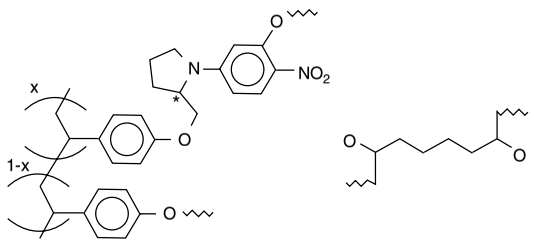 Cross-linked epoxy polymer from 1,2,7,8-diepoxyoctane and *N*-(3-hydroxy-4-nitrophenly)-(S)-prolinoxy functionalized poly(*p*-hydroxystyrene) copolymer (Park et al. 1990)	Thermal cross-linking is achieved by procuring at 100°C for 24 h and at 180°C for 1 hour under a corona poling field. High dye content: 16 wt%. diepoxide/phenol ratio: 0.5. d_{33}(1.06 μm) = 3 pm/V. Temporal stability: τ_1(25°C) = 79 days and τ_2(25°C) = 100 days.

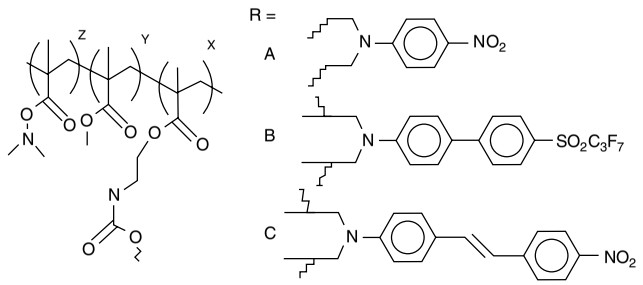

Cross-linked homo-and copolymers of isocyanatoethyl methacrylate, MMA, and dimethylaminoethyl methacrylate. (Cheng et al. 1992)

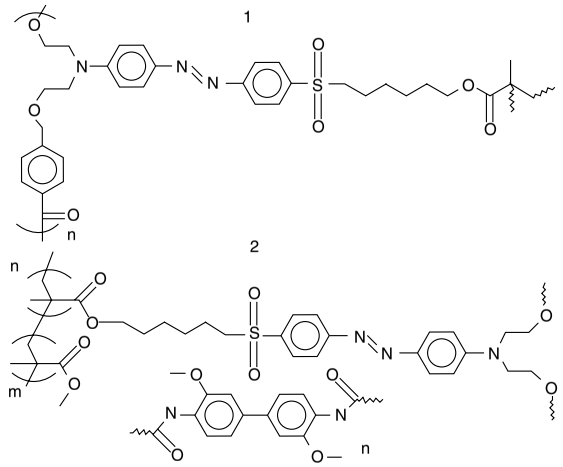

Cross-linked side-chain polymers containing 4-*N*,*N*-dialkylamino-4′-alkylsulfonylazobenzene [Xu et al. 1992b; Shi et al. 1993]

Corona poled near T_g.
d_{33} values are measured at 1.064 μm.
d_{33} of A are stable at room temperature.
Activity decays by 10% in 100 days at 80°C for polymer B and C.
$\alpha(1.06\ \mu m) \approx$ -(1.5-3) dB/cm.

(x, y, z)	$\rho^{\#}$ (10/cm^3)	d_{33} (pm/V)
A(l, 0, 0)	11	11
B(l, 1, 0)	6	10
C(l, 0, 0)	9	34
C(l, 0, 1)	6	39

Thermal cross-linking under corona poling field: (1) with initiators; (2) without initiator.

	1	2
λ_{max} (nm)	≈440	≈440
Poling temp. (°C)	115	160–180
d_{33}(pm/V) at 1.064 μm	30	50
d_{33}(100 °C 4 days)		47.5

(continued)

15018—Chapter7—26/8/2006—22:31—SJAPPIYAR—15018—XML MODEL CRC12a – pp. 1–126.

TABLE 6.3 (Continued)

Structure and Nomenclature (Ref)	Properties
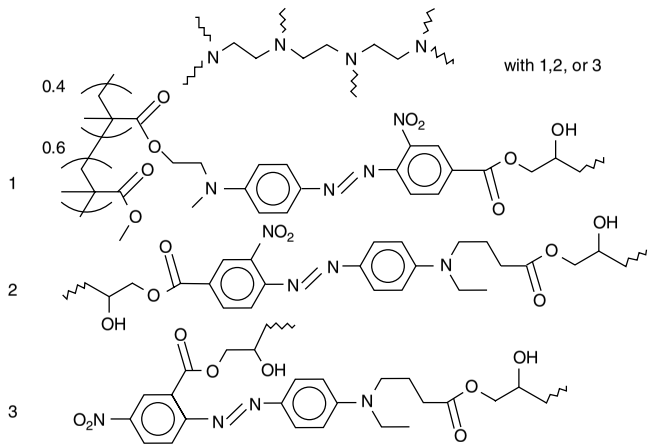 Cross-linked epoxy polymers containing dialkyamino nitroazobenzene derivatives [Muller et al. 1993]	Cross-linked polymers are prepared with 10–20 wt% PMMA as a binder. Films are characterized as having good to excellent optical quality. r_{33} values are measured at 1.32 μm after corona poling at about 140°C for 8 h.
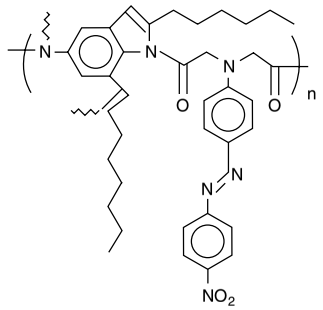 Cross-Linked polymer containing 4-amino-4′-nitroazobenzene (Yu et al. 1992)	Prepolymer containing ethynyl group is thermally cross-linked at 190°C for 2 h under a corona poling field. $\lambda_{max} \approx 470$ nm. $d_{33}(1.064\ \mu m) = 20$ pm/V. Activity decays to 75% of initial value after 30 days at 90°C.

	1	2	3
T_g(°C)	165	150	140
Precure (°C)	none	140	140
Precure (hr)	none	4.5	2.5
r_{33} (pm/V)	1.6	0.9	3.5
r_{33} (80 °C for 30 min)	8.8	7.7	1.5

15018—Chapter7—26/8/2006—22:31—SJAPPIYAR—15018—XML MODEL CRC12a – pp. 1–126.

Oligomeric prepolymer is thermally cross-linked with triethanolamine at 160°C for an hour under a corona poling field.
λ_{max} = 475 nm.
n(633 nm) = 1.753; n(800 nm) = 1.692.
d_{33}(1.06 μm) = 120 pm/V.
r_{13}(633 μm) = 13 pm/V; r_{13}(800 nm) = 5 pm/V.
No decay of activity is observed at ambient for 4 months; activity stablizes to 70% of initial value after 4 months at 90°C.

Cross-Linked polyurethane containing 4-*N*,*N*-dialkylamino-4′-nitroazobenzene(Chen et al. 1992; Shi et al. 1992)

Thermally cross-linked under a corona poling field at 125°C for 2 h.
Prepolymer $M_w = 8 \times 10^3$.
λ_{max} = 440 nm.
d_{33}(1.064 μm) = 40 pm/V.
90% activity remains stable at ambient conditions for > 3 months.

Cross-Linked random main-chain polymer containing 4-*N*,*N*-dialkamino-4′-hexylsulfonylazobenzene and 3,3′-dianisidine diisocyanate (Xu 1992; Ranon et al. 1993; Xu et al. 1993)

(*continued*)

TABLE 6.3 (Continued)

Structure and Nomenclature (Ref)	Properties
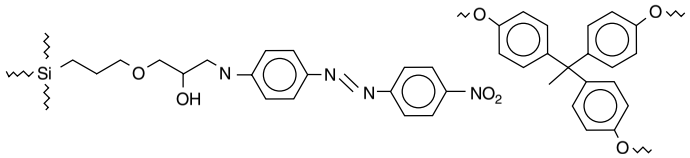 Alkoxysilane derivative of 4(-4′nitrophenylazo)-phenylamine cross-linked with 1,1,1-tris(4-hydroyphenyl)ethane (Jeng et al. 1993)	Thermally cross-linking occurs at 200°C. $T_g = 110$°C. $\lambda_{max} = 493$ nm. n(533 nm) = 1.744. Doping level: 50 mol%. Corona poled at 200°C for 30 min. d_{33}(1.06 μm) = 77 pm/V. d_{33}(24 hrs, 105°C) = 62 pm/V. No decay of activity is observed for 7 days at ambient conditions.
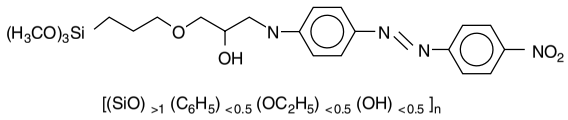 Alkoxysilane derivative of 4-(4′nitrophenylazo)-phenylamine cross-linked with phenylsiloxane polymer (Allied Signal Accuglass 204®) (Jeng et al. 1992a)	Thermal cross-linking occurs at 200°C. $\lambda_{max} = 493$ nm. n(533 nm) = 1.537. Doping level: 0.1 g dye in 4 g of A204. Corona poled at 200°C for 10 min. d_{33}(1.06 μm) = 5.28 pm/V. d_{33}(40 h, 100°C) = 2.9 pm/V.
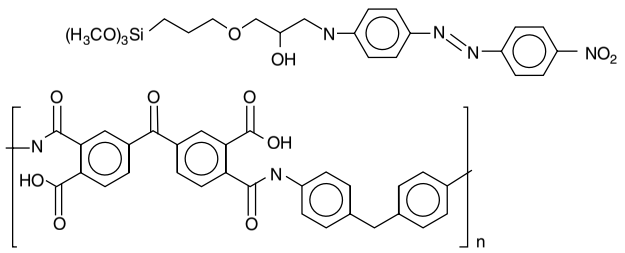 Alkoxysilane derivative of 4-(4′-nitrophenylazo)phenylamine/polyimide(Skybond®) composite (Jeng et al. 1992b)	$T_g > 275$°C. $\lambda_{max} = 466$ nm. Doping level:16 wt%. Excellent optical quality. Corona poled at 220°C. d_{33}(1.06 μm) = 13.7 pm/V. Stable d_{33} (168 h, 120°C) = 10 pm/V. Novelty: composite of polyimide and Si-O-Si network.

15018—Chapter7—26/8/2006—22:32—SJAPPIYAR—15018—XML MODEL CRC12a – pp. 1–126.

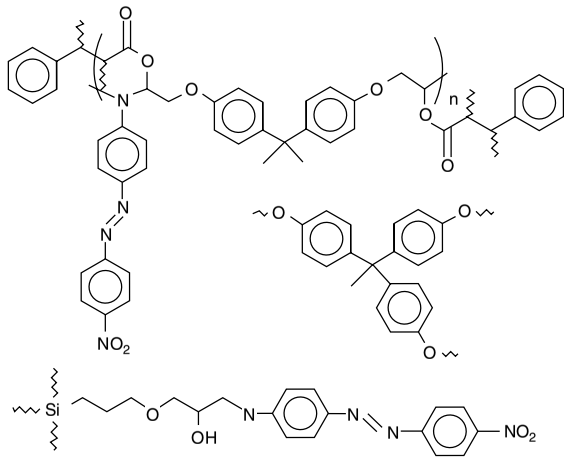

Interpenetrating network of epoxy and silicon-based cross-linked polymers(Marturunkakul et al. 1993)

Equal weight ratio of the two polymers is heated at 200°C for 1 h under a corona poling field.
Films are high optical quality.
$T_g = 176$°C.
$\lambda_{max} = 458$ nm.
N(533 nm) = 1.708.
$d_{33}(1.064\ \mu m) = 33$ pm/V.
No decay of activity is observed at 100°C for 7 days, 50% decay is observed after 15 h at 160°C.

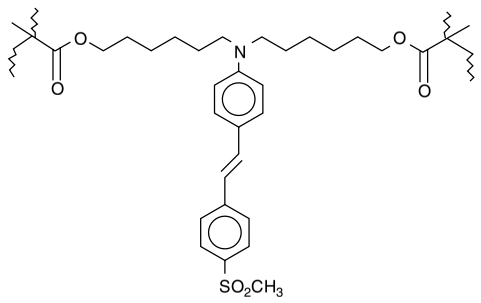

Cross-linked acrylate polymer of 4′-*N*,*N*-bis (6-methacroyloxyhexyl)-amino-4-methylsulfonylstilbene (Robello et al. 1991b)

Liquid monomers are cross-linked by UV irradiation with initiator at room temperature.
$T_g < 70$°C.
Good optical quality.
Contact poled with 6.7 V/μm.
$d_{33}(1.06\ \mu m) = 0.7$ pm/V.
Activity decays to zero in several months at ambient conditions.

(continued)

15018—Chapter7—26/8/2006—22:32—SJAPPIYAR—15018—XML MODEL CRC12a – pp. 1–126.

TABLE 6.3 (Continued)

Structure and Nomenclature (Ref)	Properties
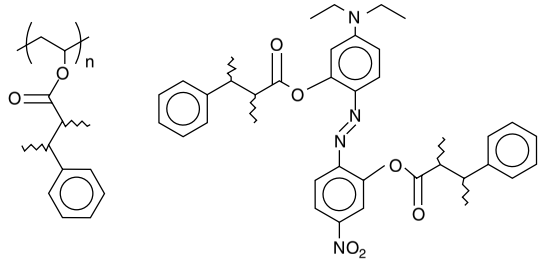 Cross-linked polymer of polyvinylcinnamate doped with 3-cinnamoyloxy-4-[4-(*N*,*N*-diethylamino)-2-cinnamoyloxy phenylazo] nitrobenzene (Mandal et al. 1991a, 1991b)	Cross-linking is induced by UV irradiation (2 mw/cm^2 at 254 nm for 3 to 10 min) at 70°C. T_g = 84°C (before cross-linking). λ_{max} = 520 nm. Doping level: 10 wt%. n(633 nm) = 1.677. Corona poled at 70°C during UV irradiation. d_{33}(1.064 μm) = 11.5 pm/V. d_{33}(1.54 μm) = 3.7 pm/V. r_{33}(633 nm) = 9pm/V. No decay of activity is observed in 22 h at ambient conditions
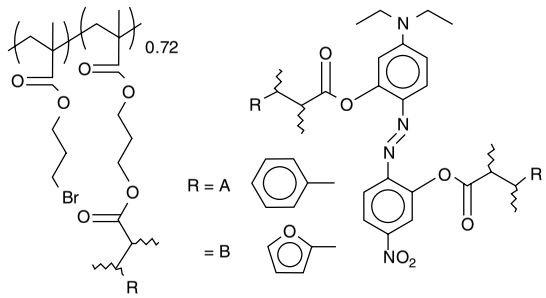 Cross-linked side-chain cinnamate or furylacrylate polymers doped with cinnamoyloxy or furylacryloyloxy functionalized 4-*N*,*N*-diethylamino 4′-azonitrobenzene (Muller et al. 1992b)	Photo-cross-linking with 1.8 mw/cm^2 at 312 nm at 75°C for 4 (A) and 2 (B) h to achieve 60% reaction. B cannot be poled under irradiation and is poled with a cycle of poling (10 min at 25°C) and cross-linking (20 min at −15°C) for a total exposure time of 2 h. r_{33}(1.32 μm) = 0.6 pm/V. Activity remains stable after 3 h at 80°C.

15018—Chapter7—26/8/2006—22:32—SJAPPIYAR—15018—XML MODEL CRC12a – pp. 1–126.

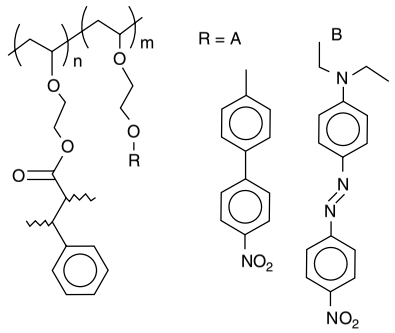

Cross-linked side-chain cinnamate copolymers functionalized with 4-alkoxy-4′-biphenyl of 4-*N*,*N*-diethylamino 4′-azonitrobenzene [Kato et al. 1993]

Photo-cross-linking with UV light under corona poling field: (A) 1.5 min at 50°C; (B) 10 min at room temperature. Both polymers were subsequently poled at 150°C for 20 min.
Activities are stable at room temperature.

	mol%	d_{33}(pm/V)
A	10	6
	33	20
	57	30
B	27	150

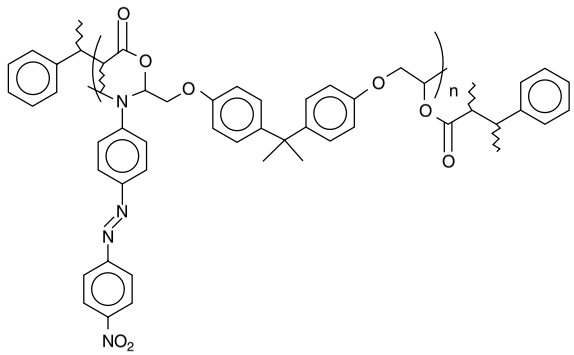

Cross-linked epoxy polymer containing 4-amino-4′-nitroazobenzene (Jeng et al. 1992c)

Prepolymer containing cinnamoyl group is cross-linked by UV irradiation at 3 MW/cm^2 for 10 min.
λ_{max}=461 nm.
n(533 nm)=1.718.
Corona poled at 115°C for 1 hour.
d_{33}(1.064 μm)=22 pm/V.
95% of SHG activity remains stable after 20 days at ambient conditions.

(continued)

15018—Chapter7—26/8/2006—22:32—SJAPPIYAR—15018—XML MODEL CRC12a – pp. 1–126.

TABLE 6.3 (Continued)

Structure and Nomenclature (Ref)	Properties
Cross-linked, random, main-chain polymer containing 4-*N*,*N*-dialkyamino-4′-hexylsulfonylazobenzene and cinnamoyl groups (Xu et al. 1993; Chen et al. 1991)	Photo-cross-linked under a corona poling field. Prepolymer $M_w = 8.5 \times 10^3$. Dye content = 53 wt%. λ_{max} = 443 nm. d_{33}(1.064 μm) = 150 pm/V. 90% activity remains stable at ambient conditions for 25 days.

References

1. Shen, Y. R. 1984. *Principles of Nonlinear Optics*. Wiley, New York.
2. Butcher, P. N. and Corter, D. 1990. *The Elements of Nonlinear Optics*. Cambridge University Press, New York.
3. Prasad, P. and Williams, D. J. 1991. *Introduction to Nonlinear Optical Effects in Molecules and Polymers*. Wiley, New York.
4. Hornak, L. A. ed. 1992. *Polymers for Lightwave and Integrated Optics*, pp. 609–661. Marcel Dekker, New York.
5. Zyss, J. ed. 1994. *Molecular Nonlinear Optics*, pp. 609–661. Academic Press, New York.
6. Nalwa, H. S. and Miyata, S. eds. 1997. *Nonlinear Optics of Organic Molecules and Polymers*, pp. 609–661. CRC Press, Boca Raton, FL.
7. Dalton, L. R. 1998. Polymers for electro-optic modulator waveguides, In *Electrical and Optical Polymer Systems: Fundamentals, Methods, and Applications*, D. L. Wise, T. M. Cooper, J. D. Gresser, D. J. Trantolo, and G. W. Wnek, eds., pp. 609–661. World Scientific, Singapore.
8. Kuzyk, M. G. and Dirk, C. W. eds. 1998. *Characterization Techniques and Tabulations for Organic Nonlinear Optical Materials*, pp. 8–33. Marcel Dekker, New York.
9. Dalton, L. R., Harper, A. W., Ren, A., Wang, F., Todorova, G., Chen, J., Zhang, C., and Lee, M. 1999. Polymeric electro-optic modulators: from chromophore design to integration with semiconductor VLSI electronics and silica fiber optics. *Industrial and Engineering Chemistry Research*, 38, 8–33.
10. Dalton, L. R. 2001. Nonlinear optical polymeric materials: from chromophore design to commercial applications. *Advances in Polymer Science*., Vol. 158 Heidelberg, pp. 1–86.
11. Dalton, L. R. 2003. Rational design of organic electro-optic materials. *Journal of Physics: Condensed Matter*, 15, R897–R934.
12. Dalton, L. R. 2004. Nonlinear optics—applications: electro-optics, EO. R.D. Guenther, ed., In *Encyclopedia of Modern Optics*, vol. 3, pp. 121–129. Elsevier, Amsterdam.
13. Bosshard, C., Sutter, K., Pretre, P., Hulliger, J., Florsheimer, M., Kaatz, P., and Gunter, P. 1995. In *Organic nonlinear optical materials*, A. Garito and F. Kajzar, eds., In *Advances in Nonlinear Optics*, vol. 1, pp. 776–789. Gordon Breach, Basel.
14. Agawal, G. P., Cojan, C., and Flytzanis, C. 1978. Nonlinear optical properties of one-dimensional semiconductors and conjugated polymers. *Physical Review B, Condensed Matter*, 17, 776–789.
15. Heflin, J. R., Wong, K. Y., Zamani-Kharmiri, O., and Garito, A. F. 1988. Nonlinear optical properties of linear chains and electron-correlation effects. *Physical Review B, Condensed Matter*, 38, 1573–1576.
16. Kanis, D. R., Ratner, M. A., and Marks, T. J. 1994. Design and construction of molecular assemblies with large second-order optical nonlinearities. Quantum chemical aspects. *Chemical Reviews*, 94, 195–242.
17. Albert, I. D. L., Marks, T. J., and Ratner, M. A. 1998. Practical computational approaches to molecular properties, In *Characterization Techniques and Tabulations for Organic Nonlinear Optical Materials*, M. G. Kuzyk and C.W. Dirk, eds., pp. 37–109. Marcel Dekker, New York.
18. Qin, A., Bai, F., and Ye, C. 2003. Design of novel X-type second-order nonlinear optical chromophores with low ground state dipole moment and large first hyperpolarizabilities. *Journal of Molecular Structure: Theochem*, 631, 79–85.
19. Kang, H., Zhu, P., Yang, Y., Facchetti, A., and Marks, T. J. 2004. Self-Assembled electrooptic thin films with remarkably blue-shifted optical absorption based on an X-shaped chromophore. *Journal of the American Chemical Society*, 126, 15974–15975.
20. Keinan, S., Zojer, E., Bredas, J., Ratner, M., and Marks, T. 2003. Twisted π-system electro-optic chromophores: a CIS vs. MRD-CI theoretical investigation. *Journal of Molecular Structure: Theochem*, 633, 227–235.

21. Kang, H., Facchetti, A., Zhu, P., Jiang, H., Yang, Y., Cariati, E., Righetto, S., Ugo, R., Liu, Z., Ho, S., and Marks, T. 2005. Exceptional molecular hyperpolarizabilities in twisted π-system chromophores. *Angewandte Chemie & Angewandte Chemie, International Edition in English*, 44, 7922–7925.
22. Breitung, E. M., Shu, C. F., and McMahon, R. J. 2000. Thiazole and thiophene analogues of donor–acceptor stilbenes: Molecular hyperpolarizabilities and structure-property relationships. *Journal of the American Chemical Society*, 122, 1154–1160.
23. Liao, Y., Eichinger, B., Firestone, K., Haller, M., Luo, J., Kaminsky, W., Benedict, J., Reid, P., Jen, A., Dalton, L., and Robinson, B. 2005. Systematic study of the structure-property relationship of a series of ferrocenyl nonlinear optical chromophores. *Journal of the American Chemical Society*, 127, 2758–2766.
24. Dalton, L. R., Robinson, B. H., Jen, A. K. Y., Reid, P., Eichinger, B., Sullivan, P., Akelaitis, A., Bale, D., Haller, M., Luo, J., Liu, S., Liao, Y., Firestone, K., Bhatambrekar, N., Bhattacharjee, S., Sinness, J., Hammond, S., Buker, N., Snoeberger, R., Lingwood, M., Rommel, H., Amend, J., Jang, S. H., Chen, A., and Steier, W. 2005. Acentric lattice electro-optic materials by rational design. *Proceedings of SPIE*, 5912, 43–54.
25. Minhaeng, C., Sun, Y. A., Hochan, L., Ledoux, I., and Zyss, J. 2002. Nonlinear optical properties of tetrahedral donor–acceptor octupolar molecules. *Journal of Chemical Physics*, 116, 9165–9173.
26. Le Bozec, H., Renouard, T., Bourgault, M., Dhenaut, C., Brasselet, S., Ledoux, I., and Zyss, J. 2001. Molecular engineering of octupolar tris(bipyridyl) metal complexes. *Synthetic Metals*, 124, 185–189.
27. Brunel, J., Juland, A., Ledoux, I., Zyss, J., and Blanchard-Desce, M. 2001. Boomerang-shaped octupolar molecules derived from triphenylbenzene. *Synthetic Metals*, 124, 195–199.
28. Stegeman, G. I. and Torreuellas 1994. Issues in organics for nonlinear optics, In *Electrical, Optical, and Magnetic Properties of Prganic Solid State Materials*, A. F. Garito, A. K. Y. Jen, C. Y. C. Lee, and L. R. Dalton, eds., pp. 397–412. Materials Research Society, Pittsburgh.
29. Perry, J. W., Marder, S. R., Perry, K. J., Sleva, E. T., Yakymyshyn, C., Stewart, K. R., and Boden, E. P. 1991. Organic salts with large electro-optic coefficient. *Proceedings of SPIE*, 1560, 302–309.
30. Burland, D. M., Miller, R. D., and Walsh, C. A. 1994. Second-order nonlinearity in poled-polymer systems. *Chemical Reviews*, 94, 31–75.
31. Dalton, L. R., Harper, A. W., Ghosn, R., Steier, W. H., Ziari, M., Fetterman, H., Shi, Y., Mustacich, R., Jen, A. K. Y., and Shea, K. J. 1995. Synthesis and processing of improved second order nonlinear optical materials for applications in photonics. *Chemistry of Materials*, 7, 1060–1081.
32. Barto, R., Bedworth, P., Frank, C., Ermer, S., and Taylor, R. 2005. Near-infrared optical-absorption behavior in high-beta nonlinear optical chromophore-polymer guest-host materials. II. Dye spacer length effects in an amorphous polycarbonate copolymer host. *Journal of Chemical Physics*, 122, 23, 1–14. 234907.
33. Barto, R., Frank, C., Bedworth, P., Ermer, S., and Taylor, R. 2004. Near-infrared optical absorption behavior in high-β nonlinear optical chromophore-polymer guest-host materials. 1. Continuum dielectric effects in polycarbonate hosts. *Journal of Physical Chemistry B: Materials, Surfaces, Interfaces & Biophysical*, 108, 8702–8715.
34. Oviatt, H. W., Shea, K. J., Kalluri, S., Shi, Y., Steier, W. H., and Dalton, L. R. 1995. Applications of organic bridged polysilsesquioxane xerogels to nonlinear optical materials by the sol-gel method. *Chemistry of Materials*, 7, 493–498.
35. Mao, S. S. H., Ra, Y., Guo, L., Zhang, C., Dalton, L. R., Chen, A., Garner, S., and Steier, W. H. 1998. Progress towards device-quality second-order nonlinear optical materials: 1influence of composition and processing conditions on nonlinearity, temporal stability and optical loss. *Chemistry of Materials*, 10, 146–155.
36. Suresh, S., Chen, S., Topping, C., Ballato, J., and Smith, D. 2003. Novel perfluorocyclo-butyl (PFCB) polymers containing isophorone derived chromophore for electro-optic [EO] applications. *Proceedings of SPIE*, 4991, 530–536.

37. Jin, D., Londergan, T., Huang, D., Wolf, N., Condon, S., Tolstedt, D., Guan, H., Cong, S., Johnson, E., and Dinu, R. 2004. Achieving large electro-optic response: DH-type chromophores in both crosslinked systems and linear high Tg systems. *Proceedings of SPIE*, 5351, 44–56.
38. Zhang, C., Zhang, H., Oh, M., Dalton, L., and Steier, W. 2003. What the ultimate polymeric electro-optic materials will be: guest-host, crosslinked, or side-chain. *Proceedings of SPIE*, 4991, 537–551.
39. Bai, Y., Song, N., Gao, J. P., Yu, G., Sun, X., Wang, X., and Wang, Z. Y. 2005. A new approach to highly electro-optically active materials using cross-linkable hyperbranched chromophore-containing oligomers as a macromolecular dopant. *Journal of the American Chemical Society*, 127, 2060–2061.
40. Song, N., Men, L., Gao, J. P., Bai, Y., Beaudin, A. M. R., Yu, G., and Wang, Z. Y. 2004. Cross-linkable zwitterionic polyimides with high electrooptic ceofficients at telecommunication wavelengths. *Chemistry of Materials*, 16, 3708–3713.
41. Ma, H., Chen, B., Takafumi, S., Dalton, L. R., and Jen, A. K. Y. 2001. Highly efficient and thermally stable nonlinear optical dendrimer for electro-optics. *Journal of the American Chemical Society*, 123, 986–987.
42. Jen, A. K. Y., Ma, J., Sassa, T., Liu, S., Suresh, S., Dalton, L. R., and Haller, M. 2001. Highly efficient and thermally stable organic/polymeric electro-optic materials by dendritic approach. *Proceedings of SPIE*, 4461, 172–179.
43. Ma, H., Liu, S., Luo, J., Suresh, S., Liu, L., Kang, S. H., Haller, M., Sassa, T., Jen, A. K. Y., and Dalton, L. R. 2002. Highly efficient and thermally stable electro-optical dendrimers for photonics. *Advanced Functional Materials*, 12, 565–574.
44. Luo, J., Haller, M., Ma, H., Liu, S., Kim, T. D., Tian, Y., Chen, B., Jang, S. H., Dalton, L. R., and Jen, A. K. Y. 2004. Nanoscale architectural control and macromolecular engineering of nonlinear optical dendrimers and polymers for electro-optics. *Journal of Physical Chemistry B*, 108, 8523–8530.
45. Sullivan, P. A., Akelaitis, A. J. P., Lee, S. K., McGrew, G., Lee, S. K., Choi, D. H., and Dalton, L. R. 2006. Novel dendritic chromophores for electro-optics: influence of binding mode and attachment flexibility on EO behavior. *Chemistry of Materials*, 18, 344–351.
46. Luo, J., Liu, S., Haller, M., Li, H., Kim, T. D., Kim, K. S., Tang, H. Z., Kang, S. H., Jang, S. H., Ma, H., Dalton, L. R., and Jen, A. K. Y. 2003. Recent progress in developing highly efficient nonlinear optical chromophores and side-chain dendronized polymers for electro-optics. *Proceedings of SPIE*, 4991, 520–529.
47. Luo, J., Kim, T. D., Ma, H., Liu, S., Kang, S. H., Wong, S., Haller, M. A., Jang, S. H., Li, H., Barto, R. R., Frank, C. W., Dalton, L. R., and Jen, A. K. Y. 2003. Nanoscale architectural control of organic functional materials for photonics. *Proceedings of SPIE*, 5224, 104–112.
48. Luo, J., Liu, S., Haller, M., Kang, J. W., Kim, T. D., Jiang, S. H., Chen, B., Tucker, N. H., Li, H., Tang, H. Z., Dalton, L. R., Liao, Y., Robinson, B. H., and Jen, A. K. Y. 2004. Recent progress in developing highly efficient and thermally stable nonlinear optical polymers for electrooptics. *Proceedings of SPIE*, 5351, 36–43.
49. Haller, M., Luo, J., Li, H., Kim, T. D., Liao, Y., Robinson, B., Dalton, L. R., and Jen, A. K. Y. 2004. A novel lattice-hardening process to achieve highly efficient and thermally stable nonlinear optical polymers. *Macromolecules*, 37, 688–690.
50. Tucker, N., Li, H., Tang, H., Dalton, L. R., Liao, Y., Robinson, B. H., Jen, A. K. J., Luo, J., Liu, S., Haller, M., Kang, J., Kim, T., Jang, S., and Chen, B. 2004. Recent progress in developinghighly efficient and thermally stable nonlinear optical polymers for electro-optics. *Proceedings of SPIE*, 5351, 36–43.
51. Jen, A., Luo, J., Kim, T. D., Chen, B., Jang, S. H., Kang, J. W., Tucker, N. M., Hau, S., Tian, Y., Ka, J. W., Haller, M., Liao, Y., Robinson, B., Dalton, L., and Herman, W. 2005. Exceptional electro-optic properties through molecular design and controlled self-assembly. *Proceedings of SPIE*, 5935, 5935061–5935113.

Q4

52. Dalton, L., Robinson, B., Jen, A., Ried, P., Eichinger, B., Sullivan, P., Akelaitis, A., Bale, D., Haller, M., Luo, J., Liu, S., Liao, Y., Firestone, K., Sago, A., Bhatambrekar, N., Bhattacharjee, S., Sinness, J., Hammond, S., Buker, N., Snoeberger, R., and Lingwood, M. 2005. Optimizing electro-optic activity in chromophore/polymer composites and in organic chromophore glasses. *Proceedings of SPIE*, 5990, 59000C-1-10.
53. Yitzchaik, S. and Marks, T. J. 1996. Chromophore self-assembled superlattices. *Accounts of Chemical Research*, 29, 197–202.
54. Zhao, Y. G., Wu, A., Lu, H. L., Chang, S., Lu, W. K., Ho, S. T., Van der Boom, M., and Marks, T. J. 2001. Traveling wave electro-optic phase modulators based on intrinsically polar self assembled chromophoric superlattices. *Applied Physics Letters*, 79, 587–589.
55. Zhu, P., van der Boom, M. E., Kang, H., Evmenenko, G., Dutta, P., and Marks, T. J. 2002. Realization of expeditious layer-by-layer siloxane-based self-assembly as an efficient route to structurally regular acentric superlattices with large electro-optic responses. *Chemistry of Materials*, 14, 4982–4989.
56. Marks, T. J., Ho, S. T., Liu, Z., Zhu, P., Sun, D. G., Ma, J., Ziao, Y., and Kang, H. 2003. Electro optic waveguide modulators by the integration of self-assembled superlattices with polymeric and semiconductor materials. *Proceedings of SPIE*, 4991, 133–143.
57. Li, J., Neyman, P. J., Vercellino, M., Heflin, J. R., Duncan, R., and Evoy, S. 2004. Active photonic crystal devices in self-assembled electro-optic polymeric materials. *Materials Research Society Symposia Proceedings*, 817, 133–138.
58. Dalton, L. R., Harper, A. W., and Robinson, B. H. 1997. The role of London forces in defining noncentrosymmetric order of high dipole moment-high hyperpolarizability chromophores in electrically poled polymeric thin films. *Proceedings of the National Academy of Sciences of the United States of America*, 94, 4842–4847.
59. Dalton, L. R., Harper, A. W., Chen, J., Sun, S., Mao, S. S., Garner, S., Chen, A., and Steier, W. H. 1997. The role of intermolecular interactions in fabricating hardened electro-optic materials. *Proceedings of SPIE*, CR68, 313–321.
60. Harper, A. W., Sun, S., Dalton, L. R., Garner, S. M., Chen, A., Kalluri, S., Steier, W. H., and Robinson, B. H. 1998. Translating microscopic optical nonlinearity to macroscopic optical nonlinearity: The role of chromophore-chromophore electrostatic interactions. *Journal of the Optical Society of America B, Optical Physics*, 15, 329–337.
61. Robinson, B. H. and Dalton, L. R. 2000. Monte Carlo statistical mechanical simulations of the competition of intermolecular electrostatic and poling field interactions in defining macroscopic electro-optic activity for organic chromophore/polymer materials. *Journal of Physical Chemistry*, 104, 4785–4795.
62. Dalton, L. R., Robinson, B. H., Jen, A. K. Y., Steier, W. H., and Nielsen, R. 2003. Systematic development of high bandwidth, low drive voltage organic electro-optic devices and their applications. *Optical Materials*, 21, 19–28.
63. Nielsen, R. D., Rommel, H. L., and Robinson, B. H. 2004. Simulation of the loading parameter in organic nonlinear optical materials. *Journal of Physical Chemistry B: Materials, Surfaces, Interfaces and Biophysical*, 108, 8659–8667.
64. Pereverzev, Y. V., Prezhdo, O. V., and Dalton, L. R. 2004. Macroscopic order and electro-optic response of dipolar chromophore-polymer materials. *Chemical Physics, Chemistry*, 5, 1–11.
65. Shi, Y., Zhang, C., Zhang, H., Bechtel, J. H., Dalton, L. R., Robinson, B. H., and Steier, W. H. 2000. Low (sub-1 volt) halfwave voltage polymeric electrooptic modulators achieved by control of chromophore shape. *Science*, 288, 119–122.
66. Baehr-Jones, T., Hochberg, M., Wang, G., Lawson, R., Liao, Y., Sullivan, P. A., Dalton, L. R., Jen, A. K. Y., and Scherer, A. 2005. Optical modulation and detection in slotted silicon waveguides. *Optics Express*, 13, 5216–5226.
67. Song, H., Oh, M., Ahn, S., and Steier, W. 2003. Flexible low-voltage electro-optic polymer modulators. *Applied Physics Letters*, 82, 4432–4434.

68. Paloczi, G., Huang, Y., Yariv, A., Luo, J., and Jen, A. 2004. Replica-molded electro-optic polymer Mach-Zehnder modulator. *Applied Physics Letters*, 85, 1662–1664.
69. Zhang, C., Dalton, L. R., Oh, M.-C., Zhang, H., and Steier, W. H. 2001. Low V_π electrooptic modulators from CLD-1: chromophore design and synthesis, materials processing, and characterization. *Chemistry of Materials*, 13, 3043–3050.
70. Sun, L., Kim, J., Jang, C., An, D., Lu, X., Zhou, Q., Taboada, J. M., Chen, R. T., Maki, J. J., Tang, S., Zhang, H., Steier, W. H., Zhang, C., and Dalton, L. R. 2001. Polymeric waveguide prism based electro-optic beam deflector. *Optical Engineering*, 40, 1217–1222.
71. Zhang, H., Oh, M.-C., Szep, A., Steier, W. H., Zhang, C., Dalton, L. R., Erlig, H., Chang, Y., Chang, D. H., and Fetterman, H. R. 2001. Push pull electro-optic polymer modulators with low half-wave voltage and low loss at both 1310 and 1550 μm. *Applied Physics Letters*, 78, 3136–3138.
72. Rabiei, P., Steier, W. H., Zhang, C., and Dalton, L. R. 2002. Polymer micro-ring filters and modulators. *Journal of Lightwave Technology*, 20, 1968–1975.
73. Liu, S., Haller, M. A., Luo, J., Jang, S. H., Ma, H., Dalton, L. R., and Jen, A. K. Y. 2003. Focused microwave-assisted synthesis of 2,5-dihydrofuran derivatives as electron acceptors for highly efficient nonlinear optical chromophores. *Materials Research Society Symposia Proceedings*, 771, 375–380.
74. Liu, S., Haller, M. A., Ma, H., Dalton, L. R., Jang, S. H., and Jen, A. K. Y. 2003. Focused microwave-assisted synthesis of 2,5-dihydrofuran derivatives as electron acceptors for highly efficient nonlinear optical chromophores. *Advanced Materials*, 15, 603–607.
75. Zhou, Z., Shaojun, L., and Cheng, Y. 2003. Poling properties of guest-host polymer films of X-type nonlinear optical chromophores. *Synthetic Metals*, 147, 1519–1520.
76. Sullivan, P. A., Bhattacharjee, S., Eichinger, B. E., Firestone, K., Robinson, B. H., and Dalton, L. R. 2004. Exploration of series type multifuctionalized nonlinear optical chromophore concept. *Proceedings of SPIE*, 5351, 253–259.
77. Firestone, K., Bale, D., Liao, Y., Casmier, D., Clot, O., Dalton, L., and Reid, P. 2005. Frequency-agile Hyper-Rayleigh Scattering studies of electro-optic chromophores. *Proceedings of SPIE*, 5935, 59350P1–59350P9.
78. Firestone, K. A., Reid, P., Lawson, R., Jang, S. H., and Dalton, L. R. 2004. Advances in organic electro-optic materials and processing. *Inorganic Chemistry Acta*, 357, 3957–3966.
79. Jang, S. H., Luo, J., Tucker, N. M., Leclercq, A., Zojer, E., Haller, M. A., Kim, T. D., Kang, J. W., Firestone, K., Bale, D., Lao, D., Benedict, J. B., Cohen, D., Kaminsky, W., Kahr, B., Bredas, J. L., Reid, P., Dalton, L. R., and Jen, A. K. Y. 2006. Pyrroline chromophores for electro-optics. *Chemistry of Materials*, 18, 13, 2982–2988.
80. Kim, W. K. and Hayden, L. M. 1999. Fully atomistic modeling of an electric field poled guest-host nonlinear optical polymer. *Journal of Chemical Physics*, 111, 5212–5222.
81. Nagtegaele, P., Brasselet, E., and Zyss, J. E. 2003. Anisotropy and dispersion of a Pockels tensor: a benchmark for electro-optic organic thin-film assessment. *Journal of the Optical Society of America B: Optical Physics*, 20, 1932–1936.
82. Teng, C. and Man, H. 1990. Simple reflection technique for measuring the electro-optic coefficient of poled polymers. *Applied Physics Letters*, 56, 1734–1736.
83. Schildkraut, J. 1990. Determination of the electrooptic coefficient of a poled polymer film. *Applied Optics*, 29, 2839–2841.
84. Park, D., Kang, J., Luo, J., Lim, T., Jen, A., Lee, C., and Herman, W. 2005. Nonlinear ellipsometric analysis of poled organic glasses having very large electro-optic coefficients. *Proceedings of SPIE*, 5935, 59350O-1-12.
85. Chen, A., Chuyanov, V., Garner, S., Steier, W., and Dalton, L. 1997. Modified attenuated total reflection for the fast and routine electrooptic measurements of nonlinear optical polymer thin films. In *Organic Thin Films for Photonic Applications*, *Vol. 14*, OSA Technical Digest Series, pp. 158–159. Optical Society of America, Washington DC.

86. Dumont, M. and Levy, Y. 1989. Measurement of electrooptic properties of organic thin films by attenuated total reflection, In *Nonlinear Optics of Organics and Semiconductors*, T. Kobayashi, ed., pp. 256–266. Springer, Berlin.
87. Levy, Y., Dumont, M., Shastaing, E., Robin, P., Chollet, P. A., Gadret, G., and Kajzar, F. 1993. Reflection method for electro-optic coefficient determination in stratified thin film structures. *Molecular Crystals and Liquid Crystals Science and Technology, Section B*, 4, 1–6.
88. Meyrueix, R., Lecomte, J., and Tapolsky, G. 1991. A Fabry-Perot interferometric technique for the electro-optic characterization of nonlinear optical polymers. *Nonlinear Optics*, 1, 201–211.
89. Meyrueix, R., Dickens, M., Lemonnier, O., Lecomte, J., and Tapolsky, G. 1994. Fabry-Perot interferometry applied to the study of piezoelectric and electro-optic properties of a poled NLO polyurethane. *Optics Communications*, 110, 445–455.
90. Kalluri, S., Garner, S., Ziari, M., Steier, W. H., and Dalton, L. R. 1996. Simple two-slit interference electrooptic coefficients measurement technique and efficient coplanar electrode poling of polymer thin films. *Applied Physics Letters*, 69, 275–277.
91. Donval, A., Toussaere, E., Hierle, R., and Zyss, J. 2000. Polarization insensitive electro-optic polymer modulator. *Journal of Applied Physics*, 87, 3258–3262.
92. Shin, M., Cho, H., Han, S., and Wu, J. 1998. Analysis of a Mach-Zehnder interferometry measurement of the Pockels coefficients in a poled polymer film with a reflection configuration. *Journal of Applied Physics*, 83, 1848–1853.
93. Chen, A., Chuyanov, V., Zhang, H., Garner, S., Steier, W. H., Chen, J., Zhu, J., He, M., Mao, S. S. H., and Dalton, L. R. 1998. "Demonstration of the full potential of second order nonlinear optic polymers for electrooptic modulation using a high $\mu\beta$ chromophore and a constant bias field. *Optics Letters*, 23, 478–480.
94. Gopalan, P. and Campbell, V. 2005. Low-loss electro-optic polymers for active wave guide components, *Pacifichem*, Honolulu, Hawaii.
95. Liao, Y., Firestone, K. A., Bhattacharjee, S., Luo, J., Haller, M., Hau, S., Anderson, C. A., Lao, D., Eichinger, B. E., Robinson, B. H., Reid, P., Jen, A. K. Y., and Dalton, L. R. 2006. Linear and nonlinear optical properties of a macrocyclic trichromophore bundle with parallel-aligned dipole moments. *Journal of Physical Chemistry B: Materials, Surfaces, Interfaces & Biophysical*, 110, 5434–5438.
96. Steier, W. H., Kalluri, S., Chen, A., Garner, S., Chuyanov, V., Ziari, M., Shi, Y., Fetterman, H., Jalali, B., Wang, W., Chen, D., and Dalton, L. R. 1996. Applications of electro-optic polymers in photonics. In *Materials Research Society Symposium Proceedings, Electrical, Optical and Magnetic Properties of Organic Solid State Materials*, *Vol. 413*, pp. 147–158, Materials Research Society, Pittsburgh.
97. Chen, A., Chuyanov, V., Marti-Carrera, F. I., Garner, S., Steier, W. H., Chen, J., Sun, S., and Dalton, L. R. 1997. Integrated polymer waveguide mode size transformer with a vertical taper for improved fiber coupling. *Proceedings of SPIE*, 3005, 65–76.
98. Chen, A., Chuyanov, V., Marti-Carrera, F. I., Garner, S. M., Steier, W. H., Chen, J., Sun, S. S., and Dalton, L. R. 2000. Vertically tapered polymer waveguide mode size transformer for improved fiber coupling. *Optical Engineering*, 39, 1507–1516.
99. Oh, M. C., Zhang, C., Lee, H. J., Steier, W. H., and Fetterman, H. R. 2002. Low-loss interconnection between electrooptic and passive polymer waveguides with a vertical taper. *IEEE Photonics Technology Letters*, 14, 1121–1123.
100. Zang, D. Y., Shu, G., Downing, T., Lin, W., Oh, C., and Bechtel, J. 2003. Insertion loss reduction in high speed polymer electrooptic modulators using tapered waveguide, fiber tip lenses and modification of waveguide structures. *Proceedings of SPIE*, 4991, 601–609.
101. Chang, D. H., Azfar, T., Kim, S. K., Fetterman, H. R., Zhang, C., and Steier, W. H. 2003. Vertical adiabatic transition between silica planar waveguide and electro-optic polymer fabricated using grayscale lithography. *Optics Letters*, 28, 869–871.

102. Ma, H., Wu, J., Herguth, P., Chen, B., and Jen, A. K. Y. 2000. A novel class of high performance perfluorocyclobutane-containing polymers for second-order nonlinear optics. *Chemistry of Materials*, 12, 1187–1189.
103. Zhang, Q., Canva, M., and Stegeman, G. 1998. Wavelength dependence of 4-dimethylamino-4'-nitrostilbene polymer thin film photodegradation. *Applied Physics Letters*, 73, 912–914.
104. Galvan-Gonzalez, A., Canva, M., Stegeman, G. I., Twieg, R., Kowalczyk, T. C., and Lackritz, H. S. 1999. Effect of temperature and atmospheric environment on the photodegradation of some Disperse Red 1 type polymers. *Optics Letters*, 24, 1741–1743.
105. Galvan-Gonzalez, A., Canva, M., Stegeman, G. I., Twieg, R. J., Chang, K. P., Kowalczyk, T. C., Zhang, X. Q., Lackritz, H. S., Marder, S., and Thayumanavan, S. 2000. Systematic behavior of electro-optic chromophore photostability. *Optics Letters*, 25, 332–334.
106. Galvan-Gonzalez, A., Canva, M., Stegeman, G. I., Sukhomilinova, L., Twieg, R. J., Chang, K. P., Kowalczyk, T. C., and Lackritz, H. S. 2000. Photodegradation of azobenzene nonlinear optical chromophores: The influence of structure and environment. *Journal of the Optical Society of America B: Optical Physics*, 17, 1992–2000.
107. DeRosa, M. E., He, M., Cites, J. S., Garner, S. M., and Tang, Y. R. 2004. Photostability of high $\mu\beta$ electro-optic chromophores at 1550 nm. *Journal of Physical Chemistry B: Materials, Surfaces, Interfaces & Biophysical*, 108, 8725–8730.
108. He, M., Leslie, T., Garner, S., DeRosa, M. E., and Cites, J. 2004. Synthesis of new electrooptic chromophores and their structure-property relationship. *Journal of Physical Chemistry B: Materials, Surfaces, Interfaces & Biophysical*, 108, 8731–8736.
109. Ashley, P., Sangnadasa, M., and Lindsay, G. 2005. Investigation of long term thermal stability of electrically poled CLD and FTC chromophores in amorphous polycarbonates, *Pacifichem*, Honolulu, Hawaii.
110. Taylor, E. W., Nichter, J. E., Nash, F. D., Haas, F., Szep, A. A., Michalak, R. J., Flusche, B. M., Cook, P. R., McEwen, T. A., McKeon, B. F., Payson, P. M., Brost, G. A., Pirich, A. R., Castaneda, C., Tsap, B., and Fetterman, H. R. 2005. Radiation resistance of electro-optic polymer-based modulators. *Applied Physics Letters*, 86, . 201122-1-3.
111. Sinyukov, A. M. and Hayden, L. M. 2004. Efficient electrooptic polymers for THz applications. *Journal of Physical Chemistry B*, 108, 8515–8522.
112. Sinyukov, A. M., Leahy, M. R., Hayden, L. M., Haller, M., Luo, J., Jen, A. K. Y., and Dalton, L. R. 2004. Resonance enhanced THz generation in electro-optic polymers near the absorption maximum. *Applied Physics Letters*, 85, 5827–5829.
113. Schneider, A. and Gunter, P. 2005. Spectrum of terahertz pulses form organic DAST crystals. *Ferroelectrics*, 318, 83–88.
114. Kawase, K., Hatanaka, T., Takahashi, H., Nakamura, K., Taniuchi, T., and Ito, H. 2000. Tunable terahertz-wave generation from DAST crystal by dual signal-wave parametric oscilation of periodically poled lithium niobate. *Optics Letters*, 25, 1714–1716.
115. Kawase, K., Mizuno, M., Sohma, S., Takahashi, H., Taniuchi, T., Urata, Y., Wada, S., Tashiro, H., and Ito, H. 1999. Difference-frequency terahertz-wave generation from 4-dimethylamino-N-methyl-4-stilbazolium-tosylate by use of an electronically tuned Ti:sapphire laser. *Optics Letters*, 24, 1065–1067.
116. Adachi, H., Tamiuchi, T., Yoshimura, M., Brahadeeswaran, S., Higo, T., Takagi, M., Mori, Y., Sasaki, T., and Nakanishi, H. 2004. High-quality organic 4-dimentylamino-N-methyl-4-stilbazolium tosylate (DAST) crystals for THz wave generation. *Japanese Journal of Applied Physics*, 43, L1121–L1123.
117. Zojer, E., Beljonne, D., Kogij, T., Vogel, H., Marder, S. R., Perry, J. W., and Bredas, J. L. 2002. Tuning the two-photon absorption response of quadrupolar organic molecules. *Journal of Chemical Physics*, 116, 3646–3658.

118. Brousmiche, D. W., Senn, J. M., Frechet, J. M. J., He, G. S., Lin, T.-C., Chung, S.-J., Prasad, P. N., Kannan, R., and Tan, L.-S. 2004. Fluorescence resonance energy transfer in novel multiphoton absorbing dendritic structures. *Journal of Physical Chemistry B*, 108, 8592–8600.

119. Drobizhev, M., Karotki, A., Rebane, A., and Spangler, C. 2001. Dendrimer molecules with record large two-photon absorption cross section. *Optics Letters*, 26, 1081–1083.

120. Hochberg, M., Baehr-Jones, T., Wang, G., Parker, J., Harvard, K., Liu, J., Chen, B., Shi, Z., Lawson, R., Sullivan, P., Jen, A. K. J., Dalton, L., and Scherer, A. Submitted. All optical modulator in silicon with terahertz bandwidth, *Nature Materials*.

Author Queries

JOB NUMBER: BK14885 / 15018

TITLE: Second- and Third-Order Nonlinear Optical Materials

Q1 We have made a change to the word 'plasticization'. Please approve.

Q2 References '118 and 119' are provided in the list but not cited in the text. Please supply citation details or delete the reference from the reference list.

Q3 Please provide forename for the author 'Torreuellas' in reference 28.